NAVAL POSTGRADUATE SCHOOL

MONTEREY, CALIFORNIA

THESIS

DIRECT TORQUE CONTROL OF A THREE-PHASE VOLTAGE SOURCE INVERTER-FED INDUCTION MACHINE

by

Darin M. Andrews

December 2013

Thesis Advisor: Alexander L. Julian
Second Reader: Roberto Cristi

Approved for public release; distribution is unlimited

THIS PAGE INTENTIONALLY LEFT BLANK

REPORT DOCUMENTATION PAGE			Form Approved OMB No. 0704-0188
Public reporting burden for this collection of information is estimated to average 1 hour per response, including the time for reviewing instruction, searching existing data sources, gathering and maintaining the data needed, and completing and reviewing the collection of information. Send comments regarding this burden estimate or any other aspect of this collection of information, including suggestions for reducing this burden, to Washington headquarters Services, Directorate for Information Operations and Reports, 1215 Jefferson Davis Highway, Suite 1204, Arlington, VA 22202-4302, and to the Office of Management and Budget, Paperwork Reduction Project (0704-0188) Washington DC 20503.			
1. AGENCY USE ONLY ***(Leave blank)***	**2. REPORT DATE** December 2013	**3. REPORT TYPE AND DATES COVERED** Master's Thesis	
4. TITLE AND SUBTITLE DIRECT TORQUE CONTROL OF A THREE-PHASE VOLTAGE SOURCE INVERTER-FED INDUCTION MACHINE		**5. FUNDING NUMBERS**	
6. AUTHOR(S) Darin M. Andrews			
7. PERFORMING ORGANIZATION NAME(S) AND ADDRESS(ES) Naval Postgraduate School Monterey, CA 93943-5000		**8. PERFORMING ORGANIZATION REPORT NUMBER**	
9. SPONSORING /MONITORING AGENCY NAME(S) AND ADDRESS(ES) N/A		**10. SPONSORING/MONITORING AGENCY REPORT NUMBER**	
11. SUPPLEMENTARY NOTES The views expressed in this thesis are those of the author and do not reflect the official policy or position of the Department of Defense or the U.S. government. IRB protocol number ____N/A____.			
12a. DISTRIBUTION / AVAILABILITY STATEMENT Approved for public release; distribution is unlimited		**12b. DISTRIBUTION CODE** A	

13. ABSTRACT (maximum 200 words)

The scope of this thesis involves various techniques to control the torque of a voltage source inverter-fed induction motor. The three methods investigated here are voltage by frequency, known as "scalar control", field-oriented control with and without space vector modulation, and direct torque control. Although all three techniques have been proven effective, each technique possesses its own advantages and disadvantages. In today's engineering world, time and money are saved by utilizing software developed to accurately model a physical system and to compare with hardware previously implemented in a lab. Comparisons can be made to determine how each of these torque control methods perform under static and dynamic modes of operation. The United States military can benefit from this study by modifying or adding onto the software models developed here with little cost and use these models to do trade studies without the cost of lab demonstrations.

14. SUBJECT TERMS Voltage source inverter-fed (VSI-fed), voltage-by-frequency (V/f), field oriented control (FOC), direct torque control (DTC), space vector modulation (SVM)			**15. NUMBER OF PAGES** 139
			16. PRICE CODE
17. SECURITY CLASSIFICATION OF REPORT Unclassified	**18. SECURITY CLASSIFICATION OF THIS PAGE** Unclassified	**19. SECURITY CLASSIFICATION OF ABSTRACT** Unclassified	**20. LIMITATION OF ABSTRACT** UU

THIS PAGE INTENTIONALLY LEFT BLANK

Approved for public release; distribution is unlimited

DIRECT TORQUE CONTROL OF A THREE-PHASE VOLTAGE SOURCE INVERTER-FED INDUCTION MACHINE

Darin M. Andrews
Lieutenant, United States Navy
B.S., Oregon State University, 2007

Submitted in partial fulfillment of the
requirements for the degree of

MASTER OF SCIENCE IN ELECTRICAL ENGINEERING

from the

NAVAL POSTGRADUATE SCHOOL
December 2013

Author: Darin M. Andrews

Approved by: Alexander L. Julian
Thesis Advisor

Roberto Cristi
Second Reader

R. Clark Robertson
Chair, Department of Electrical and Computer Engineering

THIS PAGE INTENTIONALLY LEFT BLANK

ABSTRACT

The scope of this thesis involves various techniques to control the torque of a voltage source inverter-fed induction motor. The three methods investigated here are voltage by frequency, known as “scalar control”, field-oriented control with and without space vector modulation, and direct torque control. Although all three techniques have been proven effective, each technique possesses its own advantages and disadvantages. In today’s engineering world, time and money are saved by utilizing software developed to accurately model a physical system and to compare with hardware previously implemented in a lab. Comparisons can be made to determine how each of these torque control methods perform under static and dynamic modes of operation. The United States military can benefit from this study by modifying or adding onto the software models developed here with little cost and use these models to do trade studies without the cost of lab demonstrations.

THIS PAGE INTENTIONALLY LEFT BLANK

TABLE OF CONTENTS

THIS PAGE INTENTIONALLY LEFT BLANK

LIST OF FIGURES

LIST OF TABLES

THIS PAGE INTENTIONALLY LEFT BLANK

LIST OF ACRONYMS AND ABBREVIATIONS

DTC	direct torque control
FOC	field-oriented control
PWM	pulsewidth-modulated
SVPWM	space vector pulsewidth-modulation
V/f	voltage-by-frequency
VSI-Fed	voltage source inverter-fed

THIS PAGE INTENTIONALLY LEFT BLANK

EXECUTIVE SUMMARY

The Navy is constantly looking for ways to improve the performance and efficiency of shipboard motors. Due to the current state of our national deficit and the Navy's ever-shrinking budget, development of cheaper alternatives to existing motors continues to be a primary focus. These alternatives should not sacrifice the standards for performance set by machines already in place. If we can maintain or improve upon these standards by making them more robust or improving their dynamic response while eliminating unnecessary sensors or other field monitoring devices, the money that can be saved will be substantial.

The evolution of DC drives to various forms of AC drives has been driven by the constant need for improvement in performance, simplicity, and reliability. Although many of these needs appear to encompass mutually exclusive goals, new developments strive for a better mix of advantages versus disadvantages. A simplistic viewpoint of the evolution of drive control techniques is demonstrated in Figure 1.

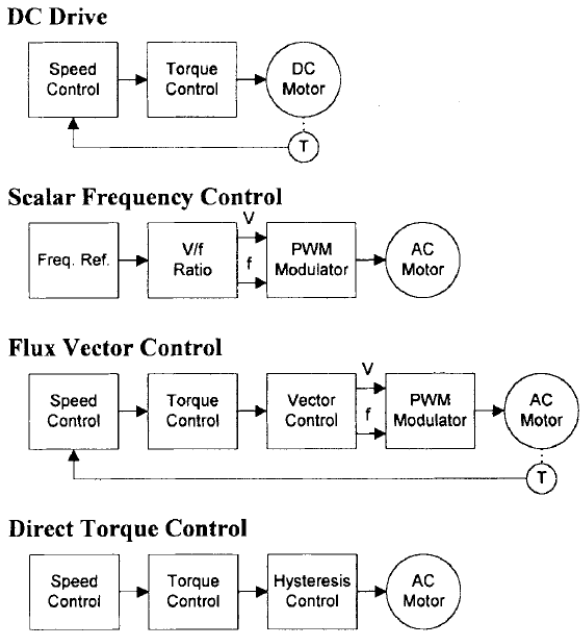

Figure 1. Evolution of drive control techniques, from [1].

The goal of this thesis is to develop an induction machine model in Simulink which is capable of accurately implementing torque control schemes and to validate this model with a hardware prototype. It is possible to model virtually every aspect of an induction machine, but a model serves only as a means to reduce time spent in the laboratory as well as cost and risk. A useful model predicts laboratory results and circuit dynamics but can only be declared accurate after experimental validation.

The construction of a three-phase voltage source, inverter-fed (VSI-fed) induction machine drive is the focus of this thesis. This physical system was tested using standard engineering principles. The physical parameters of this machine were estimated to develop an accurate model. A typical VSI-fed induction machine drive is depicted in Figure 2.

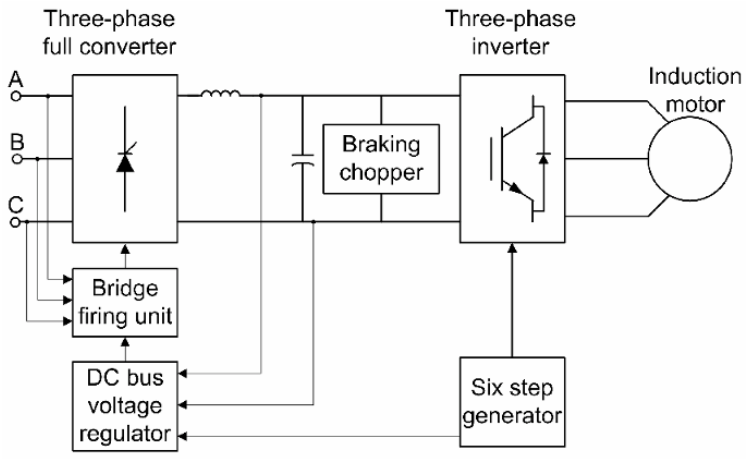

Figure 2. Three-phase VSI-fed induction machine, from [2].

The objectives of this research were to:

- Investigate various torque control schemes for an induction machine,
- Explain the control principles for each control scheme researched,
- Implement a physical system using the scalar control technique,
- Verify a Simulink model's scalar control operation by comparing measured results from the hardware prototype to the simulated results,

- Compare the performance of various torque control schemes during transient and steady state conditions,
- Compare speed, current, flux and torque responses of field oriented control to direct torque control,
- Provide recommendations as to which control technique to choose based on where they will be applied.

To control speed, torque, and position, various AC drives have been developed over the years. Depending on quality of control, these systems are classified as either low or high performance. They can also be classified as scalar (V/f) or vector-controlled based on their control principles. In general, the speed of an AC motor depends on the frequency of the stator voltage, while the developed torque is typically related to the stator current.

In V/f controlled systems, only the frequency and amplitude of the fundamental stator voltage or current are adjusted, hindering high performance of the system under transient operating conditions. Low performance V/f drives are normally employed in machinery such as adjustable speed pumps, compressors, and fans where higher quality control is unnecessary [3].

The main concept driving V/f control is to keep the ratio of the stator voltage to frequency constant to maintain constant maximum available torque. This is the most popular method of scalar control where the magnitude of the variables (frequency, voltage, or current) is controlled. The voltage applied command is calculated directly from the applied frequency maintaining a constant air gap flux in the machine. In steady-state operation, the flux is related to the ratio V_s/f_s where V_s is the amplitude of the motor phase voltage and f_s is the synchronous electrical frequency applied to the motor. This characteristic is defined by the base point of the motor. Below this base point, the motor operates at optimum excitation because of the constant V_s/f_s ratio. Above this point, the motor operates under-excited because of the DC bus voltage limit [4].

Although open loop V/f control was utilized in this thesis, closed loop speed control improves performance significantly. With closed loop control, a proportional-integral controller is employed to improve speed accuracy by regulating slip speed of the motor to maintain the motor speed at its set value.

In the 1990s the field of controlled electrical drives experienced rapid expansion due to the advances of semiconductors in power electronics culminating in better microelectronic microprocessors and digital signal processors. These technological advancements enabled development of highly effective AC drive controls with lower power dissipation and more accurate control structures. Drive controls became more accurate by managing the three-phase currents and voltages with "vector controls." The most common form of vector control is field-oriented control (FOC). Three major points establish this scheme:

- Machine current and voltage space vectors,
- Transformation of a three-phase speed and time-dependent system into a two coordinate time-invariant system,
- Effective pulsewidth-modulation (PWM).

As a result of these factors, FOC acquires all advantages of DC machine control and frees itself from the mechanical commutation drawbacks. Furthermore, FOC leads to high dynamic performance in terms of response times and power conversion by delivering accurate steady-state and transient control. A basic FOC scheme is depicted in Figure 3 [5].

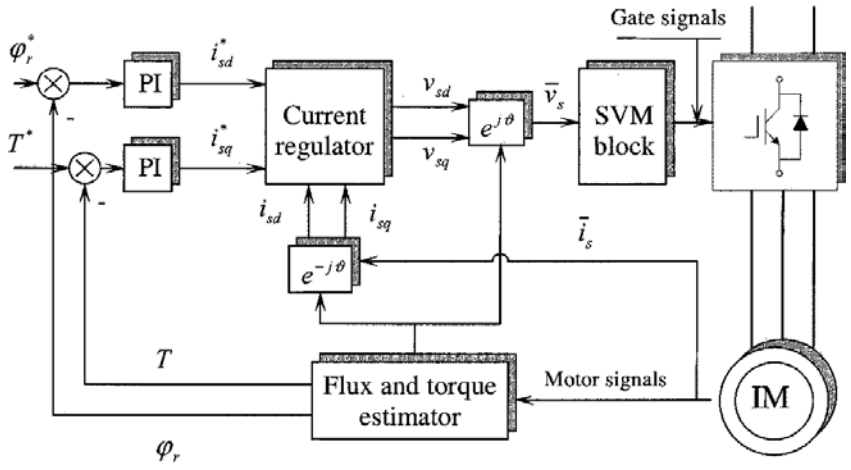

Figure 3. Basic FOC scheme, from [5].

FOC consists of controlling the stator currents represented by a vector. It is based on projections that transform a three-phase speed and time-dependent system into a two coordinate (d and q coordinates) time-invariant system. These projections led to a structure similar to that of DC machine control. FOC machines require two constants as input references: the torque component (aligned with the q-axis) and the flux component (aligned with the d-axis). As FOC is based on projections, the control structure enables accurate control in all operating conditions by seamlessly handling instantaneous electrical quantities. Thus, FOC solves classic scheme problems by easily reaching a constant reference for both the torque and flux components of the stator current [5].

Direct torque control (DTC) combines FOC theory, direct self-control theory, and advanced digital signal processing (DSP) and application specific integrated circuit (ASIC) technology to achieve a "sensorless" variable-frequency drive. On the basis of the errors between the reference and the estimated values of torque and flux, it is possible to directly control the inverter states in order to reduce the torque and flux errors within prefixed band limits. Unlike FOC, DTC does not require current regulators, coordinate transformations or a PWM modulator (as a consequence timers are not required). In spite of its simplicity, DTC allows for good torque control in both steady-state and transient operating conditions [6]. A basic DTC scheme is shown in Figure 4.

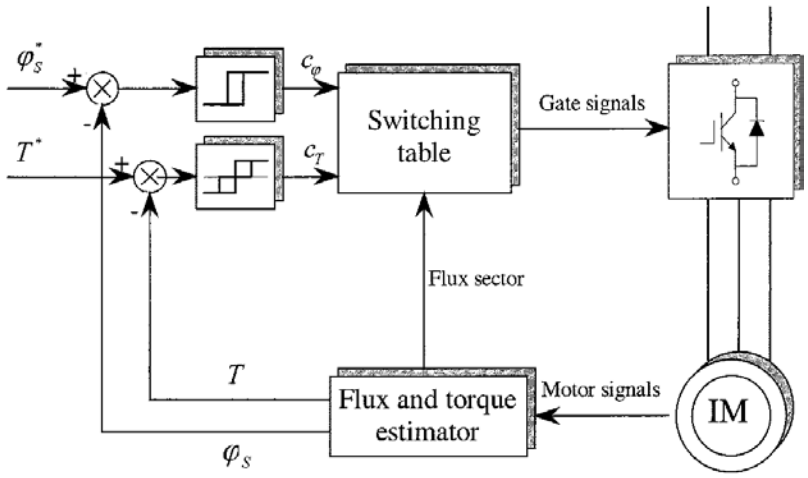

Figure 4. Basic DTC scheme, from [6].

As portrayed in Figure 4, the error between the estimated torque T and the reference torque T^* is the input of a three-level hysteresis comparator and the error between the estimated stator flux magnitude φ_S, and the reference stator flux magnitude φ_{S^*} is the input of a two-level hysteresis comparator. The selection of the appropriate voltage vector is based on the switching table given in Table 1.

Table 1. Basic switching table for DTC, from [6].

Sector		1	2	3	4	5	6
$c_\varphi = -1$	$c_T = -1$	$\overline{V}_2$	$\overline{V}_3$	$\overline{V}_4$	$\overline{V}_5$	$\overline{V}_6$	$\overline{V}_1$
	$c_T = 0$	$\overline{V}_7$	$\overline{V}_0$	$\overline{V}_7$	$\overline{V}_0$	$\overline{V}_7$	$\overline{V}_0$
	$c_T = +1$	$\overline{V}_6$	$\overline{V}_1$	$\overline{V}_2$	$\overline{V}_3$	$\overline{V}_4$	$\overline{V}_5$
$c_\varphi = +1$	$c_T = -1$	$\overline{V}_3$	$\overline{V}_4$	$\overline{V}_5$	$\overline{V}_6$	$\overline{V}_1$	$\overline{V}_2$
	$c_T = 0$	$\overline{V}_0$	$\overline{V}_7$	$\overline{V}_0$	$\overline{V}_7$	$\overline{V}_0$	$\overline{V}_7$
	$c_T = +1$	$\overline{V}_5$	$\overline{V}_6$	$\overline{V}_1$	$\overline{V}_2$	$\overline{V}_3$	$\overline{V}_4$

Appropriate use of the optimum switching look-up table requires knowledge of the stator flux linkage space vector, because the sector the vector resides in must be known [7]. This simple approach allows a quick torque response to be achieved; however, the steady-state performance is characterized by undesired ripple in current, flux and torque. This is largely due to the absence of information about torque and rotor speed values in the voltage vector selection algorithm [6].

To fairly compare FOC to DTC, their steady-state and step-response for three step events (at t=0.5, 2, and 3 seconds) were examined. In addition, their current, torque, and flux responses were observed closely. These responses are displayed in Figures 5–10.

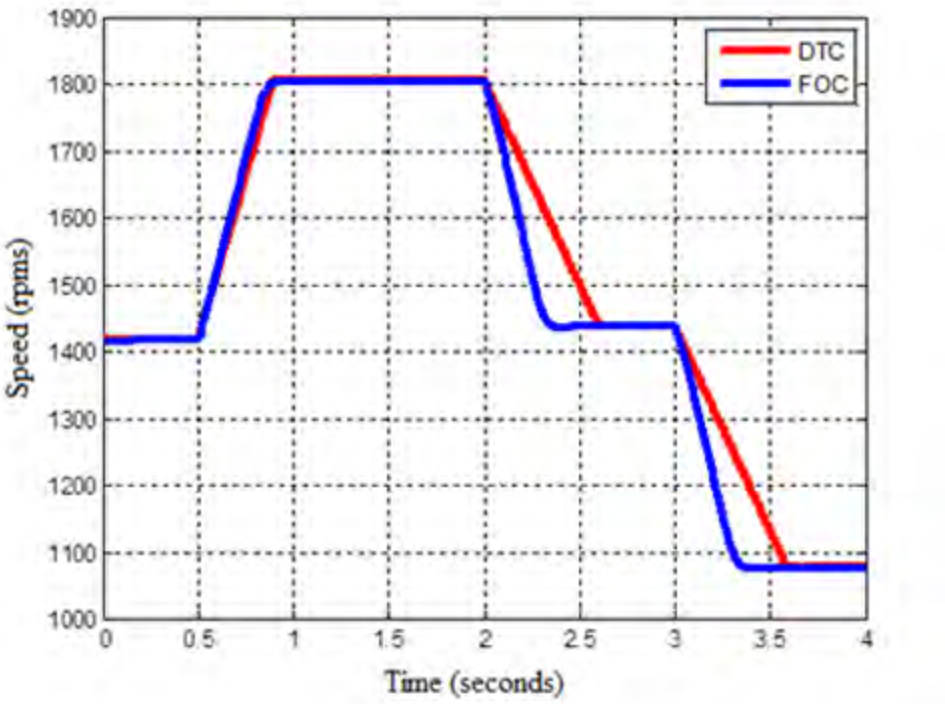

Figure 5. Speed response of DTC and FOC.

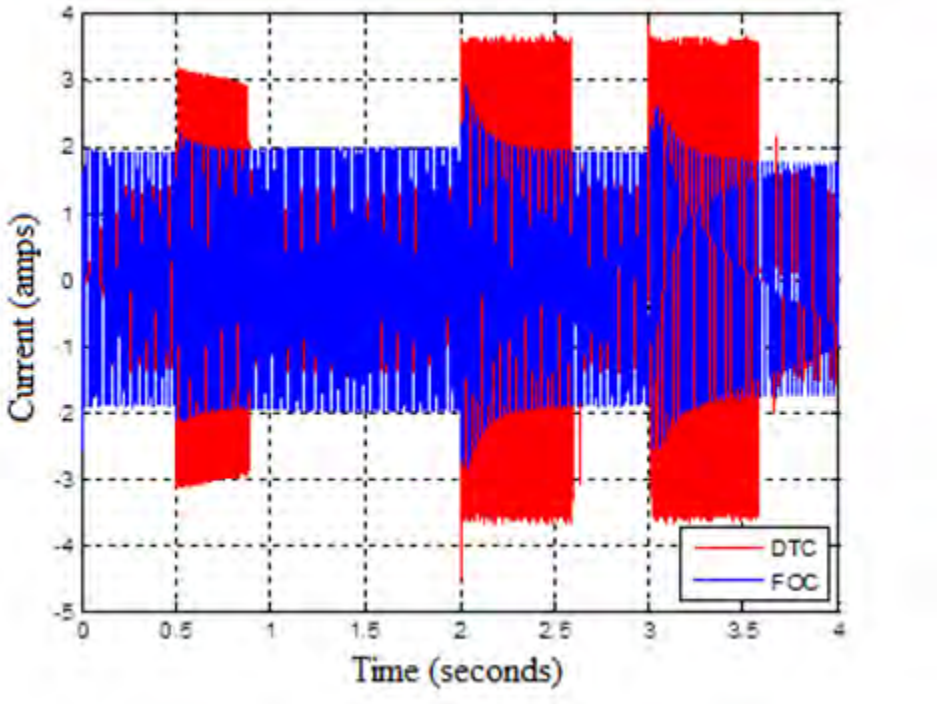

Figure 6. Phase B current of DTC and FOC filtered at 300 Hz.

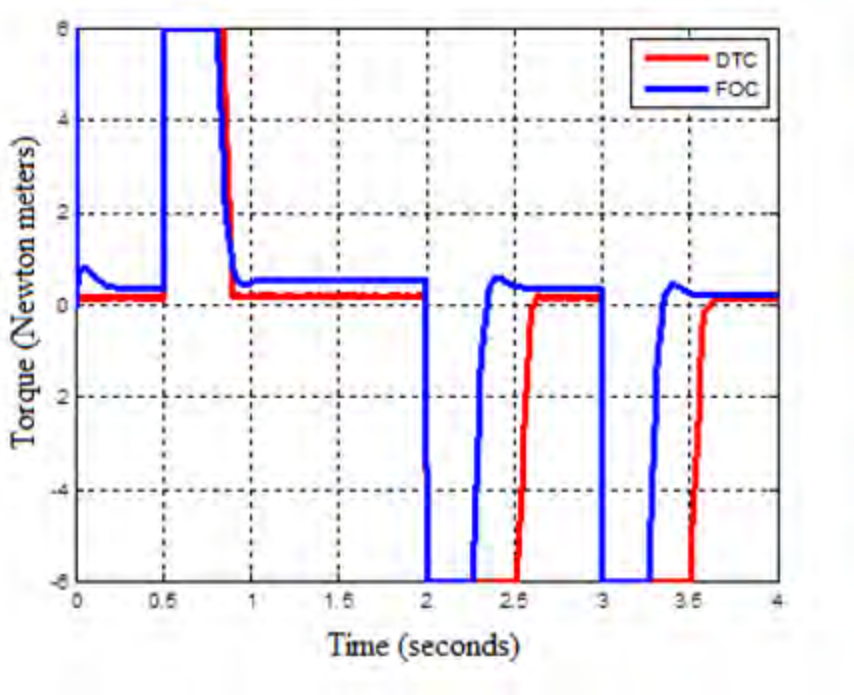

Figure 7. Reference torque for DTC and FOC.

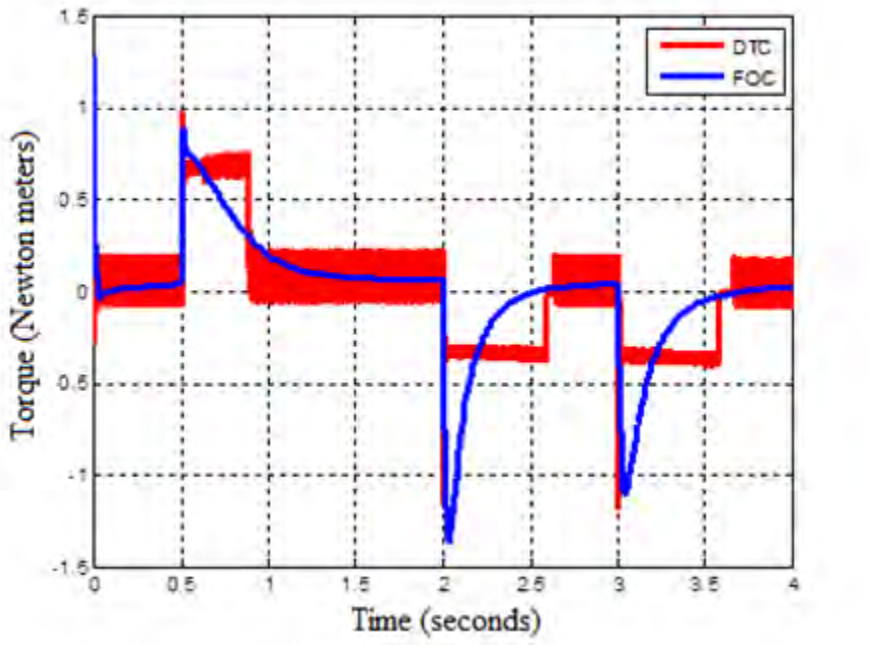

Figure 8. Electrical torque for DTC and FOC.

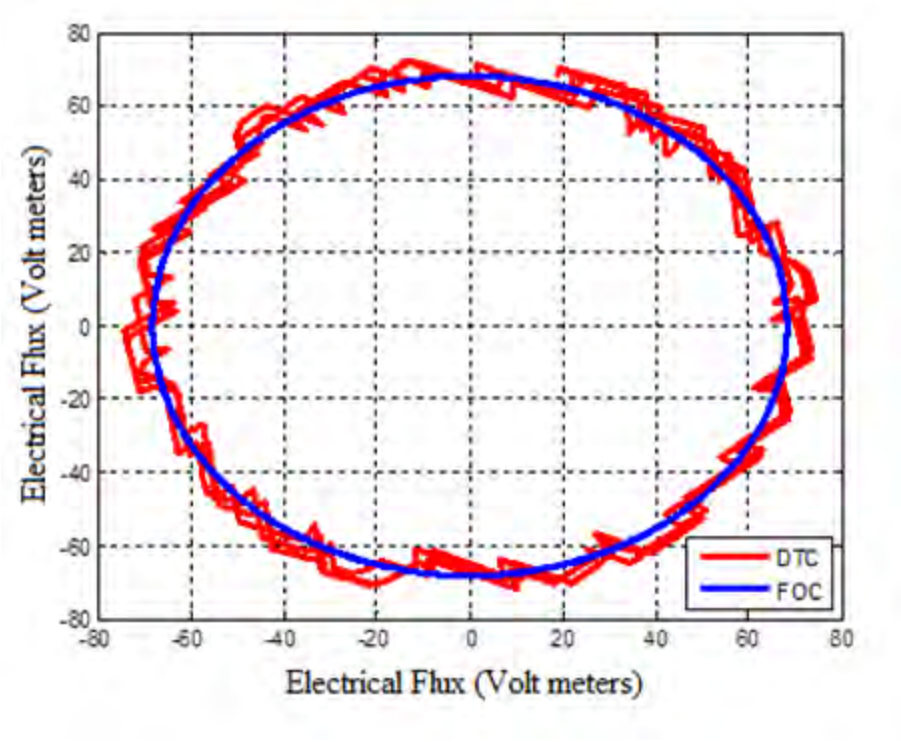

Figure 9. Stator flux for DTC and FOC.

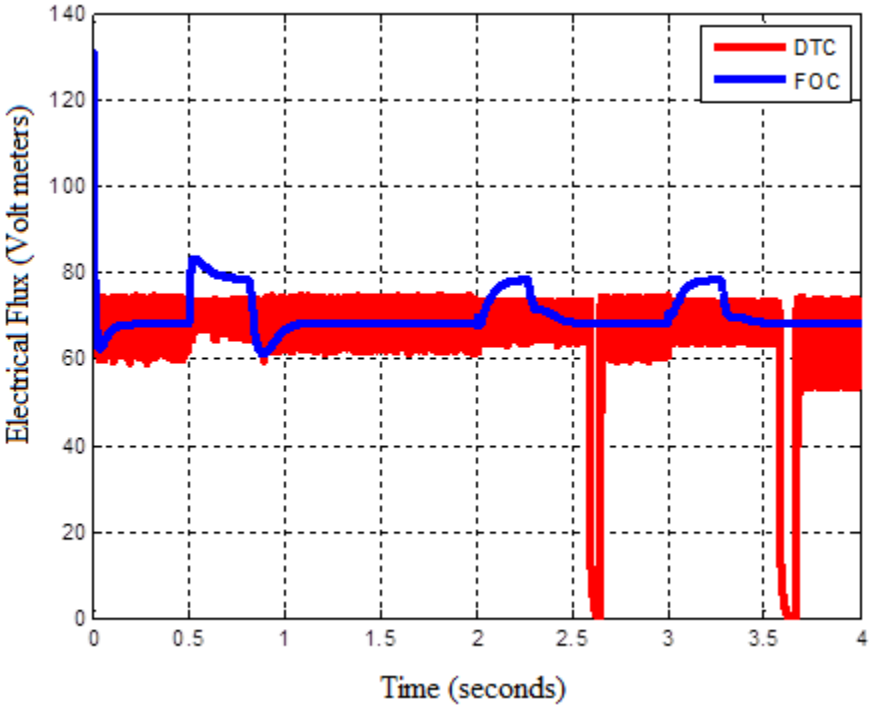

Figure 10. Electrical flux for DTC and FOC.

The results found during this research are consistent with the results shown in Table 2.

Table 2. Comparison of control schemes, from [1].

Control Type	*Torque Control*	*Flux Control*	*Response*	*Advantages*	*Disadvantages*
DC Drive	Direct	Direct	High	High accuracy Good torque response Simple	Motor maintenance Motor cost Encoder required for high accuracy
Scalar Frequency Control	None	None	Low	No encoder Simple	Low accuracy Poor torque response
Flux Vector Control	Indirect	Direct	High	High accuracy Good torque response	Encoder always required
Direct Torque Control	Direct	Direct	High	No encoder Moderate accuracy Excellent torque response	Encoder required for high accuracy

FOC and DTC possess distinct advantages over V/f control and suggest that scalar control is not a preferred control scheme for some applications. Although FOC demonstrated better accuracy (mainly because of the ability to control the current with current sensors), this accuracy comes at the expense of more complicated and expensive electronics. DTC allows for direct control of both the torque and the flux, but it is not as accurate and experiences high ripple content in both the flux and torque components. The steady-state current of DTC was significantly lower (less electrical losses) than that of FOC and should be employed with machines that operate at constant speeds for a majority of the time. FOC would better serve machines that require frequent speed changes because it experiences lower peak-to-peak currents during transients.

It was demonstrated that by using simulation to verify hardware prototypes, time and money can be saved. To further demonstrate this, the following additional research is required:

- The construction of a prototype that utilizes FOC and DTC,
- Performance improvements to the existing model, such as the addition of current sensors to the DTC scheme,
- Application of this model to machines of various sizes.

With a reliable model, the Navy has a means to build a large scale prototype for laboratory purposes and future research.

LIST OF REFERENCES

[1] J. N. Nash, "Direct torque control, induction motor vector control without an encoder," *IEEE Transactions on Industry Applications*, vol. 33, no. 2, March/April 1997.

[2] B. K. Bose, *Modern Power Electronics and AC Drives.* Prentice-Hall, NJ, 2002.

[3] S. Srilad, S. Tunyasrirut, and T. Suksri, "Implementation of a scalar controlled induction motor drive," in Bexco, Busan, Korea, pp. 3605–3610, 2006.

[4] R. Brindha, "Implementation of V/f control of three-phase induction motor using microcontroller," S.R.M Engineering College, Tamil Nadu, India, June/July 2006.

[5] Texas Instruments Europe, "Field orientated control of 3-phase AC-motors," Literature Number: BPRA073, February 1998.

[6] D. Casadei, F. Profumo, G. Serra, and A. Tani, "FOC and DTC: Two viable schemes for induction motors torque control," *IEEE Transactions on Power Electronics*, vol. 17, no. 5, September 2002.

[7] V. Peter, *Sensorless Vector and Direct Torque Control.* Oxford, United Kingdom: Oxford University Press, 1998.

THIS PAGE INTENTIONALLY LEFT BLANK

ACKNOWLEDGMENTS

I would like to thank the entire faculty and staff at the Naval Postgraduate School for giving me the opportunity to make the most out of my time in Monterey. The outstanding education and support that has been provided to me allows me to move on in my career with a genuine sense of confidence and accomplishment. I would like to extend my sincerest thanks to Professor Alexander Julian for his continual support, advice, and expansive knowledge. His efforts to pass his knowledge on to me and his patience when I struggled to understand at times were paramount in my success.

THIS PAGE INTENTIONALLY LEFT BLANK

I. INTRODUCTION

A. BACKGROUND

The Navy is constantly looking for ways to improve the performance and efficiency of shipboard motors. Due to the current state of our national deficit and the Navy's ever-shrinking budget, development of cheaper alternatives to existing motors continues to be a primary focus. These alternatives should not sacrifice the standards for performance set by machines already in place. If we can maintain or improve upon these standards by making them more robust or improving their dynamic response while eliminating unnecessary sensors or other field monitoring devices, the money that could be saved would be substantial.

The evolution of DC drives to various forms of AC drives has been driven by the constant need for improvement in performance, simplicity, and reliability. Although many of these needs appear to encompass mutually exclusive goals, new developments strive for a better mix of advantages versus disadvantages.

1. DC Drive

Torque is directly proportional to armature current in the DC motor. Direct torque control becomes possible with the use of an inner-current loop. Direct flux control is possible through the constant magnetic field orientation achieved through commutator action. These two primary factors ensure responsive control in the DC drive. Another advantage of the DC drive is that only simple electronics are required to achieve direct torque and flux control. On the other hand, initial and maintenance costs of DC motors are high, and high performance speed accuracy can only be achieved by including an encoder for feedback [1].

2. Voltage-by-Frequency (V/f) Control

Voltage-by-frequency control offers the advantage of operation without an encoder, but it possesses a major drawback in that neither torque nor flux can be controlled either directly or indirectly. Control is provided by a frequency and voltage

reference generator with constant Volts per Hertz output. This generator drives a pulsewidth-modulated (PWM) modulator. Unfortunately, this simple arrangement provides limited speed accuracy and poor torque response. Flux and torque levels are not controlled by the drive but are dictated by the response of the motor to the applied frequency and voltage [1].

3. Field-Oriented Control

FOC reestablishes direct flux control because field orientation is controlled electronically. The angular position of rotor flux is calculated and controlled directly by the drive, based on the comparison of the known stator field vector to feedback of rotor angular position and speed. The motor's electrical characteristics are mathematically modeled with microprocessor techniques to enable processing of the data. However, torque control is indirect because it is positioned prior to the vector control process in the control algorithm.

The biggest disadvantage of FOC is that to achieve high-performance speed and torque accuracy, the inclusion of a pulse encoder is necessary. The inclusion of the PWM modulator, which processes the voltage and frequency reference outputs of the vector control stage, creates a signal delay between the input references and the produced stator voltage vector. These last two factors limit the ultimate ability of FOC to achieve rapid flux and torque control [1].

4. Direct Torque Control

Just like FOC, DTC reestablishes direct flux control and implements direct torque control as well. Both flux and torque are controlled by hysteresis controllers. The PWM modulator stage is replaced by optimal switching logic, and thus, the delays associated with this stage are removed. The original benefits associated with the DC drive of direct torque control, direct flux control, and high responsiveness are all reestablished. As a result, better torque response is available with DTC. Most attractively, if moderate speed accuracy is acceptable, the need for a pulse encoder is eliminated. However, DTC has its own disadvantages that are discussed in detail later. A simplistic viewpoint of the evolution of drive control techniques is demonstrated in Figure 1 [1].

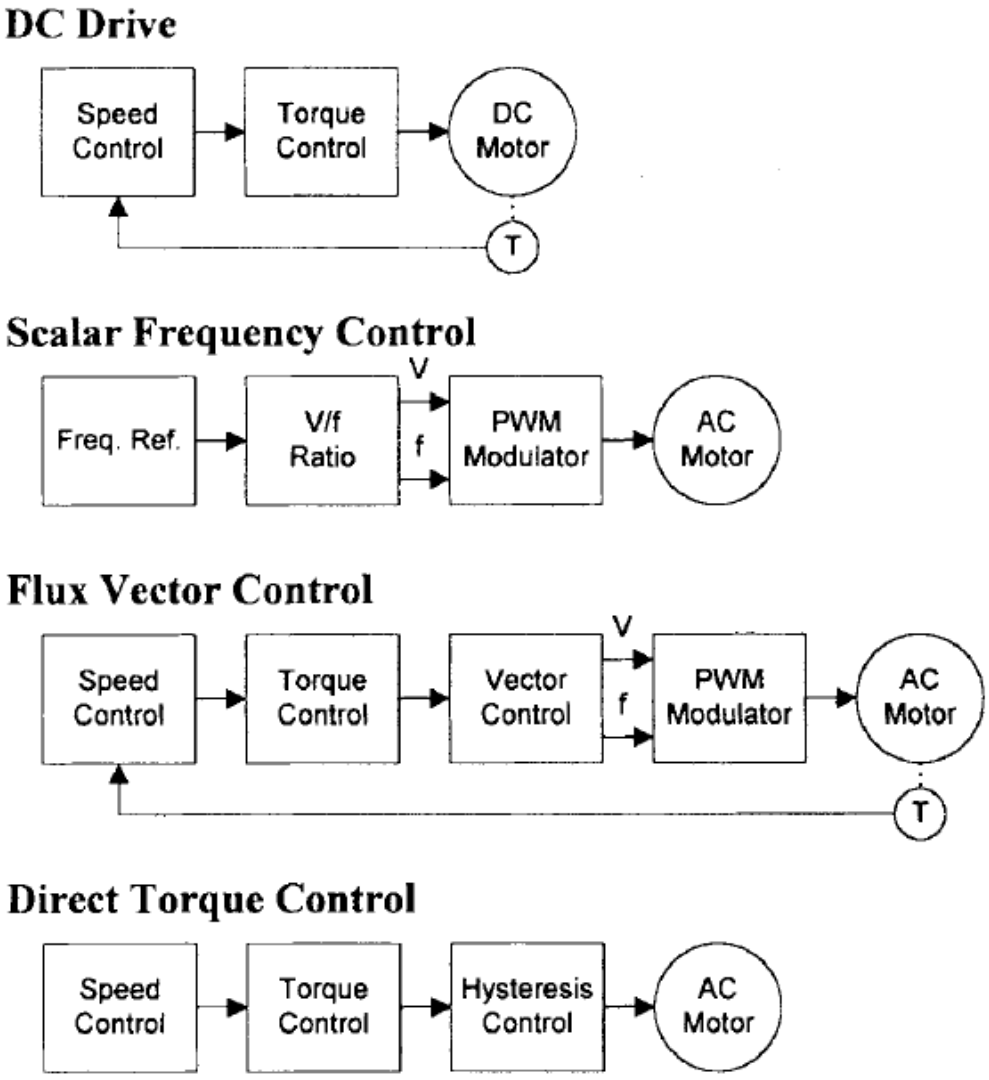

Figure 1. Evolution of drive control techniques, from [1].

B. OBJECTIVE

As previously stated, there are many schemes capable of controlling the torque of an induction machine. The purpose of this thesis is not to make conclusions as to which technique is the most effective but to demonstrate how these techniques compare both in static and dynamic performance.

The goal of this thesis is to develop an induction machine in Simulink capable of accurately implementing torque control schemes and to validate this model with a hardware prototype. It is possible to model virtually every aspect of an induction

machine, and a model serves as a means to reduce time spent in the lab as well as cost and risk. A useful model predicts laboratory results and circuit dynamics but can only be declared accurate after experimental validation.

C. APPROACH

One of the first decisions to be made was to determine which type of motor would be best for demonstrating these various techniques of torque control. One of the machine theory courses offered at the Naval Postgraduate School examined a three-phase Voltage Source Inverter-fed (VSI-fed) induction machine and determined its circuit parameters. A schematic of this machine is shown in Figure 2 and is discussed in further detail in Chapter II.

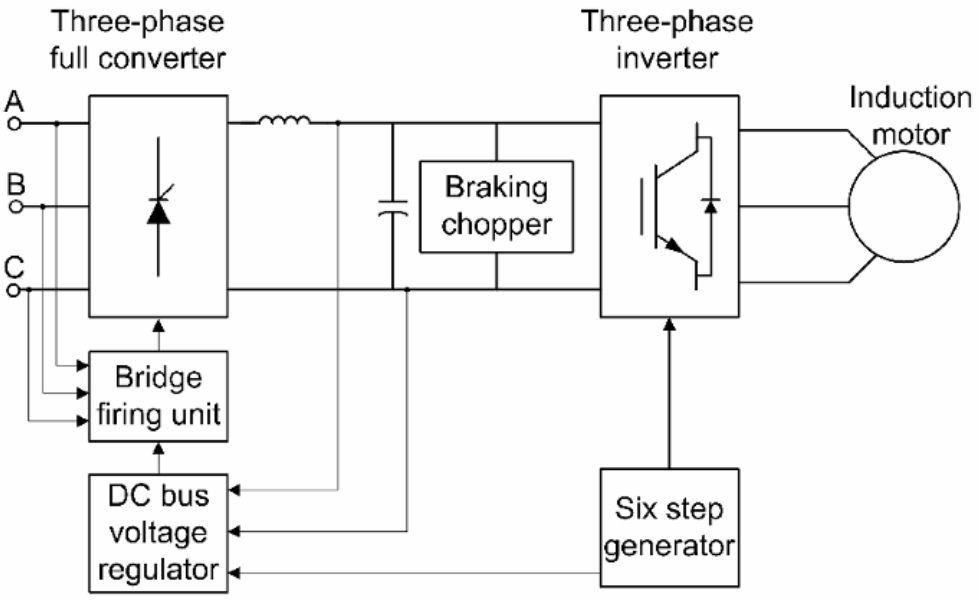

Figure 2. VSI-fed induction machine, from [2].

After calculating this machine's parameters, it was modeled in Simulink. Due to the scope of this thesis, only V/f control was implemented in the laboratory. Upon verifying that simulated and measured results utilizing V/f control matched closely, we

assumed this model behaved accurately under all torque control schemes. This model was used to simulate the other control schemes (i.e., FOC and DTC), and all three simulated torque control methods were compared.

D. THESIS ORGANIZATION

Induction machine theory and how the Simulink model was developed are presented in Chapter II. Theory behind the various torque control techniques are addressed in Chapter III. The operational modes, advantages and disadvantages of each are explained in detail. Proper functionality of the Simulink model under V/f control is verified through the comparison of simulated and experimental data and discussed in Chapter IV. The V/f simulation is used to demonstrate that both the FOC and DTC simulations accurately predict the behavior of this induction machine. A comprehensive comparison between FOC and DTC is included in Chapter IV. Conclusions and recommendations for future research are discussed in Chapter V. Data sheets for the equipment used and the Matlab code needed to regenerate the results found here are included in the appendices.

THIS PAGE INTENTIONALLY LEFT BLANK

II. INDUCTION MACHINE THEORY

A. INTRODUCTION

Simulink is a powerful tool that can be used to simulate any system that can be represented mathematically. To understand the simulated torque control techniques presented here, it is necessary to first possess a thorough understanding of the equations that represent the induction machine. The equations used to characterize this machine are discussed in further detail in [2]. Presented here are the induction machine voltage equations, flux linkage relationships, as well as the equations for stator, rotor, and mutual winding inductances. When creating an equivalent circuit, a standard convention is to refer the rotor variables to the stator windings using the appropriate turns ratio. This convention applies to the magnetizing and mutual inductances as well. More can be read concerning induction machine theory as used in this thesis application in [3].

1. From DC to AC

In the past, DC motors were used widely in variable-speed applications because their flux and torque can be controlled by the field and armature current. The existence of the commutator and brushes presents many challenges for DC machines because these parts require periodic maintenance and can only be used in certain environments. Their limitations under high speed, high voltage operational conditions, however, can be overcome by the application of AC motors. AC motors are robust, unaffected by heavy overloading, and easy to maintain while being relatively inexpensive. They can be designed with substantially higher output ratings for low weight and low rotating mass based on their size alone [4].

2. Early Misconceptions

Torque in AC and DC machines is similarly produced. This was not emphasized before the 1970s. As a result FOC did not materialize earlier. The precept given in many popular textbooks on machine theory falsely implies that the monitoring of the instantaneous electromagnetic torque of an induction machine required monitoring of the

rotor currents and position. Even more recent publications substantiated these misconceptions primarily because the convoluted expression for the instantaneous electromagnetic torque had not yet been simplified. Fundamental physical laws and space-vector theory proved that torque could be expressed as the product of a flux producing current and a torque producing current if a flux-oriented reference frame was utilized. In this case, the stator current components (normally expressed in a stationary reference frame) are transformed into a new rotating reference frame which rotates along with a selected flux-linkage space vector [4].

3. FOC and DTC

The torque in both DC and AC machines is controlled by the motor currents. Unlike DC machines, both the phase angle and the modulus of the current must be controlled in AC machines. This brings reason to the term "vector control." In addition, where the commutator and brushes of a DC machine fix the orientation of the field flux and armature magnetomotive force (analogous to emf), in AC machines, the field flux and spatial angle of the armature magnetomotive force require external control. Without this external control, the spatial angles between the various fields in an AC machine vary with the load and create unwanted oscillating dynamic response. Through external control, the torque and flux producing current components are decoupled, and the transient response characteristics emulate those of a separately excited DC machine. This system will adapt to load disturbances and/or reference value variations just as quickly as a DC machine.

Vector control is only one type of torque control. The other type of high performance torque control is DTC. DTC is achieved by direct and independent control of the flux linkages and electromagnetic torque through the selection of optimal inverter switching modes, which gives fast torque response, low inverter switching frequency, and low harmonic losses. How these control methods compare with V/f control and also with one another in both transient and dynamic operating conditions is demonstrated in this thesis [4].

B. VSI-FED INDUCTION MACHINE

The model used for this thesis and how its parameters were calculated are described in this section. This VSI-fed induction machine was implemented in the laboratory, and an equivalent model was designed using Simulink. After verifying V/f control of this machine through measured and simulated results, we assumed that the model behaves accurately regardless of which torque control scheme is utilized. Then, the Simulink model was modified to simulate FOC and DTC separately and then compared with V/f control for accuracy.

1. Balanced Three-Phase Machines

The three-phase induction machine has three-phase windings distributed on the stator iron and either three-phase windings wound on the rotor or an equivalent squirrel-cage structure. Applying balanced three-phase power to a balanced AC motor implies that the line-to-line voltages across the motor terminals are sinusoidal in steady-state. In a balanced AC motor, it can be shown that the motor voltages are also sinusoidal and, similarly to the motor currents, the three-phase voltages sum to zero on an instantaneous basis as expressed by

$$v_{an}(t) + v_{bn}(t) + v_{cn}(t) = 0 \tag{1}$$

where v_{an}, v_{bn}, and v_{cn} are these motor voltages.

This is also valid on an average basis

$$\overline{v}_{an}(t) + \overline{v}_{bn}(t) + \overline{v}_{cn}(t) = 0 \tag{2}$$

when

$$i_a(t) + i_b(t) + i_c(t) = 0 \tag{3}$$

where i_a, i_b and i_c are the phase currents [5].

The balanced power applied to the stator circuits produces a rotating magnetic field (North/South pole pair) which cuts the windings on the rotor and induces voltages. The windings are typically short circuited and current flows. In turn, the rotor currents set

up a rotating magnetic field relative to the rotor. The interaction of these fields is the mechanism of torque production in induction machines [6].

2. The *T*-Equivalent Circuit

One of the machine theory courses offered at Naval Postgraduate School required students to perform a laboratory experiment designed to calculate the parameters of a VSI-fed induction machine. From a simulation and analysis perspective, it is desirable to calculate the approximate parameters for the induction machine *T*-equivalent circuit. To do so, no-load and locked-rotor tests were performed. The *T*-equivalent circuit for steady-state operation of a symmetrical induction machine is portrayed in Figure 3.

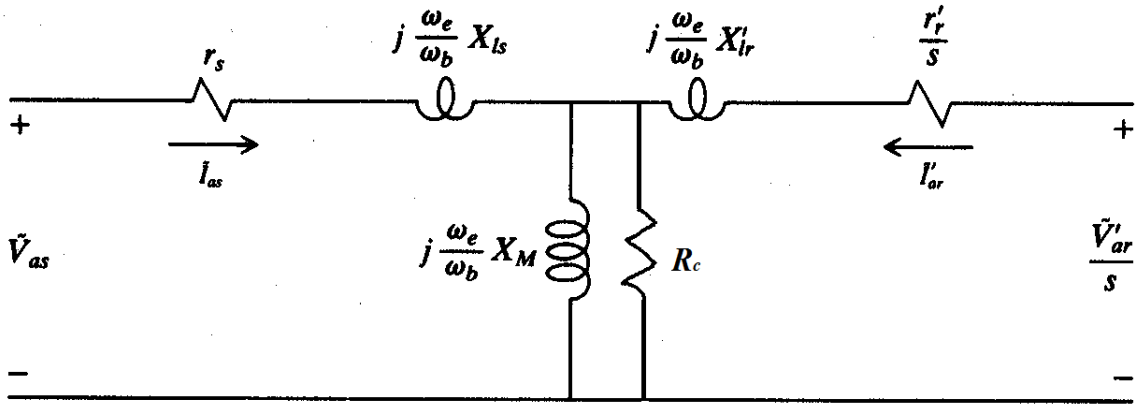

Figure 3. Equivalent circuit for steady-state operation of a symmetrical induction machine, after [2].

When an induction machine runs at no-load, the slip is exceedingly small which implies that the equivalent resistance is very large. As a result, the rotor current is negligible, and the equivalent circuit reduces to only the magnetizing branch which is modeled by a reactance X_M and a parallel resistance R_c, in series with the stator resistance and leakage reactance. The resistance R_c allows the core losses of the machine to be taken into account. The values of this reduced circuit were derived by applying rated line-to-line voltage and measuring the no-load current and total three-phase active power.

When the rotor of an induction motor is locked, the stator current is on the order of six times greater than the rated current. Furthermore, the slip is equal to one. While the slip is equal to one, the resistance is small compared to the magnetizing branch. Thus, the magnetizing branch was neglected.

3. Rated Values and Average Phase Resistance

The rated current and rated phase voltage of the stator winding as well as the machines rated speed, electrical frequency, and horsepower of the motor are listed in Table 1.

Table 1. Rated values.

Parameter name	Value
Rated current (stator winding)	1.5 A
Rated phase voltage (stator winding)	120 V_{rms}
Rated speed, ω_e	1670 rpm
Rated electrical frequency, f_e	60 Hz
Horsepower	1/4 HP

First, the number of poles was calculated from

$$p = \left(2 f_e \times 60\right) \div NLS \tag{4}$$

where p is the number of poles, f_e is the electrical frequency in Hertz, and NLS the no-load speed was measured in rpms. With a no-load speed of 1789 rpm, it was discovered that this was a four pole machine, from the horsepower and speed, the torque can also be calculated from

$$P = T\omega \rightarrow T = \frac{P}{\omega_e} \tag{5}$$

where P is ¼ horsepower, T is the calculated torque and ω_e is the rated speed in radians/second. This calculation leads to a torque of 9.4 lbf· in.

By measuring the resistance of each stator phase the average stator winding resistance can be determined from

$$\overline{R}_{ph} = \frac{R_{ph1} + R_{ph2} + R_{ph3}}{3} \tag{6}$$

where $\overline{R}_{ph}$ is the average phase resistance in ohms and is 11.91 Ω.

a. No-Load Measurements

The circuit used to measure no-load characteristics is illustrated in Figure 4.

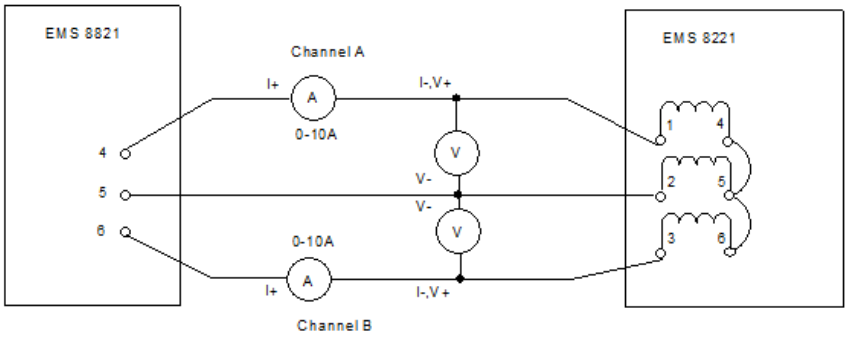

Figure 4. Circuit for measuring no-load characteristics, from [6].

By using the expression for instantaneous three-phase power and the fact that the machine is wye-connected, the setup in Figure 3 yields total steady-state three-phase power

$$P = v_{as}i_{as} + v_{bs}i_{bs} + v_{cs}i_{cs}\,. \tag{7}$$

This can be manipulated to obtain

$$P == (v_{as} - v_{bs})i_{as} + (v_{cs} - v_{bs})i_{cs} \tag{8}$$

where v_{as}, v_{bs}, and v_{cs} are the stator phase voltages and i_{as}, i_{bs}, and i_{cs} are the stator phase currents.

By applying 200 VAC and recording the line-to-line voltages, line currents, power readings, and machine speed the total three-phase power was calculated to be 138 W (no-load characteristic). These no-load measurements are listed in Table 2.

Table 2. No-load measurements.

Parameter name	Value
Channel A Line Current	0.684 A
Channel A Power	60 W
Channel B Line-to-Line Voltage	201 V
Channel B Line Current	0.68 A
Channel B Power	78 W
Machine Speed	1789 rpm

b. Locked-Rotor Measurements

For the locked-rotor test, the line-to-line voltage was adjusted to approximately 60 VAC, and 120 VAC was supplied to the dynamometer. The motor was connected to the dynamometer with a timing belt, and the dynamometer was set to provide maximum load. After measuring the appropriate currents, powers, and voltages, the total three-phase power was computed to be 234 W (locked-rotor characteristic). These locked-rotor measurements are listed in Table 3.

Table 3. Locked-rotor measurements

Parameter name	Value
Channel A Line-to-Line Voltage	99 V
Channel A Line Current	2.09 A
Channel A Power	42 W
Channel C Line-to-Line Voltage	100 V
Channel C Line Current	2.04 A
Channel C Power	192 W

c. Final T-Equivalent Circuit Parameters

From the data collected, the following parameters for the *T*-equivalent induction machine circuit were calculated: $r_s, \mathrm{X}_{ls}, \mathrm{X}'_{lr}, \mathrm{X}_{M,}$ and the core loss resistance R_c. The rms phase A stator voltage v_1 was determined from

$$\tilde{V}_{as} = \frac{\tilde{V}_{ab}}{\sqrt{3}} \tag{9}$$

where $\tilde{V}_{ab}$ is the rms line a-to-line b voltage and was 116 V_{rms}.

To calculate the no-load power of the core $P_{core,NL}$, the following expression was used

$$P_{core,NL} = P_{in,NL} - 3\left|\tilde{I}_{as,NL}\right|^2 r_s \tag{10}$$

where $P_{in,NL}$ is the no-load input power, $\tilde{I}_{as,NL}$ is the no-load phase A stator current, and r_s is the resistance of the stator. A no-load power of the core of 121.5 W was computed. Next, the core resistance R_c was determined from

$$R_c = \frac{3\left|\tilde{V}_{as,NL}\right|^2}{P_{core,NL}} \tag{11}$$

where $\tilde{V}_{as,NL}$ is the instantaneous no-load phase A stator voltage. This results in a core resistance of 332 Ω.

The phase angle difference $\Delta\theta$ was calculated using the rated frequency of 60 Hz from

$$\Delta\theta = \frac{360°\Delta t}{1/f} \tag{12}$$

where Δt is the measured difference between the voltage and current phase (3.92 msec). This phase angle difference is 84.7°.

Starting with the expression

$$\frac{\left|\tilde{V}_{as,NL}\right|}{\left|\tilde{I}_{as,NL}\right|} = \sqrt{r_s^{\,2} + (\mathrm{X}_M + X_{ls})^2} \tag{13}$$

where X_M is the mutual reactance and X_{ls} is the stator leakage reactance, and rearranging Equation (13) in the following way

$$\left(X_M + X_{ls}\right) = \sqrt{\left[\frac{\left|\tilde{V}_{as,NL}\right|}{\left|\tilde{I}_{as,NL}\right|}\right]^2 - r_s^2}\ , \tag{14}$$

we can determine the total reactance. A total reactance of 170 Ω was calculated. In turn, the resistance of the rotor on the secondary side $r_r^{'}$ can be found using the expression

$$\frac{r_r^{'}}{s} = \frac{P_{in,LR}}{3\left|\tilde{I}_{as,LR}\right|^2} - r_s \tag{15}$$

where $P_{in,LR}$ is the locked-rotor input power and $\tilde{I}_{as,LR}$ is the locked-rotor instantaneous phase A stator current. This computation resulted in a resistance of 5.95 Ω. Rearranging Equation (13) into the form

$$\frac{\left|\tilde{V}_{as,LR}\right|}{\left|\tilde{I}_{as,LR}\right|} = \sqrt{\left(r_s + \frac{r_r^{'}}{s}\right)^2 + \left(X_{lr}^{'} + X_{ls}\right)^2} \tag{16}$$

and Equation (16) into

$$\frac{\left|\tilde{V}_{as,LR}\right|}{\left|\tilde{I}_{as,LR}\right|} = \sqrt{\left(r_s + \frac{r_r^{'}}{s}\right)^2 + \left(X_{lr}^{'} + X_{ls}\right)^2} \tag{17}$$

where $X_{lr}^{'}$ is the rotor leakage reactance on the primary side and X_{ls} is the stator leakage reactance (they are equal) makes calculating the reactance possible. Rearranging Equation (17) allows for both to be solved from

$$\left(X_{lr}^{'} + X_{ls}\right) = \sqrt{\left(\frac{\left|\tilde{V}_{as,LR}\right|}{\left|\tilde{I}_{as,LR}\right|}\right)^2 - \left(r_s + \frac{r_r^{'}}{s}\right)^2}\ , \tag{18}$$

and $X_{lr}^{'}$ and X_{ls} are equal to 10 Ω apiece. Finally, the mutual reactance X_M can be obtained as

$$\left(X_M + X_{ls}\right) = 170\Omega\,. \tag{19}$$

Given that X_{ls} is 10 Ω it is easy to see that there is a total mutual reactance of 160 Ω.

The calculations performed above are summarized in Table 4.

Table 4. Circuit parameter values.

Parameter name	**Value**
Rotor resistance, $r_r^{'}$	5.95 Ω
Stator resistance, r_s	5.95 Ω
Stator linkage reactance, X_{ls}	10 Ω
Mutual reactance, X_M	160 Ω
Rotor linkage reactance, $X_{lr}^{'}$	10 Ω

This is the *T*-equivalent circuit with coil one selected as the reference coil. The values on the rotor side ($X_{lr}^{'}$ and $\tilde{I}_{ar}^{'}$) have been scaled by the turns ratio [6].

Once the values of the *T*-equivalent circuit were calculated, these values and the specifications of the machine used in this lab were used to develop an accurate model of the machine in Simulink. To ensure that the model accurately predicted the behavior of this machine, these same parameters were incorporated into the model. The simulated and measured results were then compared to ensure that the model accurately predicted the behavior of the physical machine. These results are shown in Figure 5.

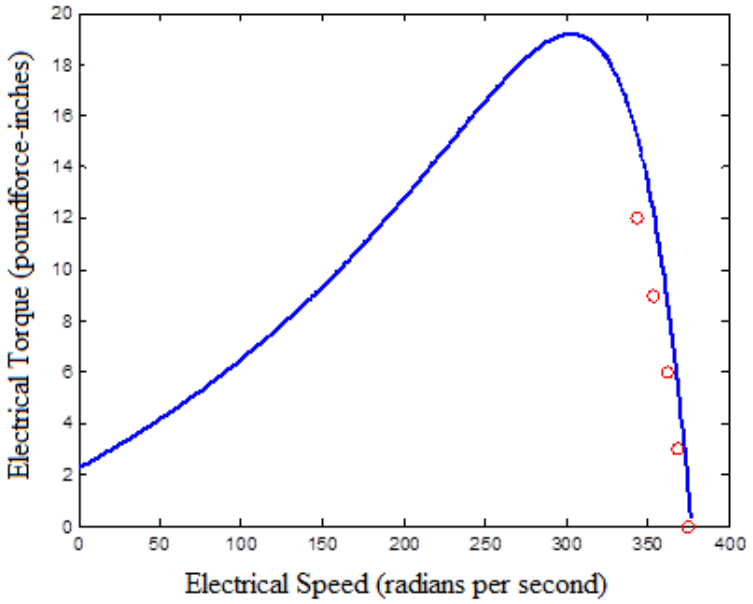

Figure 5. Measured and equivalent electrical torque versus speed.

THIS PAGE INTENTIONALLY LEFT BLANK

III. TORQUE CONTROL METHODS FOR VSI-FED INDUCTION MACHINE

A. VOLTAGE-BY-FREQUENCY CONTROL

To control speed, torque, and position, various AC drives have been developed over the years. Depending on quality of control these systems are classified as low or high performance. They can also be classified as scalar (V/f) or vector-controlled (FOC) based on their control principles. In general, the speed of an AC motor depends on the frequency of the stator voltage, while the developed torque is typically related to the stator current.

In V/f controlled systems, only the frequency and amplitude of the fundamental stator voltage or current are adjusted, hindering high performance of the system under transient operating conditions. These low performance V/f drives are normally employed in machinery such as adjustable speed pumps, compressors, and fans where higher quality control is unnecessary [5].

1. V/f Concept

The ratio of the stator voltage to frequency is kept constant to maintain maximum available torque in variable-speed induction motor drives. This is known as V/f control and is the most popular method of scalar control where the magnitude of the variables (frequency, voltage, or current) is controlled. The voltage applied command is calculated directly from the applied frequency maintaining a constant air gap flux in the machine. In steady-state operation, the flux is related to the ratio V_s/f_s where V_s is the amplitude of the motor phase voltage and f_s is the synchronous electrical frequency applied to the motor. This characteristic is defined by the base point of the motor. Below this base point, the motor operates at optimum excitation because of the constant V_s/f_s ratio. Above this point, the motor operates under excited because of the DC bus voltage limit [7].

a. Faraday's Law and the Speed of an Induction Motor

The speed of an induction motor can be controlled by varying the frequency of the three-phase power supply. To maintain constant flux density, the applied voltage must be changed in the same proportion as the frequency according to Faraday's Law. Any change in the magnetic environment of a coil or wire will cause a voltage (emf) to be induced in the coil. Although there are many ways to change this environment, this voltage is generated regardless of what causes this change. The magnetic field strength can be changed by moving a magnet toward or away from the coil, by moving the coil into or out of the magnetic field, or by rotating the coil relative to the magnet. Faraday's law is a fundamental relationship derived from Maxwell's equations and serves as a succinct summary of the ways a voltage may be generated by a changing magnetic environment. The induced emf in a coil can be expressed as

$$Emf = -N\frac{\Delta(BA)}{\Delta t} = -N\frac{\Delta\Phi}{\Delta t} \tag{20}$$

where N is the number of turns, Φ or BA is the magnetic flux, B is the external magnetic field and A is the area of the coil. The induced emf involves the interaction of charge with magnetic field [8].

b. Induction motor under V/f Control

With regard to rated speed, adherence to the V/f principle means increasing the stator voltage above the rated value, which is not permitted. With frequencies above rated speed, the applied voltage is maintained constant at the rated level, which is known as field weakening. Here, the intensity of the magnetic field in the induction motor decreases with a frequency increase (unaccompanied by a proportional voltage increase). The maximum permitted frequency is that which causes the motor to rotate with the maximum permitted speed. At low frequencies, voltage must be boosted to compensate for the effects of the stator resistance [7].

Using the parameters from Figure 4, we can express the electromagnetic torque as

$$T_e = \frac{3\left(\frac{P}{2}\right)\left(\frac{\omega_e}{\omega_b}\right)\left(\frac{X_M^2}{\omega_b}\right)\left(\frac{r_r^{'}}{s}\right)\left|\tilde{I}_{as}\right|^2}{\left(\frac{r_r^{'}}{s}\right)^2 + \left(\frac{\omega_e}{\omega_b}\right)^2 X_{rr}^{'2}} \tag{21}$$

where ω_b is the rated frequency, ω_e is the electrical frequency, X_M is the mutual reactance, s is the slip ($s = (\omega_e - \omega_b)/\omega_e$), $r_r^{'}$ is the rotor resistance scaled by the turns ratio, and $\tilde{I}_{as}$ is the instantaneous phase A current on the stator side. The reactance $X_{rr}^{'}$ is the sum of the leakage reactance on the rotor side (scaled by the turns ratio) $X_{lr}^{'}$ and the mutual reactance [2]. Torque curves (for various values of frequency and voltage) and applied voltage as a function of frequency are displayed in Figure 6.

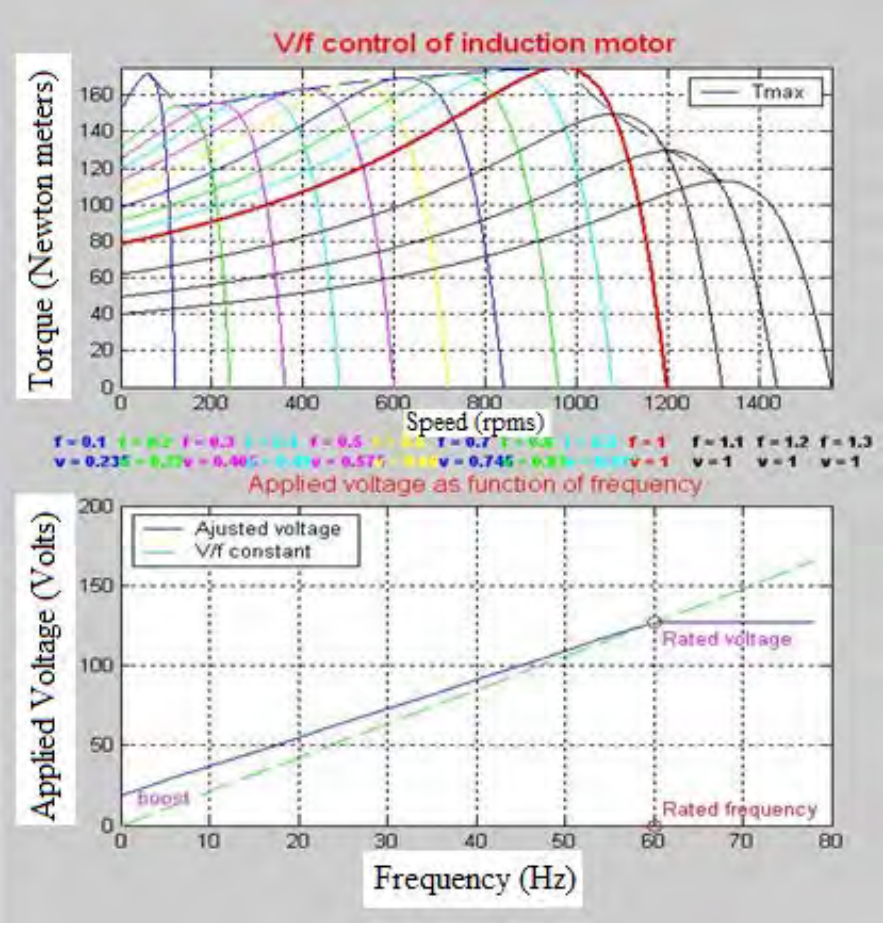

Figure 6. V/f control of induction motor, after [7].

c. Open loop V/f Control

We assume that the three-phase voltages at the stator terminals v_{an}, v_{bn}, and v_{cn} are given by

$$v_{an} = V_m \cos\left(2\pi f \cdot t\right), \tag{22}$$

$$v_{bn} = V_m \cos\left(2\pi f \cdot t - \frac{2\pi}{3}\right), \tag{23}$$

and

$$v_{cn} = V_m \cos\left(2\pi f \cdot t - \frac{4\pi}{3}\right), \tag{24}$$

respectively, where the amplitude V_m and the frequency f are variables. The V/f control algorithm implies that there is a relationship between the amplitudes of the voltage and the frequency. This relationship produces a constant ratio (*K*). We can see a top-level view of an open loop V/f controller in Figure 7 [5].

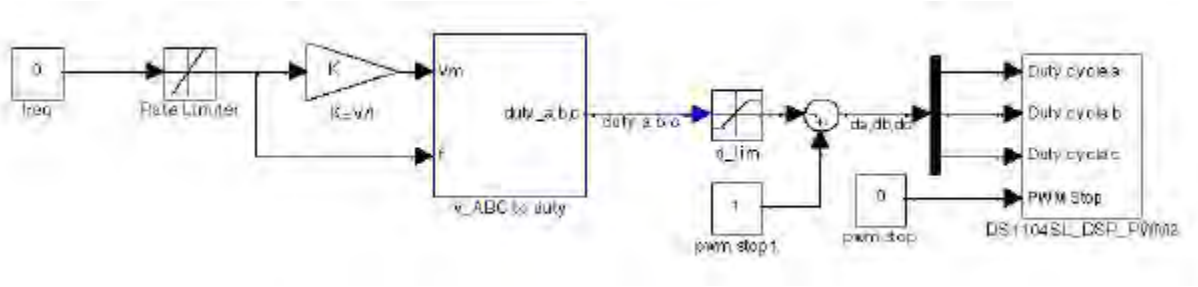

Figure 7. Open loop V/f control, from [5].

d. Closed loop V/f Control

An improvement of open loop V/f control is closed-loop speed control by slip regulation as shown in Figure 8.

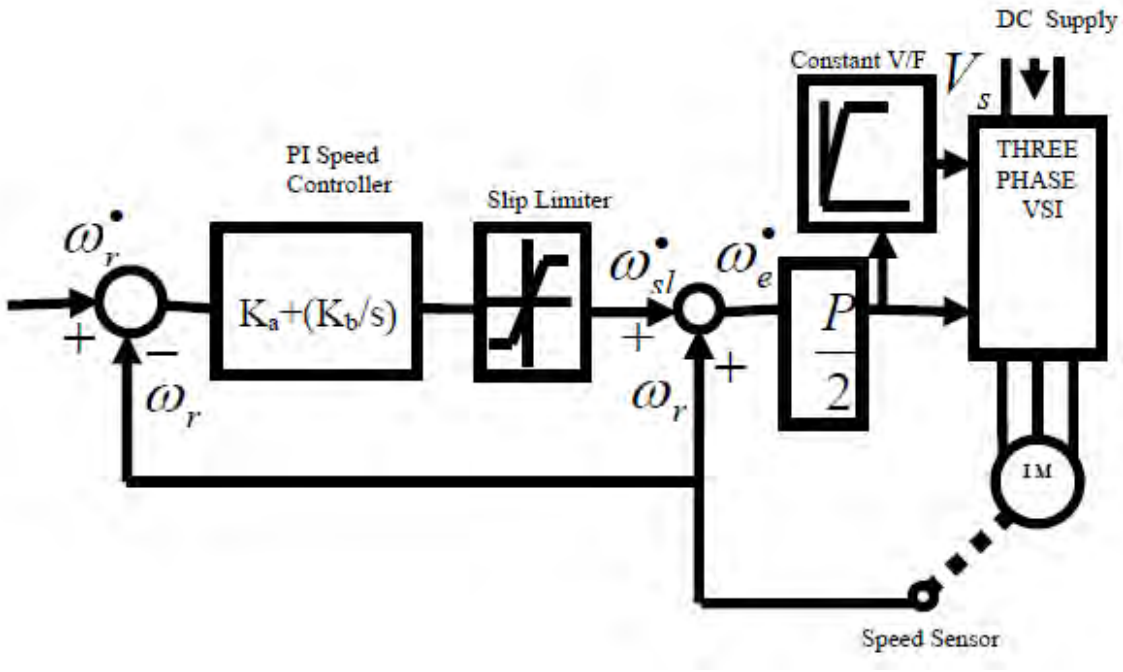

Figure 8. Closed-loop speed control utilizing V/f and slip regulation, from [9].

The variables for Figure 8 are defined in Table 5.

Table 5. Variable definitions for Figure 8.

Variable	Variable Name
ω_r^*	Rated speed command
ω_r	Speed feedback signal
ω_{sl}^*	Slip speed command
ω_e^*	Slip frequency command
IM	Induction Machine
K_a	Constant
K_b	Constant
s	slip
V_s	Stator voltage

A proportional-integral (PI) controller can be employed to improve speed accuracy by regulating slip speed of the motor to keep the motor speed at its set value. The major components consist of a DC source, a three-phase inverter and an induction motor with load. The speed loop error generates the slip command ω_{sl}^* through the PI

controller and limiter. The slip is added to the feedback speed signal to generate the frequency command as shown. The slip frequency command ω_e^* also generates the voltage command through a V/f function generator, which incorporates the low frequency stator drop compensation.

A step increase in the slip frequency command produces a positive speed error, and the slip command is set to its maximum value. The drive accelerates at the permissible inverter current, producing the maximum available torque until the speed error is reduced to a small value. Finally, the drive settles to a slip speed for which the motor torque balances the load torque. A step decrease in the slip frequency command produces a negative speed error. The slip speed is set to the maximum negative value, and the drive accelerates under regenerative braking. It continues to do so until the speed error is reduced to a small value meanwhile producing the maximum available breaking torque. The operation then shifts to motoring, and the drive settles at the slip speed for which the motor torque equals the load torque [9].

B. FIELD-ORIENTED CONTROL

In the 1990s, the field of controlled electrical drives experienced rapid expansion due to the advances of semiconductors in power electronics culminating in better microelectronic microprocessors and digital signal processors. These technological advancements enabled development of highly effective AC drive control with lower power dissipation and more accurate control structures. Drive controls became more accurate because not only were the DC current and voltage controlled but the three-phase currents and voltages were managed by vector controls. The most common form of vector control is FOC. Three major points establish this scheme:

- Machine current and voltage space vectors
- Transformation of a three-phase speed and time-dependent system into a two coordinate time-invariant system
- Effective pulsewidth-modulation (PWM).

As a result of these factors, FOC retains all advantages of DC machine control and frees itself from the mechanical commutation drawbacks. Furthermore, FOC leads to

high dynamic performance in terms of response times and power conversion by delivering accurate steady-state and transient control. A basic FOC scheme is shown in Figure 9 [10].

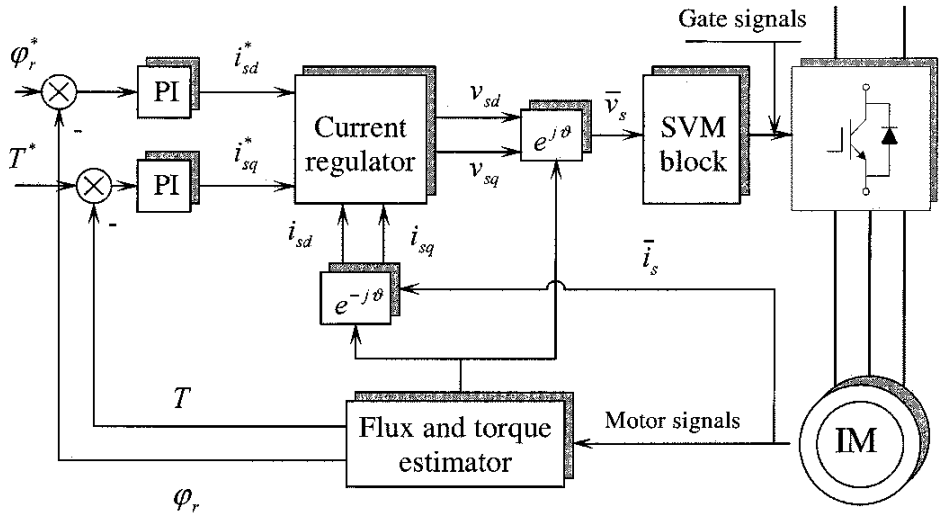

Figure 9. Basic FOC scheme, from [10].

The variables for Figure 9 are defined in Table 6.

Table 6. Variable definitions for Figure 9.

Variable	Variable Name
ω_r^*	Reference rotor flux
ω_r	Estimated rotor flux
T^*	Reference torque
T	Estimated torque
i_{sd}^*	Reference d-axis stator current
i_{sd}	Estimated d-axis stator current
i_{sq}^*	Reference q-axis stator current
i_{sq}	Estimated q-axis stator current
v_{sd}	D-axis stator voltage
v_{sq}	Q-axis stator voltage
$\bar{i}_s$	Instantaneous stator current
$\bar{v}_s$	Instantaneous stator voltage
IM	Induction Machine
SVM	Space Vector Modulation

In the majority of classic AC drives, the generation of the three sine waves is based on motor electromechanical characteristics and on an equivalent model for the motor in its steady-state. The control resembles that of three separate phase system controls rather than one control of a three-phase system, presenting some major drawbacks including:

- The machine models and characteristics are valid only in steady-state. This leads to allowing high peak voltage and current transients, which damages dynamic performance and power conversion efficiency.
- Considerable difficulty in controlling the variables with sinusoidal references; PI controllers are incapable of performing sinusoidal regulation without damaging the sinusoidal reference and hysteresis controllers introduce high bandwidth noise into the system.
- No three phase-system imbalance management and no consideration of the phase interactions.
- Lastly, the control structure must be dedicated according to motor type (synchronous or induction) [10].

1. FOC Concept

FOC consists of controlling the stator currents represented by a vector. It is based on projections which transform a three-phase speed and time-dependent system into a two coordinate (d and q coordinates) time-invariant system. These projections led to a structure similar to that of DC machine control. FOC machines require two constants as input references: the torque component (aligned with the q-axis) and the flux component (aligned with the d-axis). As FOC is based on projections, the control structure handles instantaneous electrical quantities gracefully, enabling accurate control in all operating conditions. Thus, FOC solves classic scheme problems by reaching a constant reference for both the torque and flux components of the stator current. In addition, maintaining a constant amplitude of the rotor flux ψ_R results in a linear relationship between torque and torque component i_{Sq}. We can then control the torque by controlling the torque component of the stator current vector, as can be seen from

$$m \propto \psi_R \cdot i_{Sq} \tag{25}$$

where m is the torque and is proportional to the rotor flux multiplied by the torque component [11].

2. Choosing a Reference Frame

In general, there are three possible selections for the flux-linkage vector: stator flux linkage vector, rotor flux linkage vector, or magnetizing flux linkage vector. In these three cases the instantaneous electromagnetic torque can be expressed as

$$t_e = c_{1s} \left|\bar{\psi}_s\right| i_{sy}^s \text{ (stator flux oriented control)} \tag{26}$$

$$t_e = c_{1r} \left|\bar{\psi}_r\right| i_{sy}^r \text{ (rotor flux oriented control)} \tag{27}$$

$$t_e = c_{1m} \left|\bar{\psi}_m\right| i_{sy}^m \text{ (magnetizing flux oriented control)} \tag{28}$$

where for linear magnetic conditions c_{1s}, c_{1r}, and c_{1m} are constants and $\left|\bar{\psi}_s\right|$, $\left|\bar{\psi}_r\right|$, and $\left|\bar{\psi}_m\right|$ are the modulus of the stator, rotor, and magnetizing flux linkage space vectors, respectively. Moreover, the torque-producing stator currents in the stator, rotor, and magnetizing flux oriented reference frame are denoted by i_{sy}^s, i_{sy}^r, and i_{sy}^m, respectively. The superscript denotes the reference frame used. These torque-producing stator currents take the role of the armature current in a DC drive.

Equations (26)–(28) can be derived from a single equation, according to which electromagnetic torque for an induction machine can be expressed as the cross-vector product of the stator flux linkage and current space vectors regardless of the reference frame used. It follows from Equation (26) that when the stator flux linkage modulus is constant and the torque-producing stator current changes rapidly, quick torque response is obtained. These same considerations hold for Equations (27) and (28). This physical picture is the basis for vector-controlled drives.

The expression for the electromagnetic torque contains the transformed stator currents, and in a vector-controlled drive the stator currents must clearly be transformed into the required reference frame. A common feature of all vector-controlled drives is that the modulus and phase angle of the AC excitation are controlled. This is the essence of vector control. The reference frame is aligned with the selected flux linkage space vector so the transformation contains the angle of the flux linkage space vector. This implementation depends upon the flux angle and the flux linkage modulus, and a major task for implementation requires accurate flux linkage estimation [4].

3. Defining the Space Vector

The three-phase voltages, currents, and fluxes of AC motors can be analyzed in terms of complex space vectors. With regard to the currents, the space vector are defined as follows when i_a, i_b, and i_c are defined as the instantaneous currents in the stator phases. The complex stator current $\bar{i}_s$ is defined by

$$\bar{i}_s = i_a + \propto i_b + \propto^2 i_c \tag{29}$$

where $\propto = e^{j\frac{2}{3}\pi}$ and $\propto^2 = e^{j\frac{4}{3}\pi}$ represent the spatial operators. Shown in Figure 10 is the stator current complex space vector where (a,b,c) are the three-phase system axes.

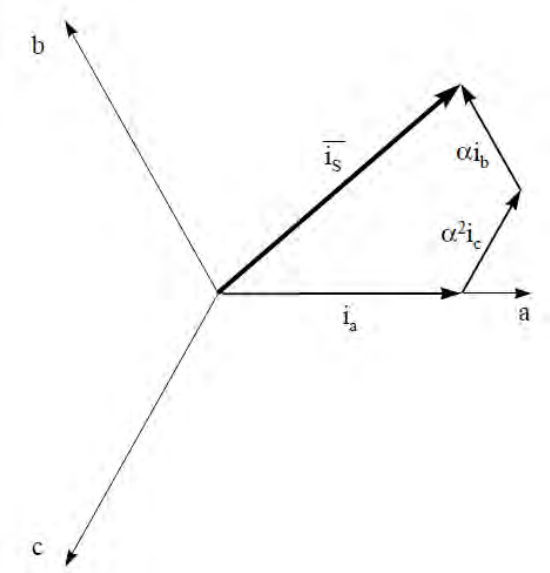

Figure 10. FOC of 3-phase AC motors, from [11].

This current space vector depicts the three-phase sinusoidal system that needs to be transformed into a two-coordinate time-invariant system. This transformation is a two-step process:

- The Clarke transformation, which outputs a two-coordinate time-invariant system $(a,b,c) \Rightarrow (\propto, \beta)$ and
- The Park transformation, which outputs a two-coordinate time-invariant system $(\propto, \beta) \Rightarrow (d,q)$.

a. Clarke Transformation

The current space vector can be reported in another reference frame with two orthogonal axis called $(\propto, \beta)$. Assuming that the axis a and the axis $\propto$ are in the same direction, we have the vector diagram illustrated in Figure 11.

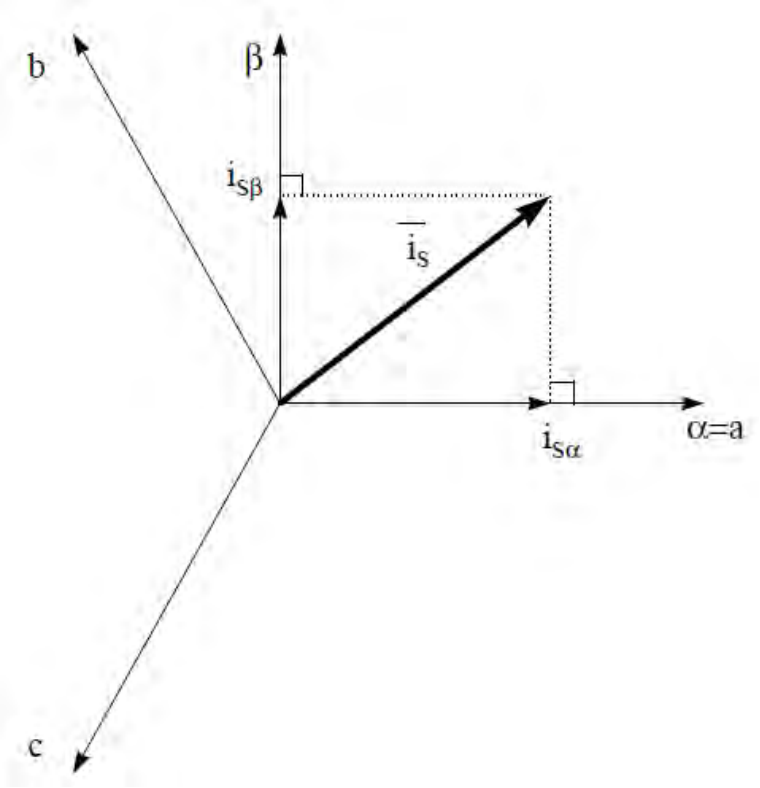

Figure 11. Clarke transformation, from [11].

The Clarke transformation is a projection that modifies the three-phase system into the $(\propto, \beta)$ two-dimension orthogonal system and is represented by

$$i_{S\propto} = i_a \tag{30}$$

and

$$i_{S\beta} = \frac{1}{\sqrt{3}} i_a + \frac{2}{\sqrt{3}} i_b; \tag{31}$$

and, thus, we obtain a two-coordinate system $(i_{S\propto}, i_{S\beta})$ that still depends on time and speed.

b. Park Transformation

The most important transformation in the FOC is the Park transformation. This projection modifies a two-phase orthogonal system $(\propto, \beta)$ into the (d, q) rotating reference frame. If we consider the *d*-axis aligned with the rotor flux for the current vector, the relationship from the two reference frames is shown in Figure 12.

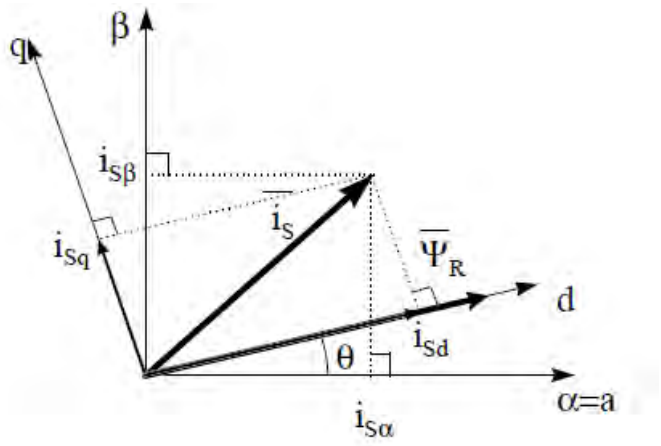

Figure 12. Park transformation, from [11].

Knowledge of the rotor flux position θ allows for the flux and torque components to be determined by

$$i_{Sd} = i_{S\propto} \cos\theta + i_{S\beta} \sin\theta \tag{32}$$

and

$$i_{Sq} = -i_{S\propto} \sin\theta + i_{S\beta} \cos\theta \tag{33}$$

where i_{Sd} and i_{Sq} are the flux and torque components, respectively. These components depend on the current vector $(\propto, \beta)$ components and on the rotor flux position. If the rotor flux position is known, then the (d, q) component is a constant. We obtain a two-coordinate system (i_{Sd}, i_{Sq}) with the following characteristics: a two coordinate time-invariant system, and with i_{Sd} and i_{Sq} direct control becomes possible.

c. Inverse Park Transformation

The inverse Park transformation introduces a voltage transformation that modifies the voltages in the (d,q) rotating reference frame in a two phase orthogonal system. This transformation is represented by

$$v_{S\propto ref} = v_{Sdref}\cos\theta - v_{Sqref}\sin\theta \tag{34}$$

and

$$v_{S\beta ref} = v_{Sdref}\sin\theta + v_{Sqref}\cos\theta \tag{35}$$

where the outputs of this block are the components of the reference vector that we call $\bar{V}_r$, the voltage space vector to be applied to the motor phases.

d. Putting It All Together

The basic FOC torque control scheme is summarized in Figure 13.

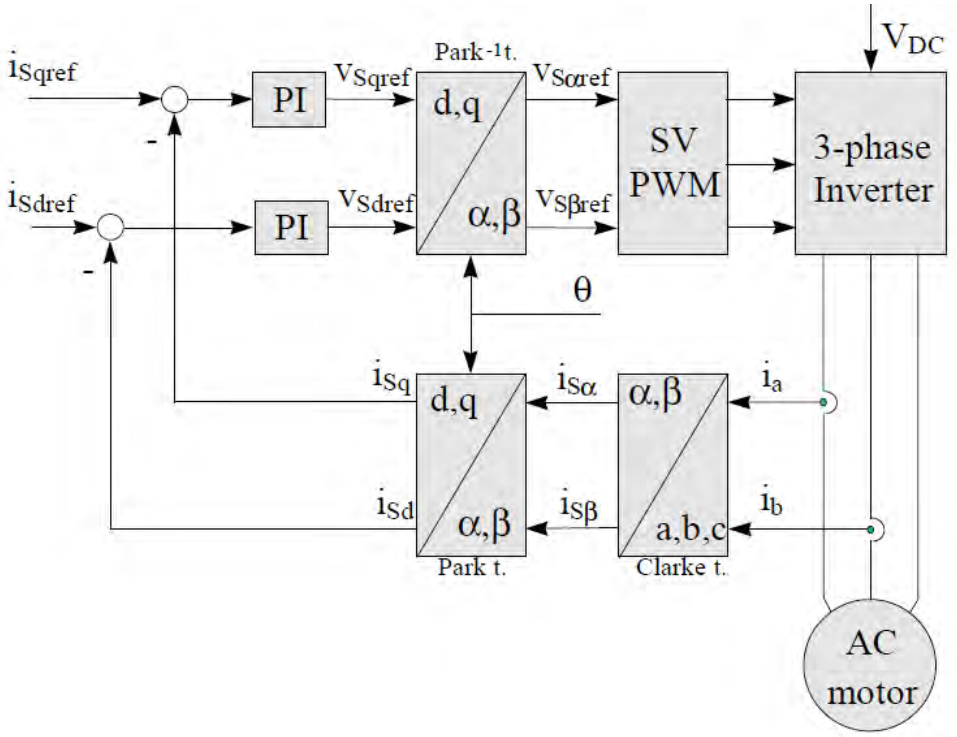

Figure 13. FOC of three-phase AC motors. [11].

The variables for Figure 13 are defined in Table 7.

Table 7. Variable definitions for Figure 13.

Variable	Variable Name
i_{Sqref}	Flux reference stator current
i_{Sdref}	Torque reference stator current
i_{Sq}	Park transformed current
i_{Sd}	Park transformed current
$i_{S\alpha}$	Clarke transformed current
$i_{S\beta}$	Clarke transformed current
i_a	Phase A current
i_b	Phase B current
V_{Sqref}	Flux reference stator voltage
V_{Sdref}	Torque reference stator voltage
$V_{S\alpha ref}$	Inverse Park transformed voltage
$V_{S\beta ref}$	Inverse Park transformed voltage
V_{DC}	DC Voltage

Two motor phase currents are measured and feed the Clarke transformation module. The outputs of this projection are designated $i_{S\propto}$ and $i_{S\beta}$. These two components of the current are the inputs of the Park transformation that projects the current in the (d,q) rotating reference frame. The i_{Sd} and i_{Sq} components are compared to the references i_{Sdref} (the flux reference) and i_{Sqref} (the torque reference), respectively.

This control structure can be used to control either synchronous or induction machines by simply changing the flux reference and obtaining the rotor flux position. In synchronous permanent magnet motors, the rotor flux is fixed (determined by the magnets) and there is no need to create one. Hence, when controlling a permanent magnet synchronous machine, i_{Sdref} should be set to zero. However, an induction motor needs a rotor flux to operate, and the flux reference must not be zero. This allows the portability from asynchronous to synchronous drives and solves a major drawback of classic control structures. The torque command i_{Sqref} is the output of the speed regulator when we use a speed FOC. The outputs of the current regulators are v_{Sdref} and v_{Sqref}, which are the inputs of the inverse Park transformation. The outputs of this projection are $v_{S\alpha ref}$ and $v_{S\beta ref}$, which are the components of the stator vector voltage in the (a,b)

stationary orthogonal reference frame. These are the inputs of the Space Vector PWM, and the outputs of this block drive the inverter. Remember both the Park and inverse Park transformations need the rotor flux position and obtaining this rotor flux position depends on the AC machine type (synchronous or asynchronous machine). Rotor flux position considerations are made in a following subsection [11].

e. The Core of FOC

Knowledge of the rotor flux position is the core of FOC. Any error in this variable causes the rotor flux to be misaligned with the d-axis. In turn, i_{Sd} and i_{Sq} are incorrect flux and torque components of the stator current. The correct position of the rotor flux, the stator current and stator voltage space vector that rotates with the (d,q) reference at synchronous speed are shown in Figure 14.

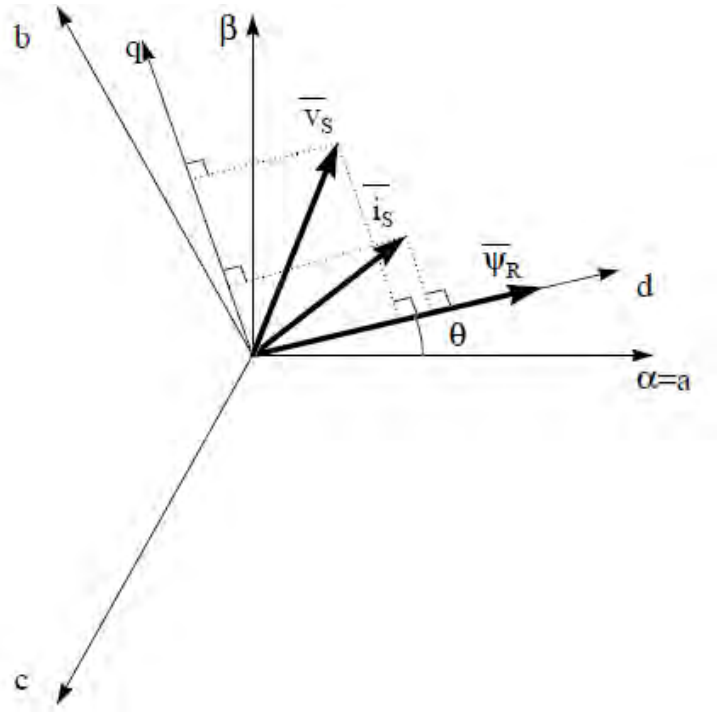

Figure 14. Current, voltage and rotor flux space vectors in the *d,q* rotating reference frame and their relationship with *a,b,c* and *a,b* stationary reference frames, from [11].

f. Space Vector PWM

The structure of a typical three-phase power inverter is shown in Figure 15, where V_A, V_B, and V_C are the voltages applied to the wye-connected motor windings, and where V_{DC} is the continuous inverter input voltage.

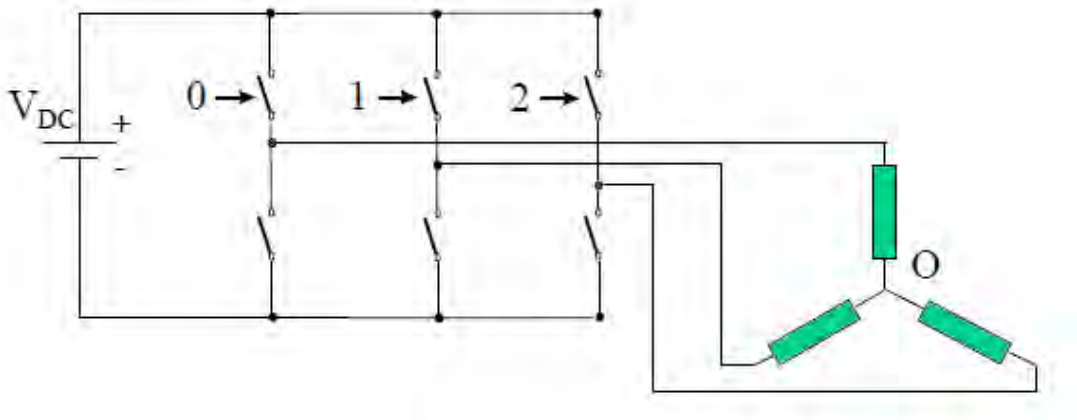

Figure 15. Basic scheme of three-phase inverter and AC motor, from [11].

These six switches must respect the following conditions:

- Three of them must always be on and three must always be off.
- The upper and lower switches of the same leg are driven with two complementary pulsed signals so that no vertical conduction is possible as long as there is no overlap in the power switch transitions.

SVPWM supplies the AC machine with the desired phase voltages. The SVPWM method of generating the pulsed signals fits the above requirements and minimizes the harmonic content. This harmonic content determines the copper losses of the machine, a major portion of the machine losses. If these two constraints are taken into account, there are eight possible combinations for the switch commands. These eight switch combinations determine eight phase voltage configurations. These combinations are depicted in Figure 16.

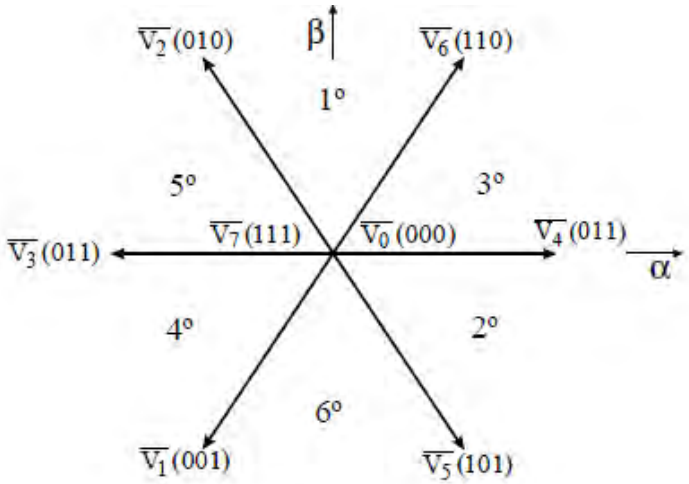

Figure 16. SVPWM, vectors and sectors, from [11].

These vectors divide the plane into six sectors. Depending on the sector that the voltage reference is in, we choose two adjacent vectors. The binary representation of two adjacent basic vectors differ in only one bit, limiting inverter switching frequency when the switching pattern moves from one vector to the next. The two vectors are time weighted in a sample period T to produce the desired output voltage.

g. An Example of SVPWM

For example, if the reference vector $\bar{V}_{ref}$ is in the 3° sector of Figure 15, we have the situation shown in Figure 17.

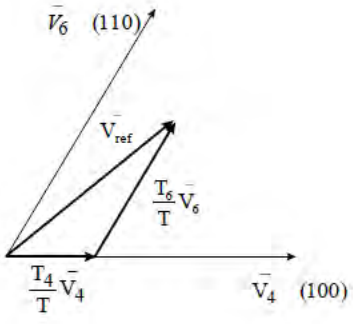

Figure 17. Reference vector as a combination of adjacent vectors, from [11].

The times T_4 and T_6 are the times during which the vectors $\bar{V}_4$ and $\bar{V}_6$ are applied, and T_0 is the time during which the zero vectors are applied. When the reference voltage and the sample periods are known, the following equations

$$T = T_4 + T_6 + T_0 \tag{36}$$

$$\bar{V}_{ref} = \frac{T_4}{T}\bar{V}_4 + \frac{T_6}{T}\bar{V}_6 \tag{37}$$

make it possible to determine the unknowns T_4, T_6, and T_0. Under these constraints the locus of the reference vector is the inside of a hexagon whose vertices are formed by the tips of the eight vectors. The generated space vector PWM waveforms are symmetrical with respect to the middle of each PWM period. The waveforms in the example presented above are pictured in Figure 18 [11].

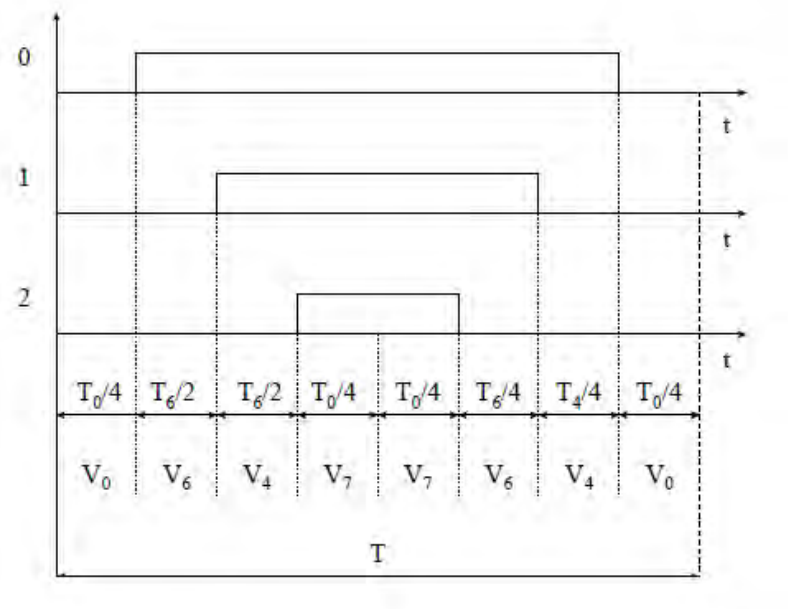

Figure 18. Pattern of SVPWM in the 3° sector, from [11].

Figure 19 illustrates the pattern of SVPWM for each sector [11].

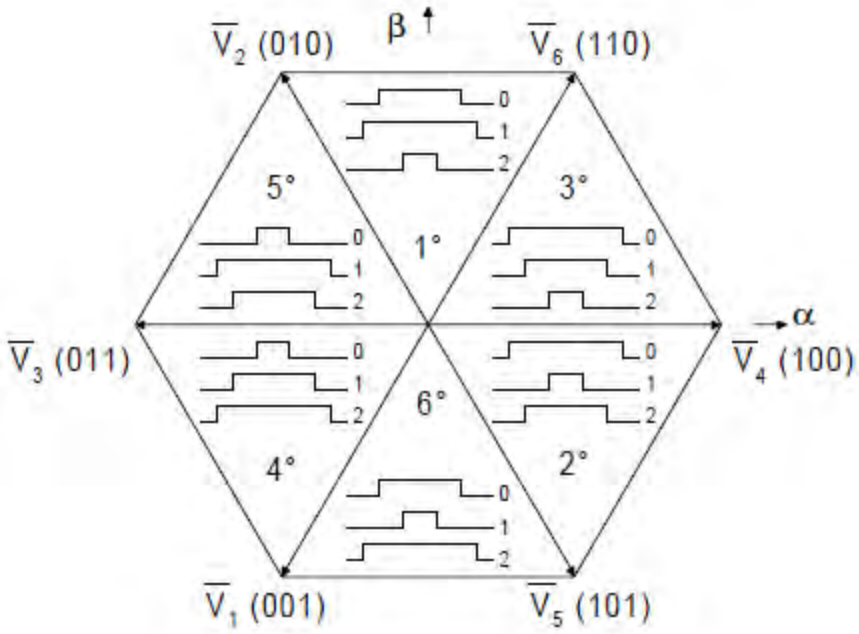

Figure 19. Hexagon of SVPWM pattern, from [11].

C. DIRECT TORQUE CONTROL

Direct torque control (DTC) combines FOC theory, direct self-control theory, and advanced DSP and application specific integrated circuit (ASIC) technology to achieve a sensorless variable-frequency drive. On the basis of the errors between the reference and the estimated values of torque and flux, it is possible to directly control the inverter states to reduce the torque and flux errors within prefixed band limits. Unlike FOC, DTC does not require any current regulator, coordinate transformation or a PWM modulator (as a consequence timers are not required). In spite of its simplicity, DTC allows for good torque control in both steady-state and transient operating conditions. On the other hand, DTC presents some significant disadvantages as follows:

- Difficulty controlling the torque and flux at very low speeds.
- Produces high current and torque ripple.
- Possesses variable switching behavior.
- Experiences high noise levels at low speed.
- Lacks of direct current control.

Research has been carried out to attempt to solve these issues faced by the DTC scheme. In particular, the following solutions have been developed:

- Use of improved switching tables.
- Use of comparators with and without hysteresis.
- Implementation of DTC schemes for constant switching frequency operation with PWM or SVM techniques.
- Introduction of fuzzy logic or neuro-fuzzy logic techniques.
- Use of sophisticated flux estimators to improve low speed behavior.

Although all of these approaches improve the performance of DTC, they also lead to more complex schemes detracting from DTC simplicity. The DTC technique is intrinsically sensorless, so only the control schemes which meet this requirement (i.e., no current or PI regulators, no coordinate transformations, and no PWM signals generator) are considered true DTC schemes [10].

1. DTC of a VSI-Fed Induction Motor

It is possible to directly control the stator flux linkage (or rotor or magnetizing flux linkages) and the electromagnetic torque by the selection of optimum inverter switching modes. The selection is made to restrict the flux and torque errors within respective flux and torque hysteresis bands, to obtain fast torque response, low inverter switching frequency, and low harmonic losses. DTC allows very fast torque responses and flexible control of an induction machine [4].

2. General, Mathematical, and Physical Fundamentals of Producing Fast Torque Response

a. Stator Flux Linkage, Rotor Flux Linkage, and Stator Current Space Vectors

In a balanced three-phase induction machine, torque is proportional to the cross-product of stator flux linkage and stator current space vectors, as given by

$$t_e = \frac{3}{2} P \bar{\varphi}_s \times \bar{i}_s \tag{38}$$

where $\bar{\varphi}_s$ is the stator flux linkage space vector and $\bar{i}_s$ is the stator current space vector. In Equation (38), both space vectors are expressed in the stationary reference frames. By considering that $\bar{\varphi}_s = |\bar{\varphi}_s| \exp(\mathrm{j}\,\rho_s)$, where ρ_s is the angle of the stator flux linkage space vector with respect to the direct axis of the stator reference frame and $\bar{i}_s = |\bar{i}_s| \exp(\mathrm{j}\,\alpha_s)$, we can put Equation (38) into the form

$$t_e = \frac{3}{2} P |\bar{\varphi}_s| |\bar{i}_s| \sin(\alpha_s - \rho_s) = \frac{3}{2} P |\bar{\varphi}_s| |\bar{i}_s| \sin\alpha \tag{39}$$

where $\alpha = \alpha_s - \rho_s$ is the angle between the stator flux linkage and stator current space vector. The relationship between the stator flux linkage and stator current space vectors is shown in Figure 20.

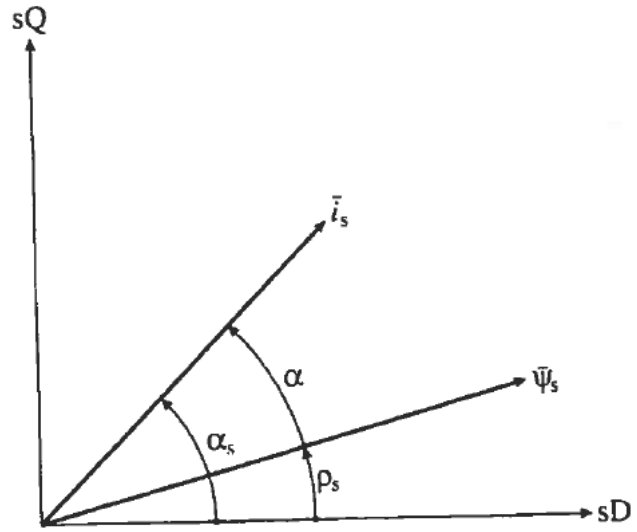

Figure 20. Stator flux linkage and stator current space vectors, from [4].

If the stator-flux linkage space vector is kept constant and ρ_s is changed quickly, the electromechanical torque t_e can also be rapidly changed ($\Delta t_e / dt \approx \Delta \rho_s / dt$). By forcing the largest $d\rho_s / dt$, the fastest torque response time is obtained.

If stator voltages are imposed on the motor which keep the stator flux constant but which quickly rotate the stator flux linkage space vector into the required

position demanded by the torque, then fast torque control is achieved. The parameter t_e can be quickly changed by controlling the stator flux linkage space vector using the appropriate stator voltages (generated by the VSI-fed induction machine). By using the appropriate stator voltages, we achieve direct stator flux and electromagnetic torque control.

An extremely clear picture of this process is painted if we consider another form of Equation (39), leading to the same results mentioned above. By considering that $\bar{\varphi}_s = L_s \bar{i}_s + L_m \bar{i}_r'$ and $\bar{\varphi}_r' = L_r \bar{i}_r' + L_m \bar{i}_s$ where the primed rotor quantities are expressed in the stationary reference frame, we see that $\bar{i}_s = \bar{\varphi}_s / \bar{L}_s - [L_m / (L_r L_s')] \bar{\varphi}_r'$ and Equation (39) takes on the form

$$t_e = \frac{3}{2} P \frac{L_m}{L_s' L_r} \bar{\varphi}_r' \times \bar{\varphi}_s = \frac{3}{2} P \frac{L_m}{L_s' L_r} \left|\bar{\varphi}_r'\right| \left|\bar{\varphi}_s\right| \sin(\rho_s - \rho_r) = \frac{3}{2} P \frac{L_m}{L_s' L_r} \left|\bar{\varphi}_r'\right| \left|\bar{\varphi}_s\right| \sin\gamma \qquad (40)$$

where γ is the angle between the stator and rotor flux linkage space vectors and ρ_r is the angle of the rotor flux linkage space vector with respect to the real axis of the stationary reference frame as shown in Figure 21.

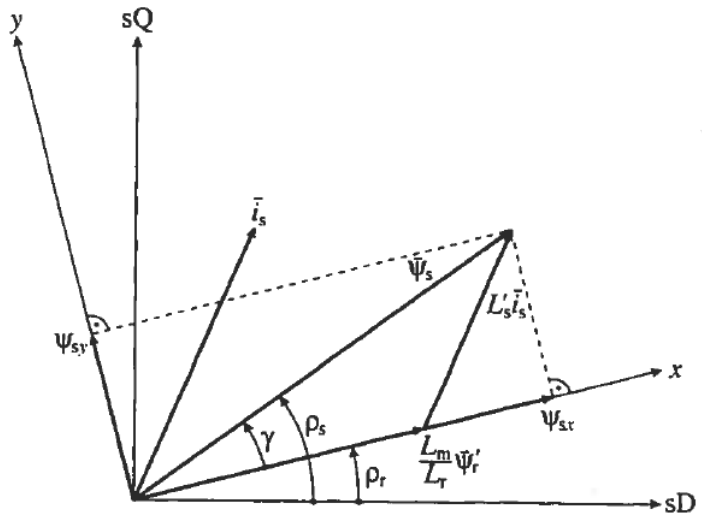

Figure 21. Stator flux linkage, rotor flux linkage, and stator current space vectors, from [4].

b. Achieving Rapid Torque Control

The rotor time constant is large; therefore, the rotor flux linkage changes slowly compared to the stator. It can be assumed to remain constant. This follows from the rotor voltage equation if the stator flux linkage is assumed to be constant. If both are assumed to be constant, the torque can be rapidly changed by changing γ in the required direction (determined by the torque command). This is the essence of DTC. By choosing the appropriate stator voltage space vector, the angle γ can be managed. Even if the stator flux linkage is not held constant, both γ and φ_s can be controlled. In FOC the stator currents are the control quantities, while in DTC the stator flux linkages are controlled. Equation (41) relates to that of a synchronous machine where the torque is controlled by the load angle between the stator and rotor flux linkages.

In summary, by rapidly changing the position or speed of the stator flux linkage space vector, rapid torque control can be achieved. Both the modulus and the angle of the stator flux linkage space vector can be changed by the stator voltages. Correct step-by-step selection of the stator voltage vector permits the stator flux to be changed in the required way. Decoupled control of the torque and stator flux is achieved by acting on the radial and tangential components of the stator flux linkage space vector. These two components are directly proportional to the components of the stator voltage space vector in the same directions; therefore, they can be controlled by the appropriate inverter switchings. The angle γ, or the relative position of the stator and rotor flux linkage space vectors, determines torque. By assuming a slow motion of the rotor, if a stator voltage is applied which causes a quick movement of the stator flux linkage away from that of the rotor flux linkage, the torque increases because γ increases. On the other hand, if a zero-voltage space vector is applied which nearly stops the rotation of the stator flux linkage, then torque decreases because the rotor flux linkage is still rotating and γ decreases. If a zero-voltage vector is applied long enough (where stator flux linkage almost does not move), the rotor flux linkage overtakes that of the stator and the sign of γ changes, and torque changes direction. For these reasons, the duration that the zero-voltage space vectors are applied have a direct effect on torque oscillations [4].

c. PWM VSI Inverter Switching States and Space Vectors

A six-pulse PWM VSI-fed inverter is shown in Figure 22.

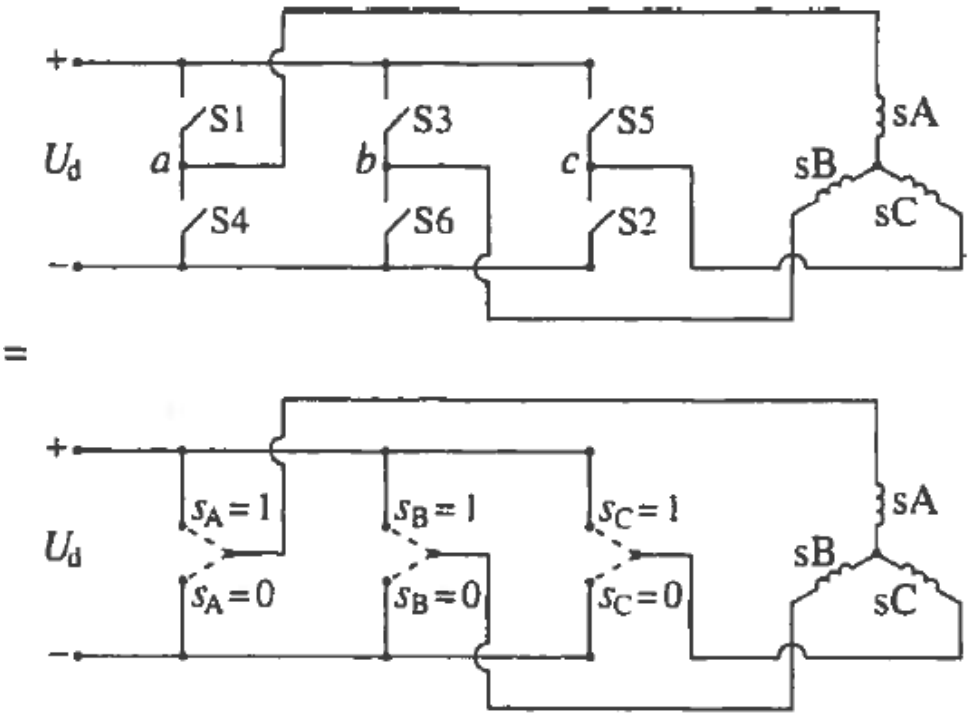

Figure 22. Schematic of PWM VSI inverter, from [4].

This inverter produces six non-zero active voltage-switching space vectors ($\bar{u}_1$, $\bar{u}_2$, … $\bar{u}_6$) and two zero space vectors ($\bar{u}_7$, $\bar{u}_8$). These eight switching states are shown in Figure 23, and their corresponding switching vectors are shown in Figure 24. The six active inverter-switching vectors can be expressed as

$$\bar{u}_s = \bar{u}_k = \frac{2}{3} U_d \exp[j(k-1)\frac{\pi}{3}] \tag{42}$$

where U_d is the DC link voltage and k=1,2,…6. For k=7 and 8, $\bar{u}_k = 0$ holds for the two zero-switching states where the stator windings are short circuited, and $\bar{u}_s = \bar{u}_k = 0$.

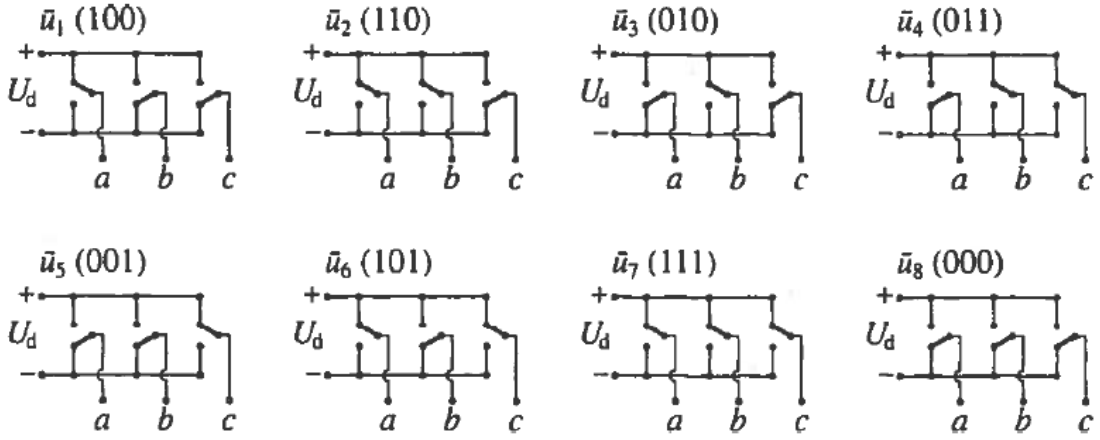

Figure 23. Eight switching states of the PWM VSI inverter, from [4].

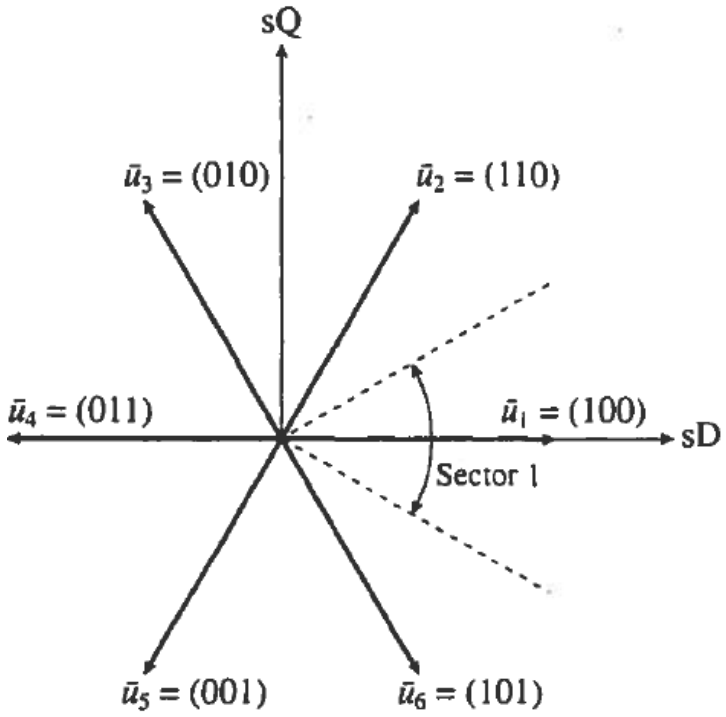

Figure 24. Eight corresponding switching space vectors, from [4].

d. Controlling Torque and Flux through Hysteresis

During every sampling period, we select switching vectors to keep the stator flux linkage errors within the required tolerance band and the torque error within the hysteresis band. The widths of these bands are $2\Delta t_e$ and $2\Delta\varphi_s$, respectively. The

upper limit is one Δ above the reference, and the lower limit is one Δ below. In terms of low order harmonics, the flux hysteresis band mainly affects the stator current distortion. The torque hysteresis band affects the switching frequency and, thus, the switching losses. This scheme requires the use of flux linkage and torque estimators. Stator flux linkage components can be obtained by integrating appropriately monitored terminal voltages. On the other hand, it is unnecessary to monitor stator voltages because they can be reconstructed by using the inverter switching modes and monitored DC link voltage.

The goal is to keep the modulus of the stator flux linkage space vector $|\bar{\varphi}_s|$ within the hysteresis band, denoted by the two circles whose width is $2\Delta\varphi_s$ as shown in Figure 25.

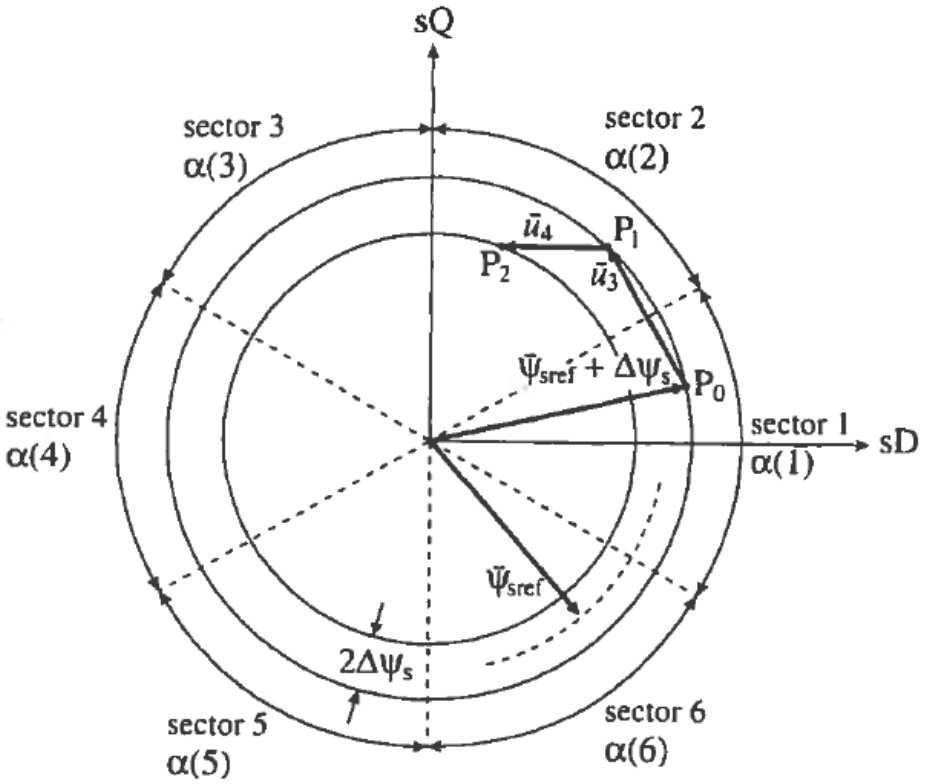

Figure 25. Control of the stator flux linkage space vector: stator flux linkage space vector locus and inverter switching errors, from [4].

Due to the six-step inverter, the locus of the flux linkage space vector is divided into the six sectors shown in Figure 24. If the stator flux linkage space vector is initially at point P_0 (sector one) and rotating counterclockwise, then the stator flux linkage is at the upper limit and must be reduced. As shown in Figure 25, applying $\overline{u}_3$ achieves this reduction. The stator flux linkage space vector moves from P_0 to P_1 (sector 2) and, once again, reaches the upper limit. Once again (when rotating counterclockwise), applying the switching vector $\overline{u}_4$ reduces the stator flux linkage appropriately. Now, $\overline{\varphi}_s$ moves from P_1 to P_2 (still in sector 2). If at point P_1, the rotation of the stator flux linkage space vector must be stopped, then a zero-switching vector, either $\overline{u}_7$ (111) or $\overline{u}_8$ (000), has to be applied. Since the last switching vector applied was $\overline{u}_3$ (010), then $\overline{u}_8$ is used because only the switching of the second switch from 1 to 0 is required. The switching vector that requires the minimum amount of switching should always be chosen [4].

As discussed above, stopping the rotation of the stator flux linkage space vector corresponds to the case when the electromagnetic torque does not have to be changed. When it has to be changed in either the clockwise or counterclockwise direction, then the stator flux linkage space vector has to be rotated in the appropriate direction. When the stator flux rotates counterclockwise and if an increase in torque is required (i.e., the stator flux linkage space vector is at point P_1 where the flux linkage is at its upper limit), then the increase in torque is achieved by applying switching vector $\overline{u}_4$. If a decrease in torque is required but the flux linkage is at the lower limit and must be increased, then this is achieved by applying switching vector $\overline{u}_1$ because this moves the stator flux linkage space vector in the clockwise direction (or in the direction of negative torque) and also increases the flux linkage.

e. Choosing the Optimum Voltage Switching Vector

The positions of the various stator flux linkage vector, if the stator flux linkage space vector is in one of the six sectors are shown in Figure 26.

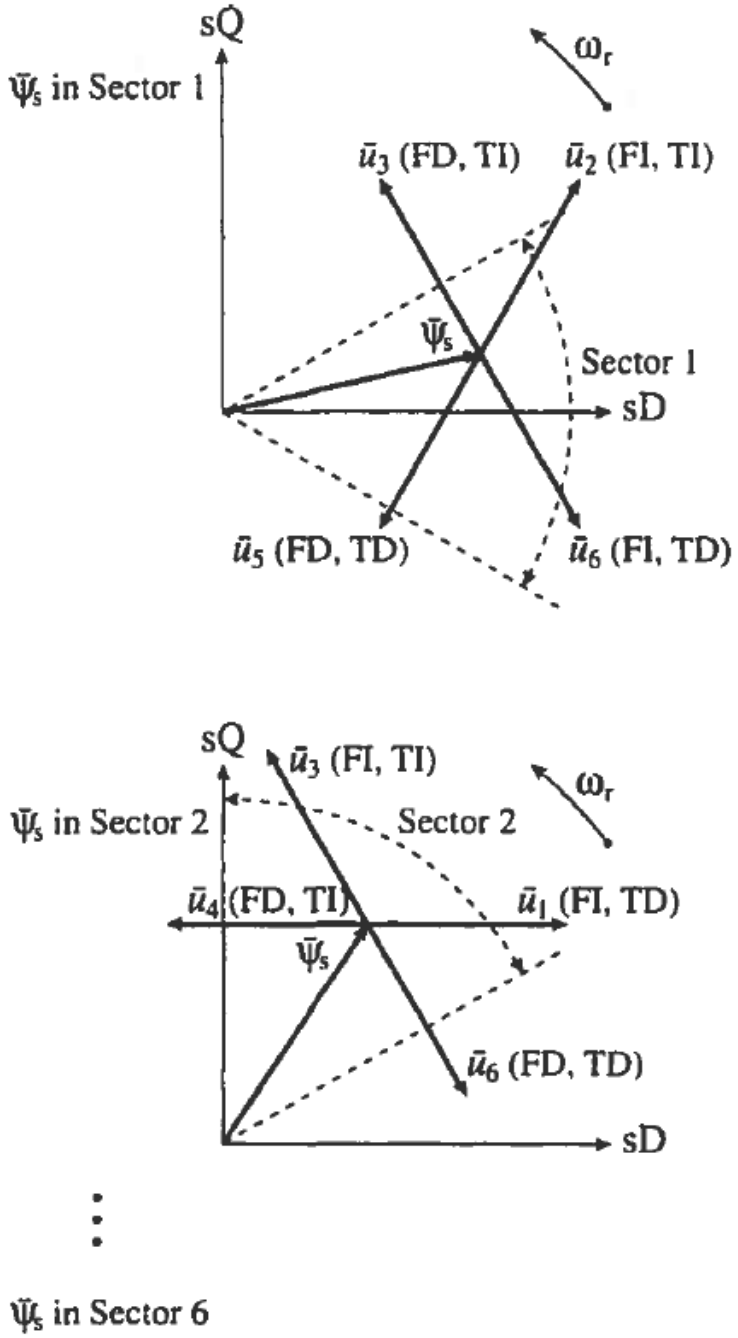

Figure 26. Position of various stator flux linkage space vectors and selection of the optimum switching vectors. FI: flux increase; FD: flux decrease; TI: torque increase; TD: torque decrease, from [4].

In general, if an increase of the torque is required, then the torque is controlled by applying voltage vectors that advance the flux linkage space vector in the direction of rotation. If a decrease is required, voltage vectors are applied which oppose

the direction of torque. If zero torque is required, the zero-switching vector is applied that minimizes inverter switching. The angle of the stator voltage space vector is indirectly controlled through the flux vector modulus and torque, and increasing torque results in an increased angle. The torque demand is reduced to a choice of increase, decrease, or zero while the stator flux linkage vector modulus can either be increased or decreased. These results are tabulated in the optimum switching vector selection table as shown in Table 8 [4].

Table 8. Optimum voltage switching vector look-up table, from [4].

$d\psi$	dt_e	$\alpha(1)$ sector 1	$\alpha(2)$ sector 2	$\alpha(3)$ sector 3	$\alpha(4)$ sector 4	$\alpha(5)$ sector 5	$\alpha(6)$ sector 6
	1	$\bar{u}_2$	$\bar{u}_3$	$\bar{u}_4$	$\bar{u}_5$	$\bar{u}_6$	$\bar{u}_1$
1	0	$\bar{u}_7$	$\bar{u}_8$	$\bar{u}_7$	$\bar{u}_8$	$\bar{u}_7$	$\bar{u}_8$
	−1	$\bar{u}_6$	$\bar{u}_1$	$\bar{u}_2$	$\bar{u}_3$	$\bar{u}_4$	$\bar{u}_5$
	1	$\bar{u}_3$	$\bar{u}_4$	$\bar{u}_5$	$\bar{u}_6$	$\bar{u}_1$	$\bar{u}_2$
0	0	$\bar{u}_8$	$\bar{u}_7$	$\bar{u}_8$	$\bar{u}_7$	$\bar{u}_8$	$\bar{u}_7$
	−1	$\bar{u}_5$	$\bar{u}_6$	$\bar{u}_1$	$\bar{u}_2$	$\bar{u}_3$	$\bar{u}_4$

Active switching vectors: $\bar{u}_1(100)$; $\bar{u}_2(110)$; $\bar{u}_3(010)$; $\bar{u}_4(011)$; $\bar{u}_5(001)$; $\bar{u}_6(101)$
Zero switching vectors: $\bar{u}_7(111)$; $\bar{u}_8(000)$.

The optimum selection of the switching vectors for all the possible stator flux linkage space vector positions and the desired control inputs (which are the reference values of the stator flux linkage modulus and the electromagnetic torque, respectively) are given in Table 8. The optimum switching look-up table requires knowledge of the position of the stator flux-linkage space vector because it must be known in which sector it resides. For this purpose, the angles $\alpha(1)$, $\alpha(2),\ldots,\alpha(6)$ shown in Figure 24 must be known. We can eliminate the need for trigonometric functions because it is not the accurate position of the stator flux linkage space vector that has to be known, but only the sector in which it resides. This information can be obtained by considering the signs of the various stator flux linkage components, allowing a simple implementation requiring only the use of comparators. The results of these signs are summarized in Table 9 [4].

Table 9. Selection of the stator flux linkage space vector sector, from [4].

Signs of flux linkages \ Sectors	α(1) sector 1	α(2) sector 2	α(3) sector 3	α(4) sector 4	α(5) sector 5	α(6) sector 6
Sign of ψ_{sD}	+	+	−	−	−	+
Sign of ψ_{sQ}	(nu; − +)	+	+	(nu; + −)	−	−
Sign of ψ_{sB} = sign of $[\sqrt{3}\psi_{sD} - \psi_{sQ}]$	−	+	+	+	−	−

nu = not useful

The relationship of the space vector $\overline{\varphi}_s$ to the various stator flux linkage components is shown in Figure 27.

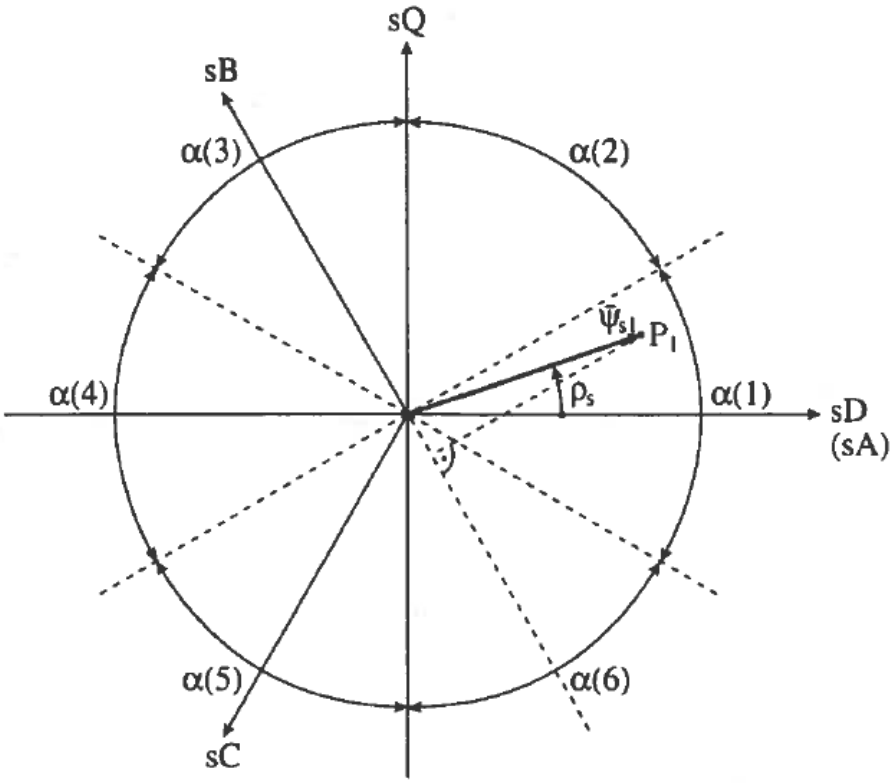

Figure 27. Relationship of the space vector $\overline{\varphi}_s$ to the stator flux linkage components φ_{sD}, φ_{sQ}, and φ_{sB}, from [4].

It should be noted that at very low speeds, such as when the machine is started, flux control can be lost during application of the switching vectors shown in

Table 5. Instead of having a circular path corresponding to constant reference flux, the space vector locus of the stator flux linkage space vector is a six-sided symmetrical locus, where during 1/6 of the cycle the modulus of the stator flux linkage space vector changes. These problems are related to the inappropriate use of switching voltage vectors in the low speed region.

f. A Basic DTC Scheme

As can be seen in Figure 28, the error between the estimated torque T and the reference torque T^* is the input of a three-level hysteresis comparator which is shown in Figure 29. The error between the estimated stator flux magnitude φ_S and the reference stator flux magnitude φ_{S^*} is the input of a two-level hysteresis comparator, which is shown in Figure 30 [10].

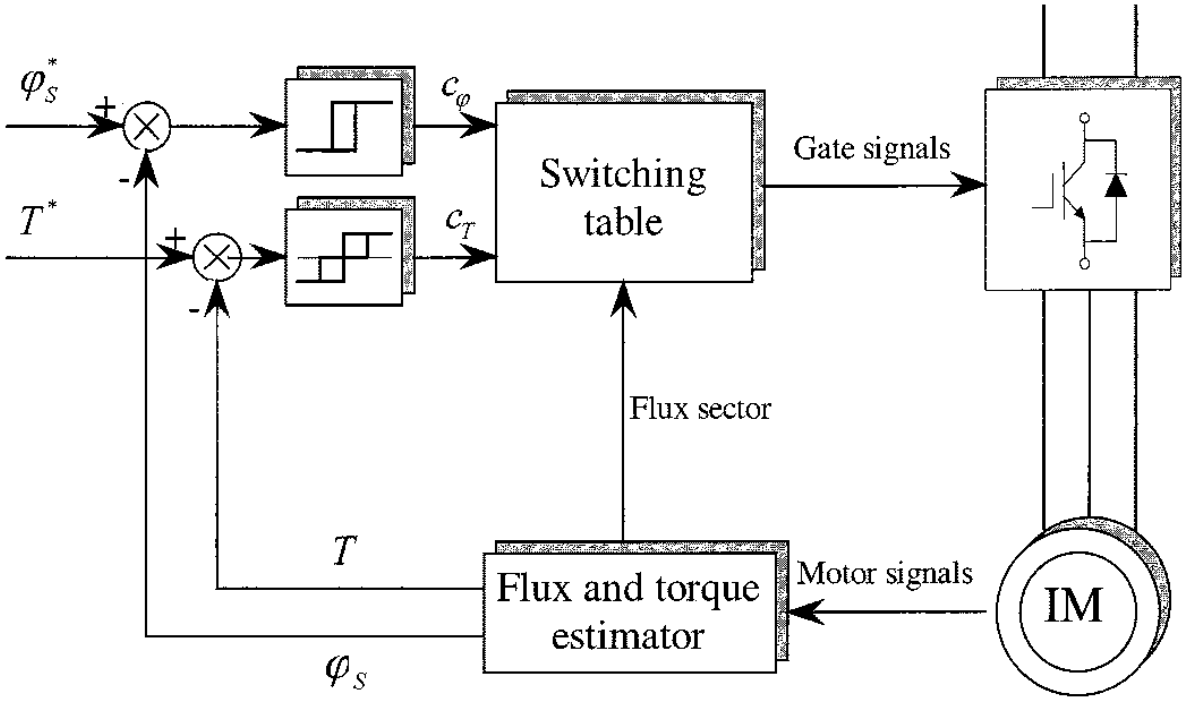

Figure 28. Basic DTC scheme, from [10].

The variables in Figure 28 are defined in Table 10.

Table 10. Variable definitions for Figure 28.

Variable	Variable Name
φ_s^*	Refernce stator flux magnitude
φ_s	Estimated stator flux magnitude
T^*	Reference torque
T	Estimated torque
c_φ	Output of flux hysteresis comparator
c_T	Output of torque hysteresis comparator
IM	Induction Machine

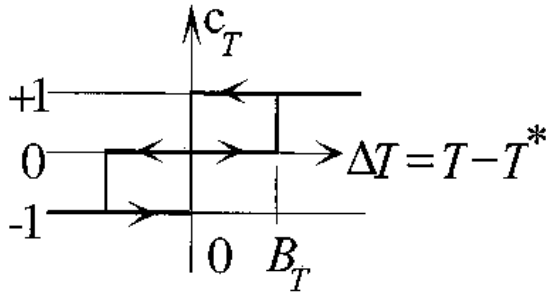

Figure 29. Torque hysteresis comparator, from [10].

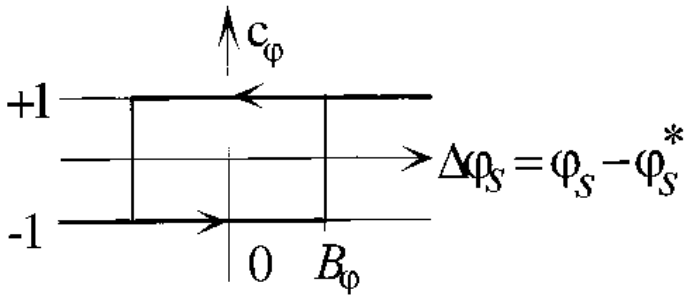

Figure 30. Flux hysteresis comparator, from [10].

The selection of the appropriate voltage vector is based on the switching table given in Table 11. Knowledge of the optimum switching look-up table requires knowledge of the stator flux linkage space vector since it must be known in which sector the vector is [4].

Table 11. Basic switching table for DTC, from [10].

Sector		1	2	3	4	5	6
$c_\varphi = -1$	$c_T = -1$	$\overline{V}_2$	$\overline{V}_3$	$\overline{V}_4$	$\overline{V}_5$	$\overline{V}_6$	$\overline{V}_1$
	$c_T = 0$	$\overline{V}_7$	$\overline{V}_0$	$\overline{V}_7$	$\overline{V}_0$	$\overline{V}_7$	$\overline{V}_0$
	$c_T = +1$	$\overline{V}_6$	$\overline{V}_1$	$\overline{V}_2$	$\overline{V}_3$	$\overline{V}_4$	$\overline{V}_5$
$c_\varphi = +1$	$c_T = -1$	$\overline{V}_3$	$\overline{V}_4$	$\overline{V}_5$	$\overline{V}_6$	$\overline{V}_1$	$\overline{V}_2$
	$c_T = 0$	$\overline{V}_0$	$\overline{V}_7$	$\overline{V}_0$	$\overline{V}_7$	$\overline{V}_0$	$\overline{V}_7$
	$c_T = +1$	$\overline{V}_5$	$\overline{V}_6$	$\overline{V}_1$	$\overline{V}_2$	$\overline{V}_3$	$\overline{V}_4$

The input quantities are the stator flux sector and the outputs of the two hysteresis comparators. If the stator flux vector is lying in sector one of the (d,q) plane, then the voltage vectors used by DTC technique are shown in Figure 31.

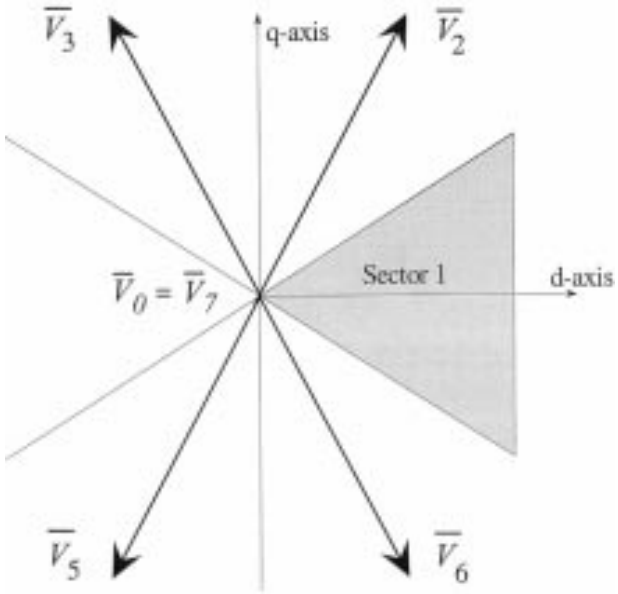

Figure 31. Voltage vectors utilized in basic DTC scheme when stator flux in sector 1, from [10].

This simple approach allows a quick torque response to be achieved; however, the steady-state performance is characterized by undesired ripple in current, flux and torque. This is largely due to the absence of information about torque and rotor speed values in the voltage vector selection algorithm [10].

g. Limitations of DTC

(1) Torque and Flux Ripple. In DTC drives there are torque and flux ripples because none of the inverter switching vectors are able to generate the exact stator voltage required to produce the desired changes in torque and stator flux linkage. Various schemes can be used to reduce these ripples. Although increased switching frequency is desirable (because it reduces harmonic content of stator currents and leads to reduced torque harmonics), it significantly increases switching losses, leading to reduced efficiency and added stress on the semiconductor devices of the inverter. In the case of high switching frequency, a faster processor is required, increasing cost. In addition, changed inverter topology can be used to limit ripples.

(2) Problems at Low Speed. When a DTC drive is operated in the zero-speed region, problems occur. During magnetization, the stator flux comparator selects only non-zero vectors. At that time, the output of the torque comparator takes one state, and the inverter cannot apply zero vectors to the motor. The introduction of an additional carrier signal to the input of the torque comparator is one solution to this problem. This carrier signal is only applied in the zero-speed region and forces zero vectors improving stator flux linkage and stator current waveforms. This ensures robust start and operation in the zero-speed region.

(3) Duty Ratio Control. In DTC motor drives, a voltage vector is applied for the entire switching period, which causes stator current and torque to increase for that entire period. For small errors, torque exceeds its reference value early and continues to increase, causing a high torque ripple. Then, zero-vectors are applied to reduce the torque back to its reference value. A solution can be obtained to reduce the ripples by applying the inverter switching vector for only a part of the switching period and a zero-vector for the remainder of the period, thus, a non-zero vector is used to increase torque to its reference value and, when it reaches that value, a zero-vector is

applied. During the application of a zero-vector, there is no voltage forced on the machine and torque is nearly constant. The average input voltage during application is δU_d (δ is the duty ratio from 0 to 1). So any voltage between 0 and U_d can be applied. This increases the number of choices for the voltage vector, which was previously limited to the six switching vectors [4].

THIS PAGE INTENTIONALLY LEFT BLANK

IV. MEASUREMENTS AND SIMULATIONS

A. APPROACH

It is possible to model virtually every aspect of an induction machine, but this model serves only as a means to reduce time spent in the laboratory, cost and risk to personnel. A useful model must be able to predict laboratory results and circuit dynamics. Only through experimental validation is it apparent that a simulated model predicts the behavior of an implemented hardware prototype accurately. Upon verifying the V/f control simulation functioned properly, we used this model was used to simulate FOC and DTC. Ultimately, three types of torque control for a VSI-fed induction machine were compared.

The experimental data presented here was captured through the use of Chipscope, an embedded, software based logic analyzer. This program allowed monitoring of all of the signals in the design and provided a convenient software based interface for controlling the integrated logic analyzer, including setting triggering options and viewing the waveforms. The program also provided a fast, easy, and interactive setup and simple debugging of input/output channels in high-speed FPGA designs. Up to 4000 data points were captured from four separate channels. The data collected included the flux (CH1), Phase B current in amps (CH2), commanded voltage in volts (CH3), and the speed in rpm (CH4). These signals were captured at the speed of operation and brought out through the programming interface. Captured signals were displayed and analyzed using the Chipscope Pro Analyzer tool.

B. V/F CONTROL

To show that the simulation accurately predicted the behavior of the machine, simulated results were compared with measured data. It can be seen in Figure 32 that the speed response of the measured and simulated results match closely.

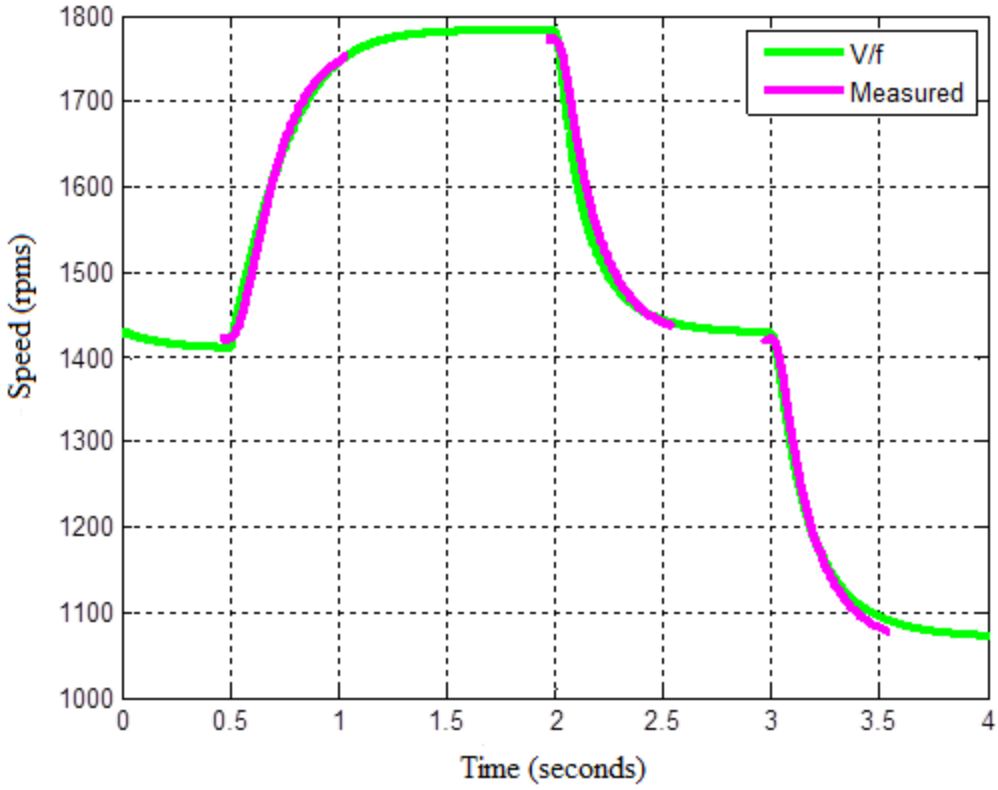

Figure 32. Measured and simulated speed response of an induction machine with V/f control.

Although only a certain number of samples were gathered (due to limitations on available lab equipment), the data that was collected sufficiently demonstrates that the simulation accurately predicted the behavior of a hardware prototype.

The primary objective was to illustrate the operation of both the physical machine and the simulation in transient and steady-state operating conditions. This was achieved by creating three distinct step events and recording the results. The machine was originally set to 80 percent of its rated speed (approximately 1440 rpm). The first step event occurs at 0.5 seconds, where the speed is increased from 80 percent of the rated value to the rated value itself (1800 rpm). Although the maximum rated value was never reached (due to slip and friction), neither the model nor the machine itself reached this speed. The second step event occurs at two seconds, where the speed was decreased from the rated value back to the original 80 percent level. Finally, the third step event occurs at

three seconds, and the speed was decreased from 80 percent to 60 percent (approximately 1080 rpm) of the rated value. Throughout these step events, the measured and simulated data align and demonstrate similar response times.

The Phase B current during these same step events was also monitored. This current was filtered at 300 Hz, and the step response of the step event occurring at 0.5 seconds (from 80 percent to 100 percent of the rated speed) is shown in Figure 33.

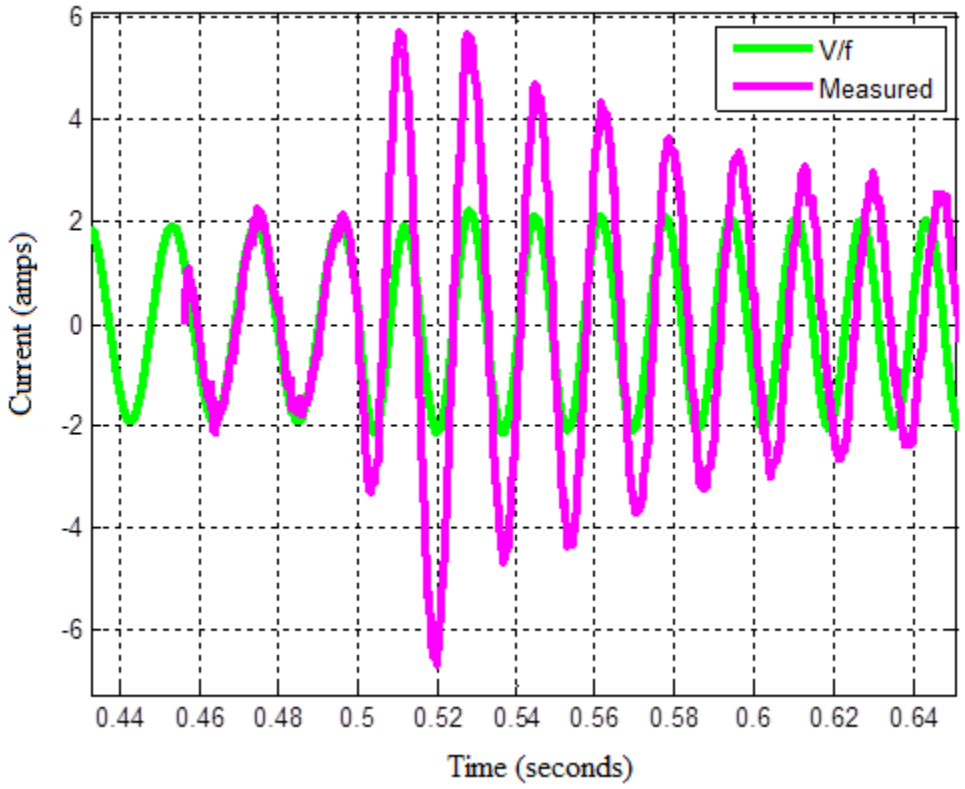

Figure 33. Phase B current filtered at 300 Hz of an induction machine under V/f control.

At steady-state, the measured and simulated currents are in phase. As this model was developed using steady-state operating conditions, the two did not obtain the same transient response. This observation was made for the other two step events as well. With the measured data, we see a current spike of over 6.0 A, whereas the maximum simulated current spike is only about 2.3 A. In addition, during the transient response, the currents

fell out of phase, and the simulated current led the measured current. This error was predicted to occur because the steady-state equivalent circuit model does not accurately model the dynamic response; however, the error is small. Upon settling back to steady-state, the behavior of the machine fell right in line with what the simulation predicted. Based on the speed and current response to the three created step events, the model accurately predicted the behavior of an induction machine utilizing V/f control. This verification allowed the model to be used for simulating FOC and DTC.

C. V/F CONTROL VERSUS FOC AND DTC

Time and money can be saved through the use of simulation because it is unnecessary to physically implement all of the control schemes covered in this thesis. The developed Simulink model has proven to successfully demonstrate the behavior of an induction machine utilizing V/f control and can be built upon to simulate FOC and DTC as well.

1. V/f Control Versus FOC

The simulation was modified to incorporate FOC capability. After these modifications were made, this control scheme was compared to V/f control by introducing the same step events used earlier. This comparison is shown in Figure 34.

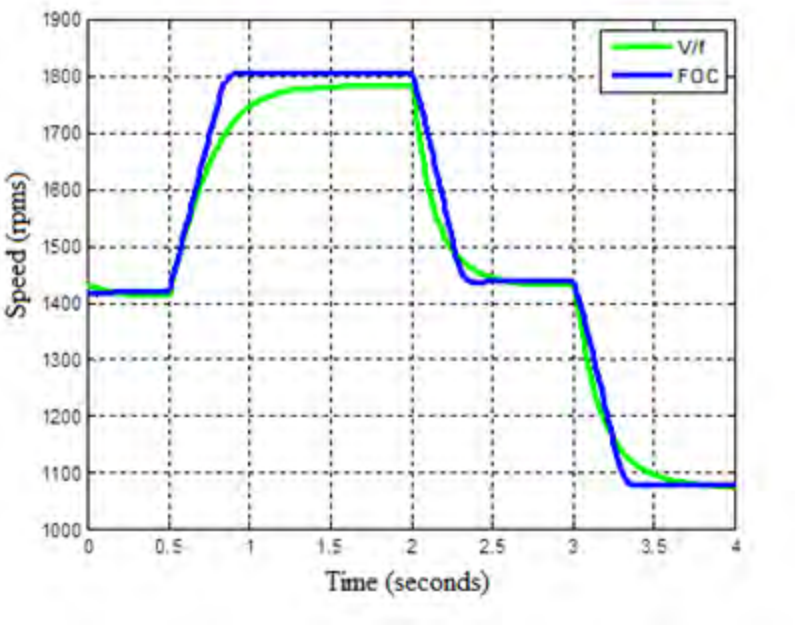

Figure 34. Comparison of simulated V/f control and FOC.

FOC possesses a much better dynamic response time (it reaches its maximum speed much quicker than V/f control). Moreover, the full rated speed of the induction machine is accomplished (1800 rpm). These two facts prove that FOC possesses distinct advantages over V/f control.

2. V/f Versus DTC

Next, DTC capability was developed and incorporated into the Simulink model. In the same way that FOC was compared to V/f control, so was DTC. This comparison is shown in Figure 35.

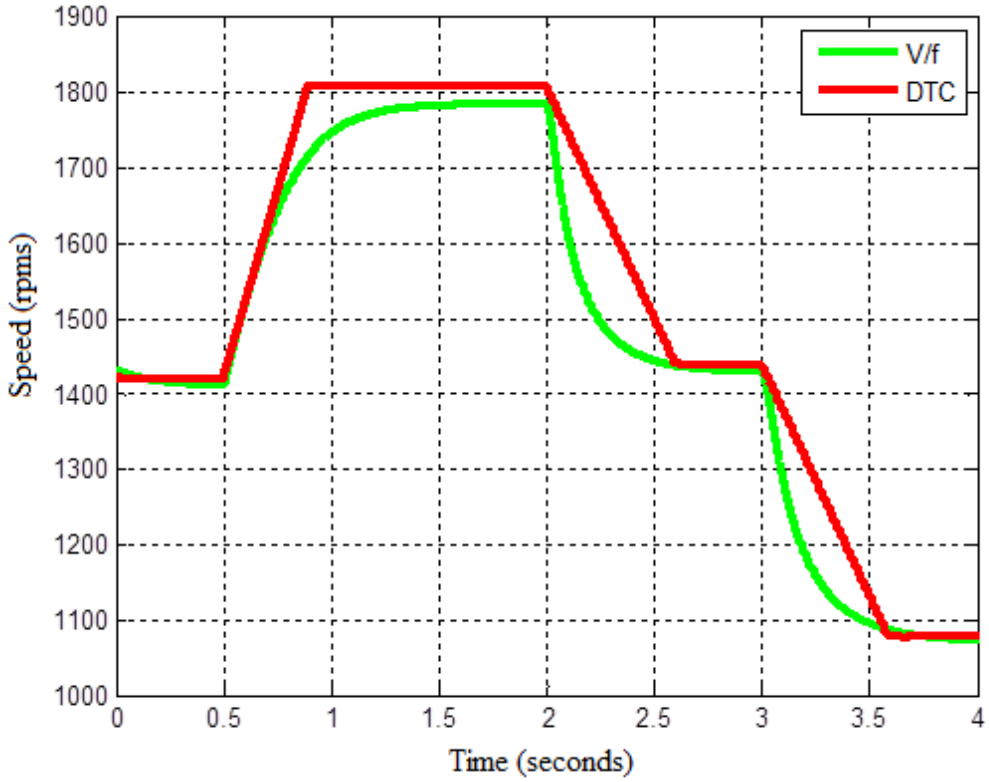

Figure 35. Comparison of simulated V/f control and DTC.

DTC shows a distinct advantage over V/f control for increasing speeds but is slightly sluggish for speed decreases. Much like FOC, DTC allows the machine to reach the full rated speed. Both the FOC and DTC simulations illustrate clear benefits over V/f control.

D. FOC Versus DTC

FOC induction machines were introduced nearly 40 years ago and today are an industrial reality and widely available. DTC was introduced shortly thereafter and was characterized by simplicity, good performance and robustness. The use of DTC made dynamic control of torque possible without any mechanical transducers on machine shafts. Often DTC is referred to as a sensorless type control technique [1]. It was the aim of this thesis to fairly compare these two techniques in all modes of operation. First, DTC and FOC speed responses are compared and are displayed in Figure 36.

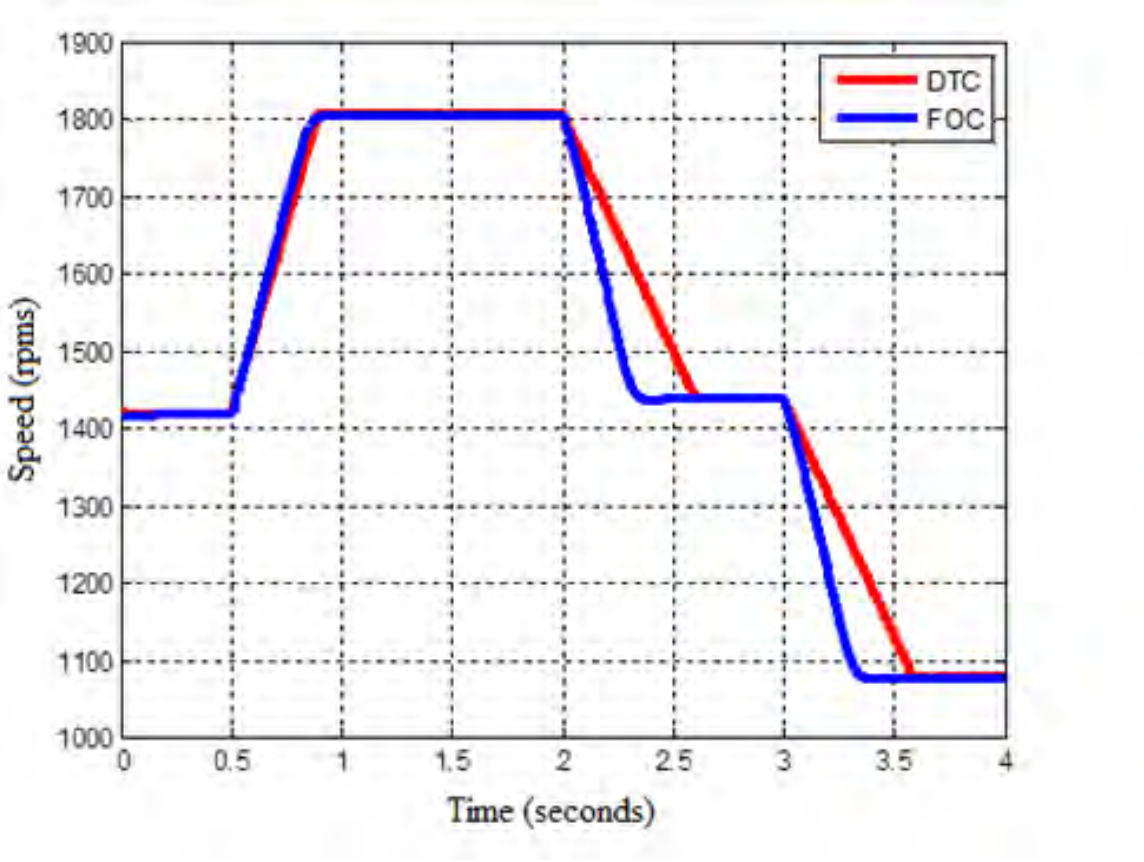

Figure 36. Comparison of simulated speed response of DTC and FOC.

Both control schemes reach the rated speed and do so relatively quickly. However, FOC performs considerably better than DTC upon both decreases from 100 percent to 80 percent and from 80 percent to 60 percent. It is also important to examine the Phase B currents of both control strategies (still filtered at 300 Hz) for the speed profiles shown in Figure 36. They are displayed in Figure 37.

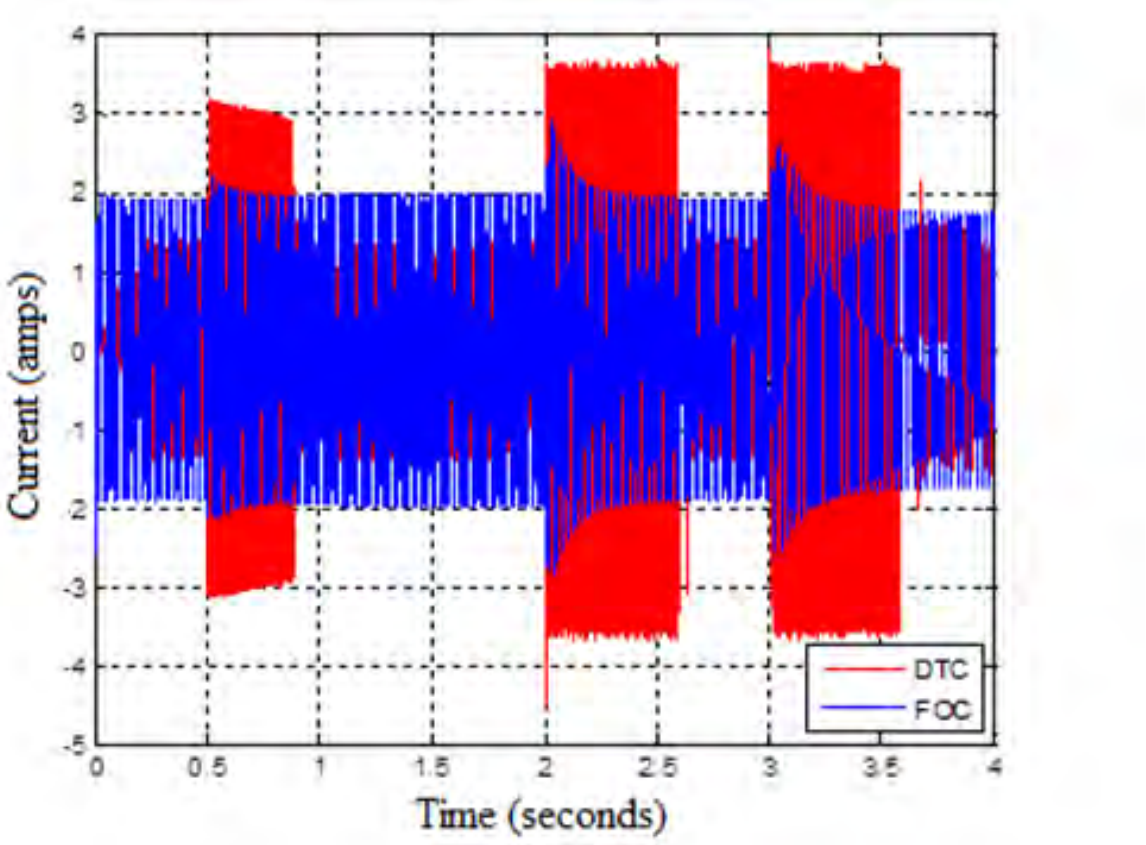

Figure 37. Phase B current for DTC and FOC.

DTC's peak-to-peak current during steady-state operation is much lower than the peak-to-peak current of FOC. This lower current leads to lower electrical losses of the machine. Although FOC constantly controls the current through the use of current sensors, DTC does not have this same control and experiences high current peaks during transient operation. As discussed earlier, DTC experiences high current ripples because the optimum switching vectors cannot generate the exact stator voltage required to produce the desired changes in torque and stator flux linkage. Based on these results, each control scheme possesses advantages, and the application of a machine determines which one to employ. If the machine is going to be used mostly in steady-state operation, such as a water pump, DTC is the better choice. If the machine changes speeds frequently, such as an electric drive for an electric car, then the preferred choice is FOC.

Next, the reference torque of both DTC and FOC are examined and shown in Figure 38.

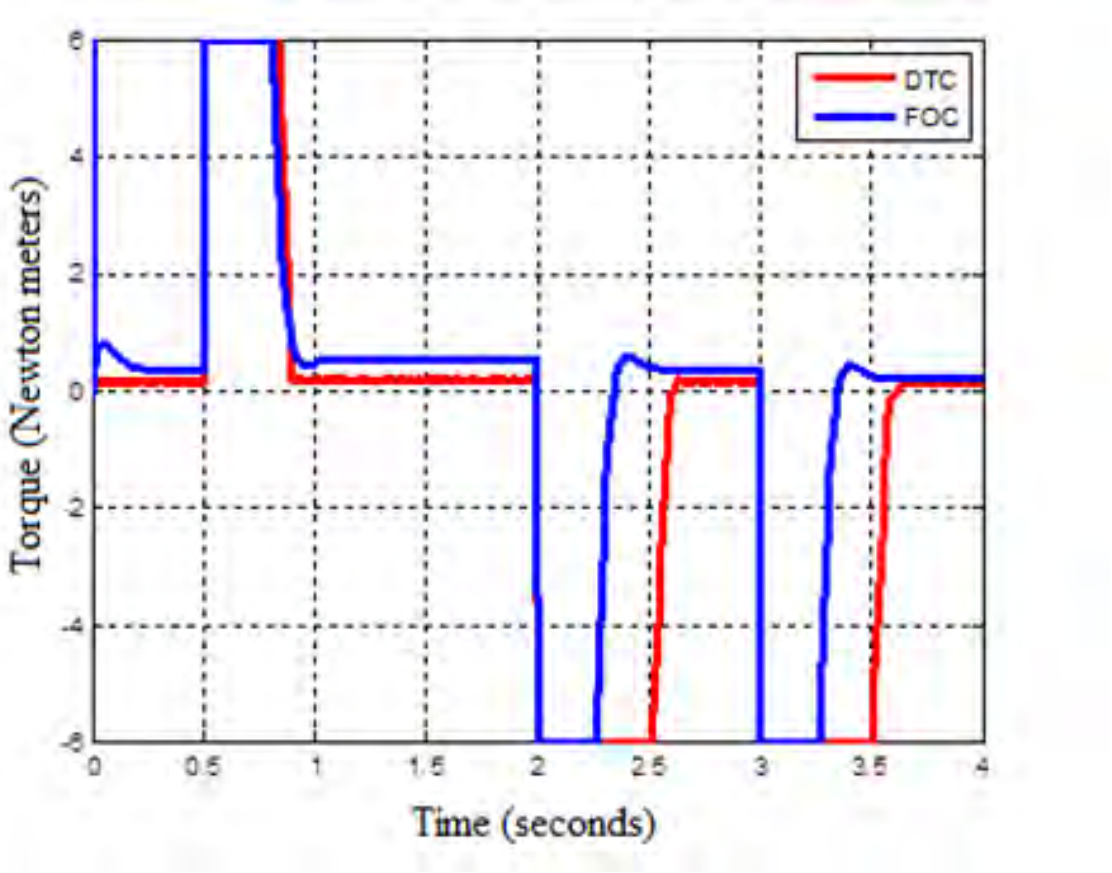

Figure 38. Reference torque for DTC and FOC.

When considering the reference torque, it should be noted that the absolute value of the reference torque was set to two Newton meters as determined by a saturation block in the controller of this model. It is also important to understand that the signed values of torque imply the demanded direction of torque where positive values imply rotation in the counterclockwise direction, while negative values imply rotation in the clockwise direction. During the first step event (at 0.5 seconds), we see that both control schemes demand the maximum available torque in the counterclockwise direction in an attempt to

speed the machine from 80 percent of the rated value to the rated value itself. Although both schemes call for torque in similar ways, FOC is noticeably more responsive upon speed decreases.

While the reference torque is the torque the machine calls for, the electrical torque is what the machine actually receives. The electrical torque is displayed in Figure 39.

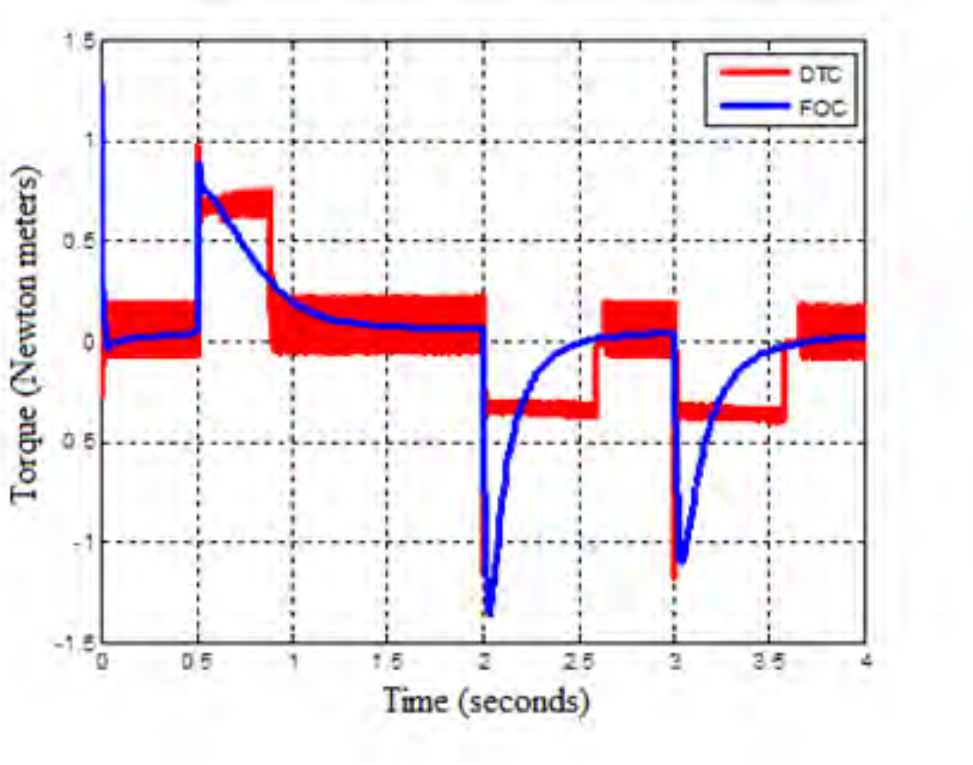

Figure 39. Electrical torque for DTC and FOC.

The first observance from the electrical torque is the different shapes of both. FOC has a pulsed response, while DTC has a stepped response. FOC has a slightly slower response time than DTC, and the torque for DTC is controlled through a hysteresis comparator and, therefore, is bouncing between the upper and lower limits of this comparator.

Finally, we need to consider how the flux behaves under these two control schemes. The stator flux of DTC and the stator flux of FOC can be seen in Figure 40.

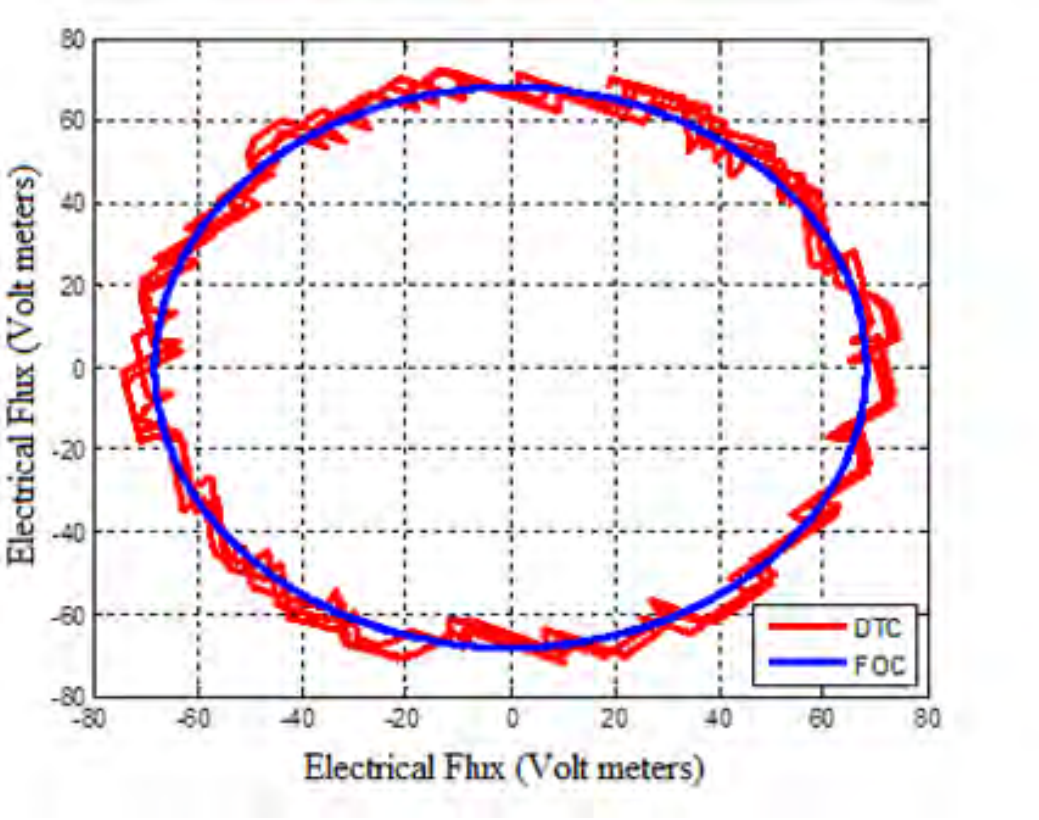

Figure 40. Simulated flux for DTC and FOC.

The results in Figure 40 were produced by capturing a few cycles of the electrical flux during steady-state operation at the rated speed. These cycles were captured from 1.45 to 1.55 s. FOC maintains constant flux throughout the duration of this cycle (producing a circle), while DTC does not. As discussed earlier, DTC attempts to keep the flux within a preset hysteresis band with upper and lower limits, and the uneven response is a result of bouncing back and forth between these two limits. With FOC the torque and flux producing current components are decoupled, and the transient response characteristics emulate those of a separately excited DC machine. Observing the dynamic response of flux is also beneficial. This is shown in Figure 41.

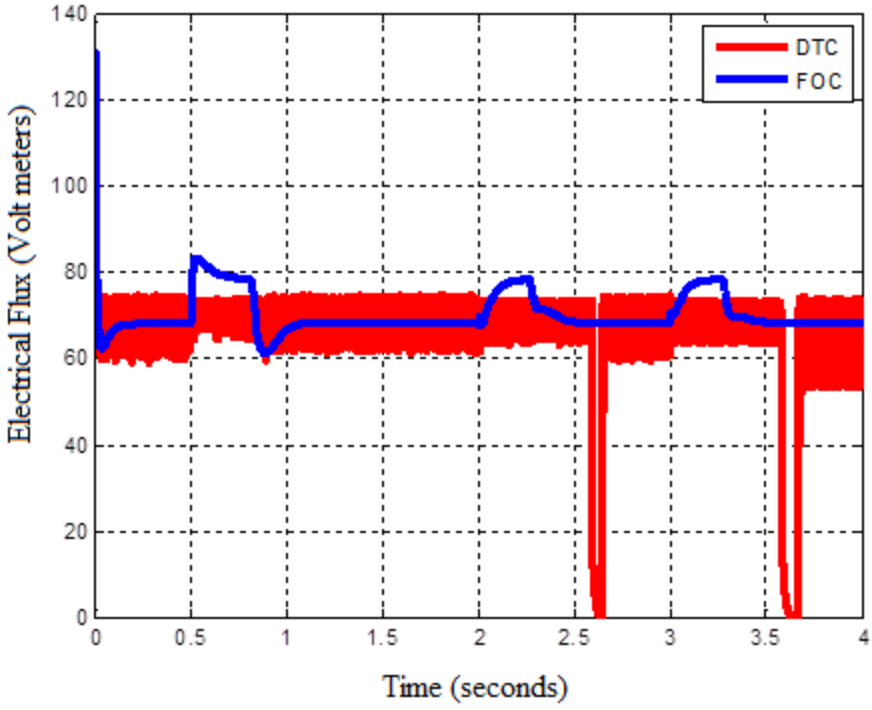

Figure 41. Electrical flux for DTC and FOC.

Again, DTC maintains the flux within the hysteresis band. DTC's electrical torque drops to zero and back again because the direction of the flux linkage space vector is changed by 180 degrees at these times. Flux is a product of the current and, thus, FOC experiences increased flux when the current is increased to supply the demanded torque.

In summary, the verification of V/f control through the comparison of measured and simulated results allowed FOC and DTC to be simulated with confidence that they accurately predict a physical system using these control techniques. These three control schemes were compared to one another, and conclusions are discussed in the next chapter.

V. CONCLUSIONS

A. CONCLUSIONS

Using parameters from a VSI-fed induction machine, a Simulink model of this machine was designed, simulated, constructed and tested using standard engineering principles and theory. Thorough research and simulation phases allowed for relatively short development and construction phases. Experimental results demonstrated that this model accurately predicted the behavior of the machine. The simulation was used to evaluate three different torque control schemes (V/f, FOC, and DTC).

The results found during this thesis are summarized in Table 12.

Table 12. Comparison of control schemes, from [1].

Control Type	*Torque Control*	*Flux Control*	*Response*	*Advantages*	*Disadvantages*
DC Drive	Direct	Direct	High	High accuracy Good torque response Simple	Motor maintenance Motor cost Encoder required for high accuracy
Scalar Frequency Control	None	None	Low	No encoder Simple	Low accuracy Poor torque response
Flux Vector Control	Indirect	Direct	High	High accuracy Good torque response	Encoder always required
Direct Torque Control	Direct	Direct	High	No encoder Moderate accuracy Excellent torque response	Encoder required for high accuracy

The evolution from DC drives to various forms of AC drives has been driven by the need for better response times, higher accuracy, and control of torque and flux (directly or indirectly). Theory and principles for V/f control, FOC, and DTC were covered in detail. The distinct advantages that FOC and DTC possess over V/f control allow the reader to conclude that scalar control is not a preferred control scheme. FOC demonstrated better accuracy mainly because of the ability to control the current, but this accuracy comes at the necessity of current sensors. DTC allows for direct control of both the torque and the flux, but it is not as accurate and experiences high ripple content in both the flux and torque components. The steady-state current of DTC was significantly

lower (less electrical losses) than that of FOC. If the machine is going to be used mostly at constant speeds, DTC is the better choice. If the machine changes speeds frequently, then the preferred choice is FOC.

With a reliable model, the US Navy has the means to build a large scale prototype for laboratory purposes and future research. Future research on this topic will go above and beyond current publications and will have an enabled freedom to exploit the capabilities of the VSI-fed induction machine.

B. FUTURE RESEARCH

While the hardware prototype used in this thesis utilized only V/f control, a prototype that utilizes the other two control schemes can be built. One could use a similar process developed here to verify that the simulation accurately predicts the behavior of an induction machine using FOC and DTC. Improvements leading to substantially higher performance of both control schemes should be investigated. For example, current sensors could be introduced to DTC to improve accuracy and reduce the ripple component of torque and flux. In addition, to evaluate whether the trends developed here are consistent, machines of different sizes should be studied. Many questions remain, but a foundation leading to those answers was provided by this thesis.

APPENDIX A. DATASHEETS

Model 8231 Three-Phase Wound-Rotor Induction Motor

Each phase of the stator windings of this motor is independently terminated and identified on the faceplate to permit operation in either delta or star (wye) configuration. The rotor windings are brought out to the faceplate via external slip rings and brushes. This machine can be used as a wound-rotor induction motor, phase shifter, single-phase variable coupling transformer, three-phase transformer, selsyn control, frequency converter or asynchronous induction generator. The speed of this machine can be controlled through the use of the Three-Phase Rheostat (Model 8731).

SPECIFICATIONS

Model 8211 DC Motor/Generator		120/208 V – 60 Hz	220/380 V – 50 Hz	240/415 V – 50 Hz
Power Requirement		120/208 V	220/380 V	240/415 V
Rating	Motor Output Power	175 W		
	Generator Output Power	120 W	110 W	120 W
	Armature Voltage	120 V – DC	220 V – DC	240 V – DC
	Shunt Field Voltage	120 V – DC	220 V – DC	240 V – DC
	Full Load Speed	1800 r/min	1500 r/min	1500 r/min
	Full Load Motor Current	2.8 A	1.3 A	1.1 A
	Full Load Generator Current	1 A	0.5 A	0.5 A
Physical Characteristics	Dimensions (H x W x D)	308 x 291 x 440 mm (12.1 x 11.5 x 17.3 in)		
	Net Weight	14.1 kg (31 lb)		
Model 8221 Four-Pole Squirrel-Cage Induction Motor		**120/208 V – 60 Hz**	**220/380 V – 50 Hz**	**240/415 V – 50 Hz**
Power Requirement		120/208 V	220/380 V	240/415 V
Rating	Output Power	175 W		
	Stator Voltage	120/208 V, 3-phase	220/380 V, 3-phase	240/415 V, 3-phase
	Full Load Speed	1670 r/min	1360 r/min	1395 r/min
	Full Load Current	1.2 A	0.52 A	0.46 A
Physical Characteristics	Dimensions (H x W x D)	308 x 291 x 440 mm (12.1 x 11.5 x 17.3 in)		
	Net Weight	13.5 kg (29.7 lb)		
Model 8231 Three-Phase Wound-Rotor Induction Motor		**120/208 V – 60 Hz**	**220/380 V – 50 Hz**	**240/415 V – 50 Hz**
Power Requirement		120/208 V	220/380 V	240/415 V
Rating	Output Power	175 W		
	Stator Voltage	120/208 V, 3-phase	220/380 V, 3-phase	240/415 V, 3-phase
	Rotor Voltage	60/104 V, 3-phase	110/190 V, 3-phase	120/208 V, 3-phase
	Full Load Speed	1500 r/min	1240 r/min	1315 r/min
	Full Load Current	1.3 A	0.53 A	0.48 A
Physical Characteristics	Dimensions (H x W x D)	308 x 291 x 440 mm (12.1 x 11.5 x 17.3 in)		
	Net Weight	14 kg (30.8 lb)		

POWER SUPPLY
MODEL 8821

The Power Supply provides fixed and variable AC and DC voltage sources, all terminated by color-coded 4 mm safety sockets. Independent circuit breakers, reset at the front panel, protect the input to and output from the Power Supply. Indicator lamps monitor the presence of input voltage in each phase. When a phase leg of the site's power service is out, the lamp goes off to reflect this condition.

A voltmeter, connected through a selector switch, monitors the variable AC and DC outputs and fixed DC output. A 24 V AC output provides a low-voltage supply required to operate other EMS equipment such as metering modules and modules used in the Power Electronics Training System.

SPECIFICATIONS

Model 8821 – Power Supply		120/208 V – 60 Hz	220/380 V – 50 Hz	240/415 V – 50 Hz
Input	Line Voltage	120/208 V	220/380 V	240/415 V
	Line Current	15 A	10 A	
	Service Installation	20 A, 3-phase, 5 wires, star (Wye)- connected, including neutral and ground		
Outputs	Fixed AC 3-Phase	120/208 V – 15 A	220/380 V – 10 A	240/415 V – 10 A
	Variable AC 3-Phase	0-120/208 V – 5 A	0-220/380 V – 3 A	0-240/415 V – 3 A
	Variable DC	0-120 V – 8 A	0-220 V – 5 A	0-240 V – 5 A
	Fixed DC	120 V – 2 A	220 V – 1 A	240 V – 1 A
	Low Power AC	24 V – 3 A		
Wall Outlet included		NEMA L21-20	NEMA L22-20	CLIPSAL 56SO520
Power Cord		3 m (10 ft)		
Physical Characteristics	Dimensions (H x W x D)	308 x 287 x 500 mm (12.1 x 11.3 x 19.7 in)		
	Net Weight	18.4 kg (40.5 lb)		

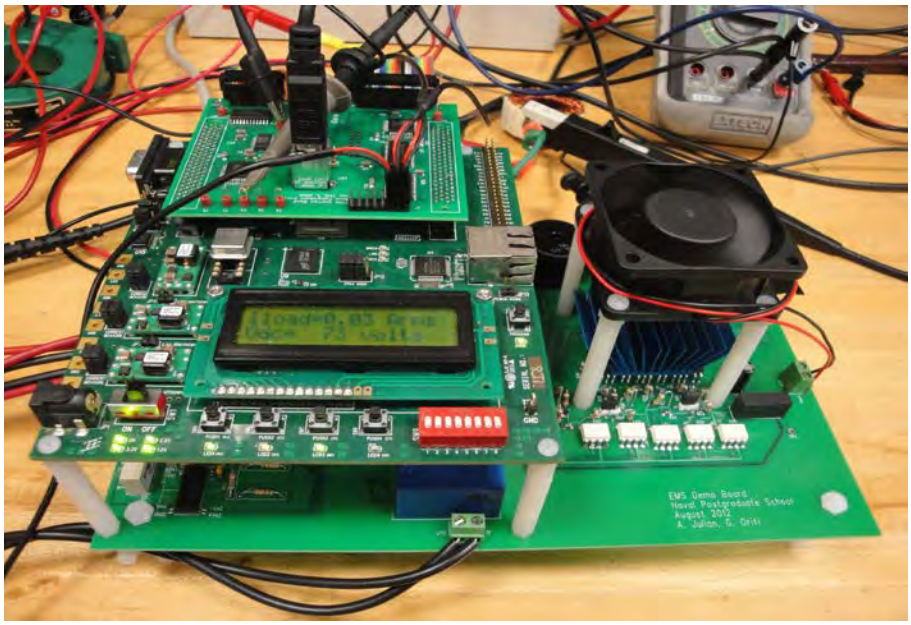

Laboratory Setup

MECHANICAL LOADS
MODELS 8911, 8913, AND 8960

Model 8911 Electrodynamometer

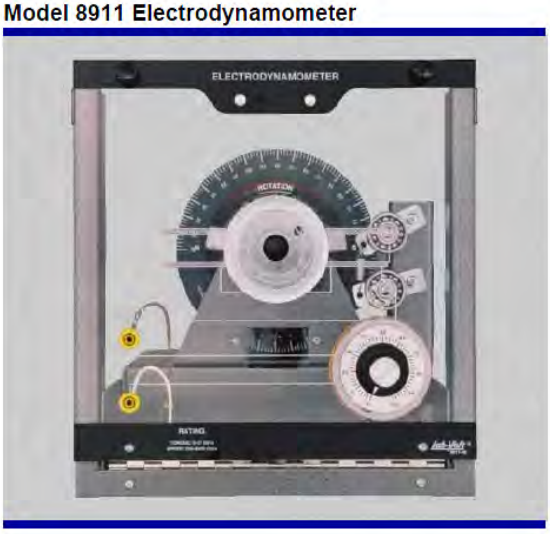

The Model 8911 Electrodynamometer is equipped with a clear plastic faceplate fitted with a chrome piano hinge. It can be coupled to a 0.2-kW drive motor through the use of the Timing Belt (Model 8942). The faceplate can be lowered to provide access to the inside for coupling the Electrodynamometer to the drive motor. When closed, the faceplate is secured by two quick-lock fasteners.

The Electrodynamometer is made of a squirrel-cage rotor fitted in a DC-excited stator. Mechanical loading is achieved by increasing the stator field current, which generates eddy currents in the driven rotor. The stator is trunnion-mounted on ball bearings and rotates against a helicoidal spring to oppose braking torque. The front-end bell is provided with a circular scale that indicates the torque developed. The circular scale is graduated in either Imperial Units (lbf·in) or Metric Units (N·m) depending on model numbers. The Electrodynamometer is electrically powered from standard fixed AC line supply.

SPECIFICATIONS

Model 8911 Electrodynamometer		120/208 V – 60 Hz	220/380 V – 50 Hz	240/415 V – 50 Hz
Rating	Torque Range (8911-1)	-0.3 to +3 N·m		
	Torque Range (8911)	-3 to +27 lbf·in		
	Speed	250 to 3000 r/min		
	Accuracy	2%		
	Input Voltage	120 V – AC	220-240 V – AC	
	Input Current	2 A	0.9 A	
Physical Characteristics	Dimensions (H x W x D)	308 x 291 x 490 mm (12.1 x 11.5 x 19.3 in)		
	Net Weight	17.4 kg (38.3 lb)		
Model 8913 Prony Brake				
Rating	Torque Range (8913-1)	0 to 3.4 N·m		
	Torque Range (8913)	0 to 30 lbf·in		
	Speed	0 to 5000 r/min		
	Accuracy	2%		
Physical Characteristics	Dimensions (H x W x D)	308 x 291 x 440 mm (12.1 x 11.5 x 17.3 in)		
	Net Weight	8.8 kg (19.4 lb)		

SPECIFICATIONS (cont'd)

Model 8960 Prime Mover / Dynamometer		120/208 V – 60 Hz	220/380 V – 50 Hz	240/415 V – 50 Hz
Prime Mover / Dynamometer	Magnetic Torque	0 to 3 N·m (0 to 27 lbf·in)		
	Rotation	CW / CCW		
	Display	Torque/Speed		
	Torque Units	N·m or lbf·in (user selectable)		
	Friction Torque	0.15 N·m (1.3 lbf·in) @ 1500 r/min		
	Low Power Input	24 V – AC		
	Shaft Encoder Output	A/B - 360 pulses/r – TTL Compatible		
	Torque Output Signal	0.3 N·m/V (2.655 lbf·in/V)		
	Speed Output Signal	500 r/min / V		
	Indicators	Overspeed, Overheat, Power On		
Prime Mover	Mechanical Power	750 W		
	Input Voltage Range	0 to 150 V – DC		
	Overvoltage Detector	NO	YES	
	Input Current	6.5 A		
	Speed Range (@ 3.0 N·m (26.6 lbf·in))	0 to 2500 r/min		
Dynamometer	Mechanical Power	250 W continuous - 750 W maximum		
	Speed Range (@ 3.0 N·m (26.6 lbf·in))	290 to 3000 r/min		
	Speed Range (@ 1.5 N·m (13.3 lbf·in))	155 to 3000 r/min		
	Load Control	Manuel/External		
	Load Control External Input	0 to +10 V		
	External Load Control Input Sensitivity	0.3 N·m/V (2.655 lbf·in/V)		
Physical Characteristics	Dimensions (H x W x D)	308 x 291 x 490 mm (12.1 x 11.5 x 19.3 in)		
	Net Weight	23.6 kg (51.9 lb)		

Manually Operated P/N	Input Volts	Phase	Hertz *	Output Volts	Constant Current Rating
3PN2210B	120	1 PH	50/60	0-140	22A

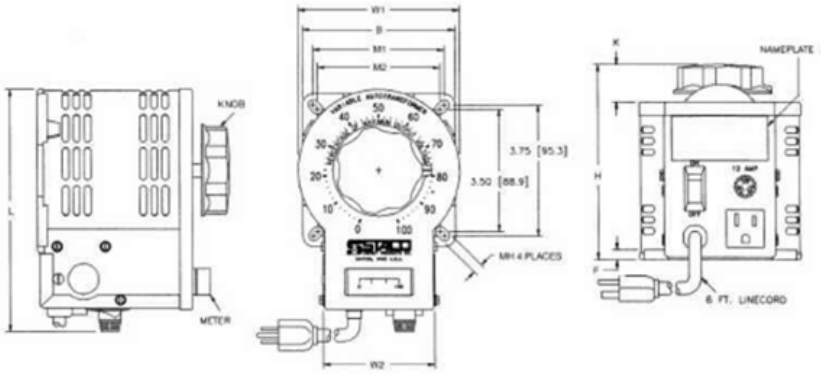

	3PN1000B 3PN1200B 3PNJ201B Series	3PN1500B 3PNJ401B Series	3PN2210B 3PN2520B
L	6.96" (176.8 mm)	9.35" (237.4 mm)	10.85" (275.6 mm)
H	5.50" (139.7 mm)	6.00" (152.4 mm)	6.31" (160.3 mm)
W1	4.62" (117.4 mm)	6.24" (158.4 mm)	7.95" (202.1 mm)
W2	3.18" (180.8 mm)	4.31" (109.6 mm)	4.31" (109.6 mm)
K	1.06" (27.0 mm)	1.00" (25.4 mm)	1.65" (41.8 mm)
B	4.38" (111.1 mm)	5.50" (139.7 mm)	7.13" (181.0 mm)
M1	3.75" (95.3 mm)	4.75" (120.7 mm)	6.38" (161.9 mm)
M2	3.50" (88.9 mm)	—	5.86" (149.2 mm)
F	0.28" (7.1 mm)	0.32" (8.1 mm)	0.32" (8.1 mm)
MH	0.29" (7.4 mm)	0.31" (7.9 mm)	0.38" (9.5 mm)

APPENDIX B. MATLAB M-FILES

A. INITIAL CONDITIONS FILE

```
omega = 2*pi*60;  %Modify this variable to change reference frame
omega_b = 2*pi*60;
omega_in = 2*pi*60;
bypass=1;
if bypass==1
    tstep=50e-6
    tstop=4;
else
    tstep=2e-6
    tstop=.9;
end;
twopiby3 = 2*pi/3;
poles = 4;
polesby2J = poles/2/(2.04e-3*3);

rs=16;
rr=8;
Xls=10.3569;
Xm=159.8850;
Xlr=10.3569;

Xm=51.6;
rr=14;  %adjustment to rr
rs=29;     % increased to improve model

rsbyXls = rs/Xls;
rrbyXlr = rr/Xlr;
Xaq = 1/(1/Xm+1/Xls+1/Xlr);
Xad = Xaq;
XaqbyXls = Xaq/Xls;
XaqbyXlr = Xaq/Xlr;
XadbyXls = Xad/Xls;
XadbyXlr = Xad/Xlr;
V_phase = 220*sqrt(2)/sqrt(3);  %Peak value used in Simulink for source
model
XaqbyXm = Xaq/Xm;
XadbyXm = Xad/Xm;
%Steady state analysis
omega_rotor = .79*omega_in;
slip = (omega_in-omega_rotor)/omega_in;
Z1 = rs + j*omega_in/omega_b*Xls;
Z2 = j*omega_in/omega_b*Xm;
Z3 = rr/slip + j*omega_in/omega_b*Xlr;
Ias = V_phase/sqrt(2)/(Z1 + Z2*Z3/(Z2+Z3));
Iar = -Ias*(Z2*Z3/(Z2+Z3))/Z3;
Te = 3*poles/2*Xm/omega_b*real(j*conj(Ias)*Iar);
Iqse = sqrt(2)*real(Ias);
Idse = -sqrt(2)*imag(Ias);
Iqre = sqrt(2)*real(Iar);
```

```
Idre = -sqrt(2)*imag(Iar);
psi_mqe = Xm*(Iqse+Iqre);
psi_mde = Xm*(Idse+Idre);
psi_qse = Iqse*Xls + psi_mqe;
psi_dse = Idse*Xls + psi_mde;
psi_qre = Iqre*Xlr + psi_mqe;
psi_dre = Idre*Xlr + psi_mde;
Te2 = 3/2*4/2*(psi_dse*Iqse - psi_qse*Idse)/omega_b;
psi_mqic=psi_mqe;
psi_mdic=psi_mde;
psi_qsic=psi_qse;
psi_dsic=psi_dse;
psi_qric=psi_qre;
psi_dric=psi_dre;
omegar_ic = omega_rotor;

t_event1=.5;
speed1=1*omega_b
t_event2=2;
speed2=0.8*omega_b
t_event3=3;
speed3=0.6*omega_b

Vdc=300;
Tsw=1/15000;
gain1 = 1/2;
gain2 = 1;
oversample=2;
Kp_i=25*4;
Ki_i=500*6;
swv0=[0 0 0];
swv1=[1 0 0];
swv2=[1 1 0];
swv3=[0 1 0];
swv4=[0 1 1];
swv5=[0 0 1];
swv6=[1 0 1];
swv7=[1 1 1];
```

B. MACHINE PARAMETERS

```
clc;
clear all;

P_rated=746/4;       % 1/4 HP machine
wrm=1670/60*2*pi;    %rad/sec mechanical
T_rated=P_rated/wrm/.113    %in in*lbf
%measured data
I1= [.694 .770 .903 1.082 1.308];
I2= [.692 .761 .895 1.083 1.297];
W1= [87 121 160 203 249];
W2= [44 13 23 60 93];
speed= [1789 1760 1726 1686 1640 0.1]/60*4*pi; %radians per second
```

```
torque= [0 3 6 9 12 18];
power=W1+W2;

%No Load
Vasnl=201/sqrt(3);
Iasnl=.68;
rs=11.91;     %
XmXls_sq=(Vasnl/Iasnl)^2-rs^2;  % Eq. 1.6 in lab report
P_core=(138-3*Iasnl^2*rs);      % Eq. 1.4 in lab report
rc=3*Vasnl^2/P_core;            % Eq. 1.5 in lab report

%Blocked rotor
Vasbr=99/sqrt(3);
Iasbr=2.09;
rr=(234/3/Iasbr^2-rs);    % Eq. 1.9 in lab report
Xls=sqrt((Vasbr/Iasbr)^2-(rs+rr)^2)/2;  % Eq. 1.10 in lab report
XM=sqrt(XmXls_sq)-Xls       % from line 16 above
Xlr=Xls;
Vas=201/sqrt(3);
wb=2*pi*60;    % base omega, page 152
we=wb;          %this means we/wb=1

rr_adj=8;  %adjustment to rr
rs=16;     % increased to improve model
wr=[0:.5:0.9999*wb];
slip=(we-wr)./we;
Z1=rs+j*Xls;
Z2=rc*j*XM./(rc+j*XM);
Z3=rr_adj./slip+j*Xlr;
Zin=Z1+Z2.*Z3./(Z2+Z3);
Ias=Vas./Zin;
Iar=-Ias.*Z2./(Z2+Z3);
Ic=Ias+Iar.*(j*XM./(rc+j*XM));
Pcore=3*rc*Ic.*conj(Ic);
Pscu=3*rs*Ias.*conj(Ias);
Prcu=3*rr_adj*Iar.*conj(Iar);
Te=3*4/2*XM/wb*real(j.*conj(Ias).*Iar);
power_out=Iar.*conj(Iar).*rr_adj.*(1-slip)./slip;

figure(1);
plot(wr,Te/1.3558179*12,'linewidth',2);  %torque expressed in in*lbf
hold on;
% plot(wr,abs(Ias),'g','linewidth',2);  %torque expressed in in*lbf
plot(speed,torque,'ro');    %torque expressed in in*lbf
hold off;
title('Measured and Equivalent circuit torque vs speed');
xlabel('Elec. Speed, rad. per sec.');

% Stall voltage, section 8 in the lab
speedb=[1722 1701 1665 1585 1713 1683 1629 1463]/60*4*pi;
V_LLb=[199.4 176.8 157.1 136.5 187.3 166.8 146.9 126.3];
slipb=(we-speedb)./we;
Z3b=rr_adj./slipb+j*Xlr;
Zinb=Z1+Z2.*Z3b./(Z2+Z3b);
```

```
Iasb=V_LLb./sqrt(3)./Zinb;
Iarb=-Iasb.*Z2./(Z2+Z3b);
Teb=3*4/2*XM/wb*real(j.*conj(Iasb).*Iarb)/1.3558179*12; %torque
expressed in in*lbf
% figure(2);
% plot(speedb,Teb,'ro');
% title('Prediction of torque for the stall voltages that were
measured');
% xlabel('Elec. Speed, rad. per sec.');
```

C. SPEED COMPARISON FILE

```
%Run both speed simulations first to create the data for these plots.
close all;
clear all;

load data_80_100b;
Ia_80_100 = adc1;
Ib_80_100 = adc2;
Vqs_80_100 = adc3;
RPM_80_100 = adc4;
load data_100_80b;
Ia_100_80 = adc1;
Ib_100_80 = adc2;
Vqs_100_80 = adc3;
RPM_100_80 = adc4;
load data_80_60b;
Ia_80_60 = adc1;
Ib_80_60 = adc2;
Vqs_80_60 = adc3;
RPM_80_60 = adc4;
time_shift1=.44+.0164;
time_shift2=1.4+.06+.5;
time_shift3=2.4+.055+.5;

alpha=2*pi*500;
Ib_80_100_fil=zeros(1,4095);
Ib_80_100_fil2=zeros(1,4095);
Ib_100_80_fil=zeros(1,4095);
Ib_100_80_fil2=zeros(1,4095);
Ib_80_60_fil=zeros(1,4095);
Ib_80_60_fil2=zeros(1,4095);
for ii=2:4095
    Ib_80_100_fil(ii)=Ib_80_100_fil(ii-1)+deltat*alpha*(Ib_80_100(ii-
1)-Ib_80_100_fil(ii-1));
    Ib_100_80_fil(ii)=Ib_100_80_fil(ii-1)+deltat*alpha*(Ib_100_80(ii-
1)-Ib_100_80_fil(ii-1));
    Ib_80_60_fil(ii)=Ib_80_60_fil(ii-1)+deltat*alpha*(Ib_80_60(ii-1)-
Ib_80_60_fil(ii-1));
end
for ii=2:4095
    Ib_80_100_fil2(ii)=Ib_80_100_fil2(ii-
1)+deltat*alpha*(Ib_80_100_fil(ii-1)-Ib_80_100_fil2(ii-1));
```

```
    Ib_100_80_fil2(ii)=Ib_100_80_fil2(ii-
1)+deltat*alpha*(Ib_100_80_fil(ii-1)-Ib_100_80_fil2(ii-1));
    Ib_80_60_fil2(ii)=Ib_80_60_fil2(ii-
1)+deltat*alpha*(Ib_80_60_fil(ii-1)-Ib_80_60_fil2(ii-1));
end

vbyf=0;
DTC=1
sim ind_machine_3hp_speed_control_DTCver4
simout_DTC=simout_vec;
sw_state_DTC=sw_state;
fluxout=flux;

vbyf=0;
DTC=0
sim ind_machine_3hp_speed_control_DTCver4
simout_FOC=simout_vec;
sw_state_FOC=sw_state;
fluxout_FOC=flux;

vbyf=1;
DTC=0
sim ind_machine_3hp_speed_control_DTCver4
temp1=length(simout_DTC);
time_vec=[1:temp1]/temp1*tstop;
sw_state_pwm=sw_state_1;

figure(1);
plot(time_vec,simout_vec(:,2),'g','linewidth',3);
hold on;
plot(time+time_shift1,RPM_80_100,'m','linewidth',3);
plot(time+time_shift2,RPM_100_80,'m','linewidth',3);
plot(time+time_shift3,RPM_80_60,'m','linewidth',3);
hold off;
title('Measured and simulated results (V/f control)');
legend('V/f','Measured','location','northeast');
xlabel('Time (seconds)');
ylabel('Speed (rpms)');
grid on;
saveas(1,'fig1.jpg','jpg');

figure(2);
plot(time_vec,simout_vec(:,4),'g','linewidth',3);
hold on;
plot(time+time_shift1,Ib_80_100_fil2,'m','linewidth',3);
% plot(time+time_shift1,Ib_80_100,'r');
plot(time+time_shift2,Ib_100_80_fil2,'m','linewidth',3);
plot(time+time_shift3,Ib_80_60_fil2,'m','linewidth',3);
hold off;
title('Phase B current filtered at 300 Hz');
xlabel('Time (seconds)');
ylabel('Current (amps)');
grid on;
if vbyf == 1
```

```
legend('V/f','Measured','location','northeast');
else
legend('---','---','location','northeast');
end

figure(3);
plot(time_vec,simout_vec(:,2),'g','linewidth',3);
hold on;
plot(time_vec,simout_FOC(:,2),'b','linewidth',3);
hold off;
title('Speed response: V/f vs. FOC');
legend('V/f','FOC','location','northeast');
xlabel('Time (seconds)');
ylabel('Speed (rpms)');
grid on;
saveas(1,'fig13.jpg','jpg');

figure(4);
plot(time_vec,simout_vec(:,2),'g','linewidth',3);
hold on;
plot(time_vec,simout_DTC(:,2),'r','linewidth',3);
hold off;
title('Speed response: V/f vs. DTC');
legend('V/f','DTC','location','northeast');
grid on;
xlabel('Time (seconds)');
ylabel('Speed (rpms)');
saveas(1,'fig12.jpg','jpg');

figure(5);
plot(time_vec,simout_DTC(:,2),'r','linewidth',3);
hold on;
plot(time_vec,simout_FOC(:,2),'b','linewidth',3);
hold off;
title('Speed response: DTC vs. FOC');
legend('DTC','FOC','location','northeast');
xlabel('Time (seconds)');
ylabel('Speed (rpms)');
grid on;
saveas(1,'fig11.jpg','jpg');

figure(6);
plot(time_vec,simout_DTC(:,4),'r');
hold on;
plot(time_vec,simout_vec(:,4),'b');
title('Phase B current filtered at 300 Hz');
legend('DTC','FOC','location','southeast');
xlabel('Time (seconds)');
ylabel('Current (amps)');
grid on;

figure(7);
plot(time_vec,simout_DTC(:,3),'r','linewidth',3);
hold on;
```

```
plot(time_vec,simout_FOC(:,3),'b','linewidth',3);
title('Reference Torque');
legend('DTC','FOC','location','northeast');
xlabel('Time (seconds)');
ylabel('Torque (Newton meters)');
grid on;

figure(8);
plot(time_vec,simout_DTC(:,1),'r','linewidth',3);
hold on;
plot(time_vec,simout_vec(:,1),'b','linewidth',3);
% axis([0 time_vec(temp1) -2000 6000]);
title('Electrical torque');
legend('DTC','FOC','location','northeast');
xlabel('Time (seconds)');
ylabel('Torque (Newton meters)');
grid on;


start1=29000;
start2=30000;


figure(9);
plot(fluxout(start1:start2,1),fluxout(start1:start2,2),'r','linewidth',
3);
hold on;
plot(fluxout_FOC(start1:start2,1),fluxout_FOC(start1:start2,2),'b','lin
ewidth',3);
hold off;
title('Stator flux of DTC vs. Stator flux of FOC');
legend('DTC','FOC','location','southeast');
xlabel('Electrical flux (Volt meters)');
ylabel('Electrical flux (Volt meters)');
grid on;

figure(10);
plot(time_vec,sqrt(fluxout(:,1).^2+fluxout(:,2).^2),'r','linewidth',3);
hold on;
plot(time_vec,sqrt(fluxout_FOC(:,1).^2+fluxout_FOC(:,2).^2),'b','linewi
dth',3);
hold off;
title('Electrical Flux');
legend('DTC','FOC','location','northeast');
xlabel('Time (seconds)');
ylabel('Flux (Volt-meters)');
grid on;

sw_ct=0;
for ii=1:temp1-1
    if sw_state_DTC(ii,2) ==0 & sw_state_DTC(ii+1,2) == 1
        sw_ct=sw_ct+1;
    end
end
```

```
sw_ctpwm=0;
for ii=1:temp1-1
    if sw_state_pwm(ii,1) ==0 & sw_state_pwm(ii+1,1) == 1
        sw_ctpwm=sw_ctpwm+1;
    end
end
```

D. CHIPSCOPE PLOTTER FILE

```
close all;
clear all;

datain=importdata('im_data100_80b.prn');
vecsize=length(datain.data);
deltat=1/(25e6/3600);
% datasize=round(1/60/deltat);
datasize=vecsize-1;
adc1raw=zeros(1,datasize);
adc2raw=zeros(1,datasize);
adc3raw=zeros(1,datasize);
adc4raw=zeros(1,datasize);
for ii=1:datasize
    index=ii+vecsize-datasize-1;
    if datain.data(index,12+2)==0

adc1raw(ii)=datain.data(index,1+2)+2*datain.data(index,2+2)+2^2*datain.
data(index,3+2)+...
        2^3*datain.data(index,4+2)+2^4*datain.data(index,5+2)+...
        2^5*datain.data(index,6+2)+2^6*datain.data(index,7+2)+...
        2^7*datain.data(index,8+2)+2^8*datain.data(index,9+2)+...
        2^9*datain.data(index,10+2)+2^10*datain.data(index,11+2);
    else

adc1raw(ii)=datain.data(index,1+2)+2*datain.data(index,2+2)+2^2*datain.
data(index,3+2)+...
        2^3*datain.data(index,4+2)+2^4*datain.data(index,5+2)+...
        2^5*datain.data(index,6+2)+2^6*datain.data(index,7+2)+...
        2^7*datain.data(index,8+2)+2^8*datain.data(index,9+2)+...
        2^9*datain.data(index,10+2)+2^10*datain.data(index,11+2)-2^11;
    end

    if datain.data(index,12+14)==0

adc2raw(ii)=datain.data(index,1+14)+2*datain.data(index,2+14)+2^2*datai
n.data(index,3+14)+...
        2^3*datain.data(index,4+14)+2^4*datain.data(index,5+14)+...
        2^5*datain.data(index,6+14)+2^6*datain.data(index,7+14)+...
        2^7*datain.data(index,8+14)+2^8*datain.data(index,9+14)+...
        2^9*datain.data(index,10+14)+2^10*datain.data(index,11+14);
    else
```

```
adc2raw(ii)=datain.data(index,1+14)+2*datain.data(index,2+14)+2^2*datai
n.data(index,3+14)+...
        2^3*datain.data(index,4+14)+2^4*datain.data(index,5+14)+...
        2^5*datain.data(index,6+14)+2^6*datain.data(index,7+14)+...
        2^7*datain.data(index,8+14)+2^8*datain.data(index,9+14)+...
        2^9*datain.data(index,10+14)+2^10*datain.data(index,11+14)-
2^11;
    end

    if datain.data(index,12+26)==0

adc3raw(ii)=datain.data(index,1+26)+2*datain.data(index,2+26)+2^2*datai
n.data(index,3+26)+...
        2^3*datain.data(index,4+26)+2^4*datain.data(index,5+26)+...
        2^5*datain.data(index,6+26)+2^6*datain.data(index,7+26)+...
        2^7*datain.data(index,8+26)+2^8*datain.data(index,9+26)+...
        2^9*datain.data(index,10+26)+2^10*datain.data(index,11+26);
    else

adc3raw(ii)=datain.data(index,1+26)+2*datain.data(index,2+26)+2^2*datai
n.data(index,3+26)+...
        2^3*datain.data(index,4+26)+2^4*datain.data(index,5+26)+...
        2^5*datain.data(index,6+26)+2^6*datain.data(index,7+26)+...
        2^7*datain.data(index,8+26)+2^8*datain.data(index,9+26)+...
        2^9*datain.data(index,10+26)+2^10*datain.data(index,11+26)-
2^11;
    end


adc4raw(ii)=datain.data(index,1+38)+2*datain.data(index,2+38)+2^2*datai
n.data(index,3+38)+...
        2^3*datain.data(index,4+38)+2^4*datain.data(index,5+38)+...
        2^5*datain.data(index,6+38)+2^6*datain.data(index,7+38)+...
        2^7*datain.data(index,8+38)+2^8*datain.data(index,9+38)+...
        2^9*datain.data(index,10+38)+2^10*datain.data(index,11+38);

end

adc1=adc1raw/2^6;
adc2=adc2raw/2^6;
adc3=adc3raw/2^11*251/sqrt(3);
adc4=adc4raw;

time=[0:datasize-1]*deltat;

set(0,'DefaultAxesFontName','times')
set(0,'DefaultAxesFontSize',14)
set(0,'DefaultTextFontName','times')
figure(1);
plot(time,adc1,'b','linewidth',2);
hold on;
plot(time,adc2,'g','linewidth',2);
hold off;
```

```
xlabel('Time')
ylabel('DC bus Magnitude')
grid on

figure(2);
plot(time,adc3,'r','linewidth',2);
hold on;
plot(time,adc4,'m','linewidth',2);
hold off;
xlabel('Time')
ylabel('Magnitude')
grid on
%axis([.0055 .006 -1 1]);
```

APPENDIX C. SIMULINK MODEL

A. INDUCTION MACHINE MODEL

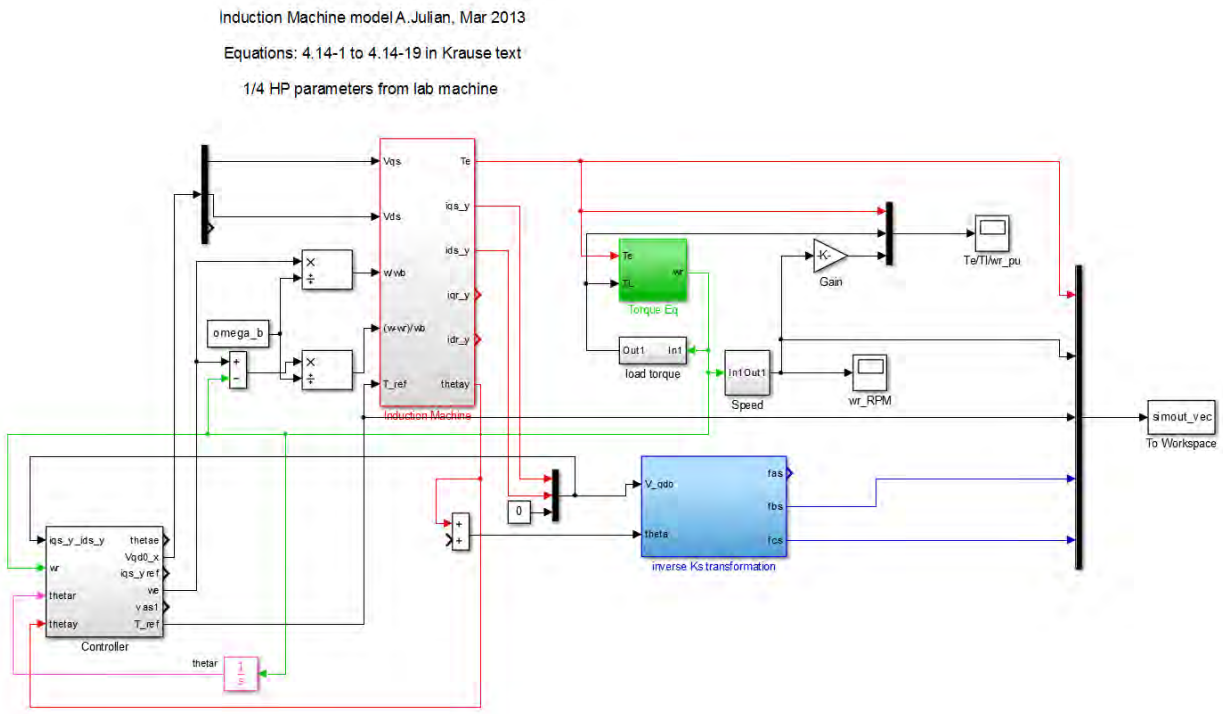

B. CONTROLLER

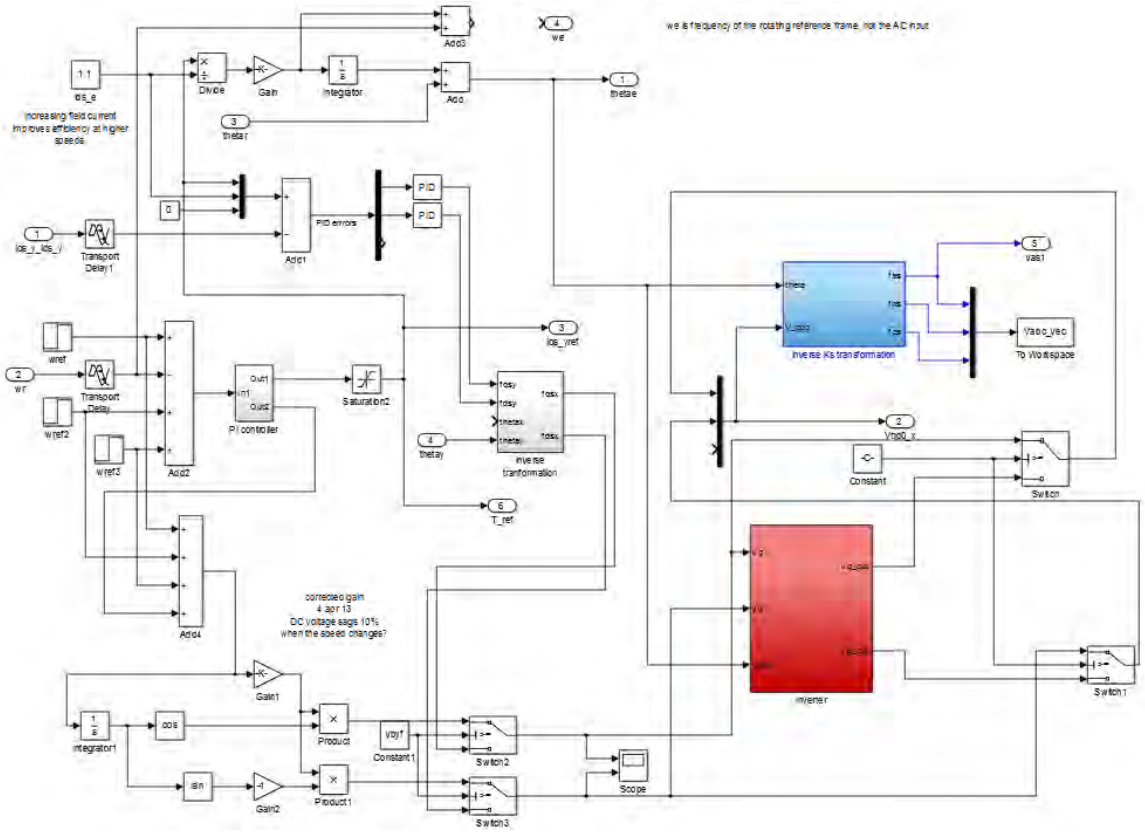

1. Inverter

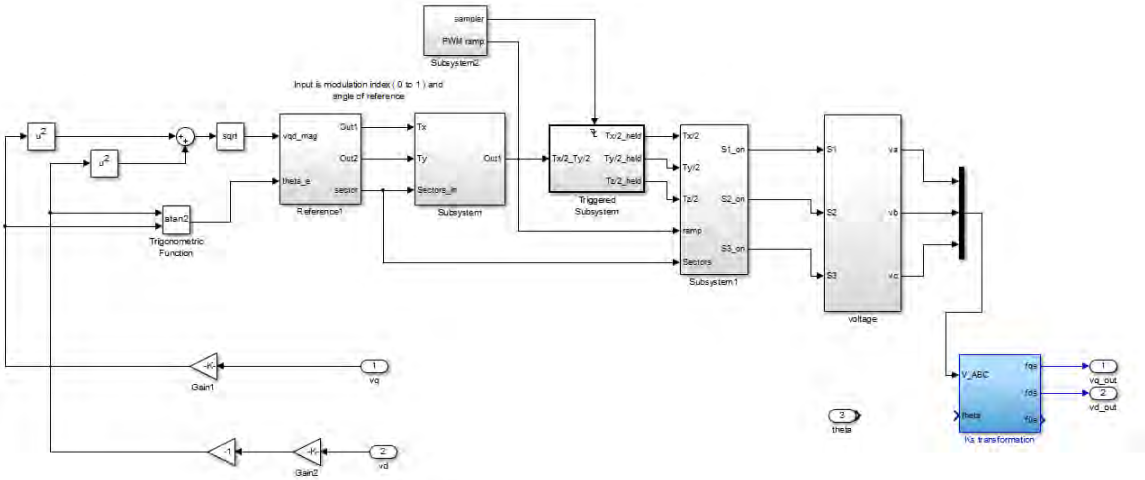

a. K_s ***Transformation***

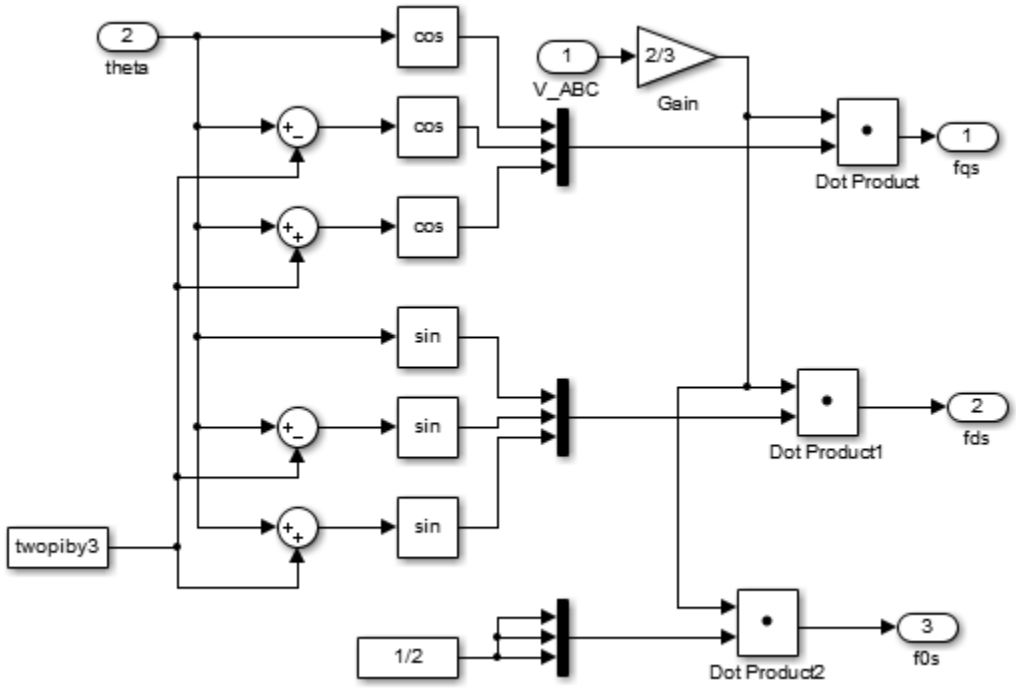

b. ***Reference 1***

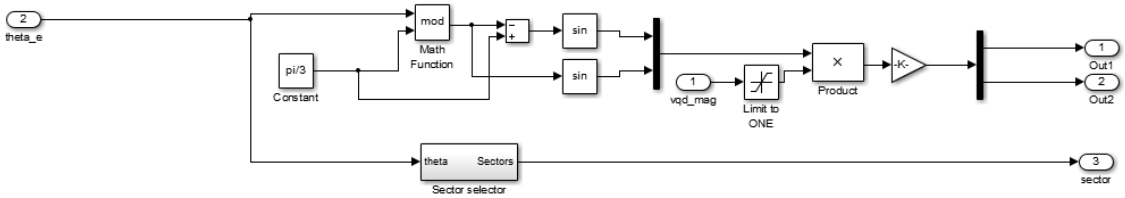

c. Sector Selector

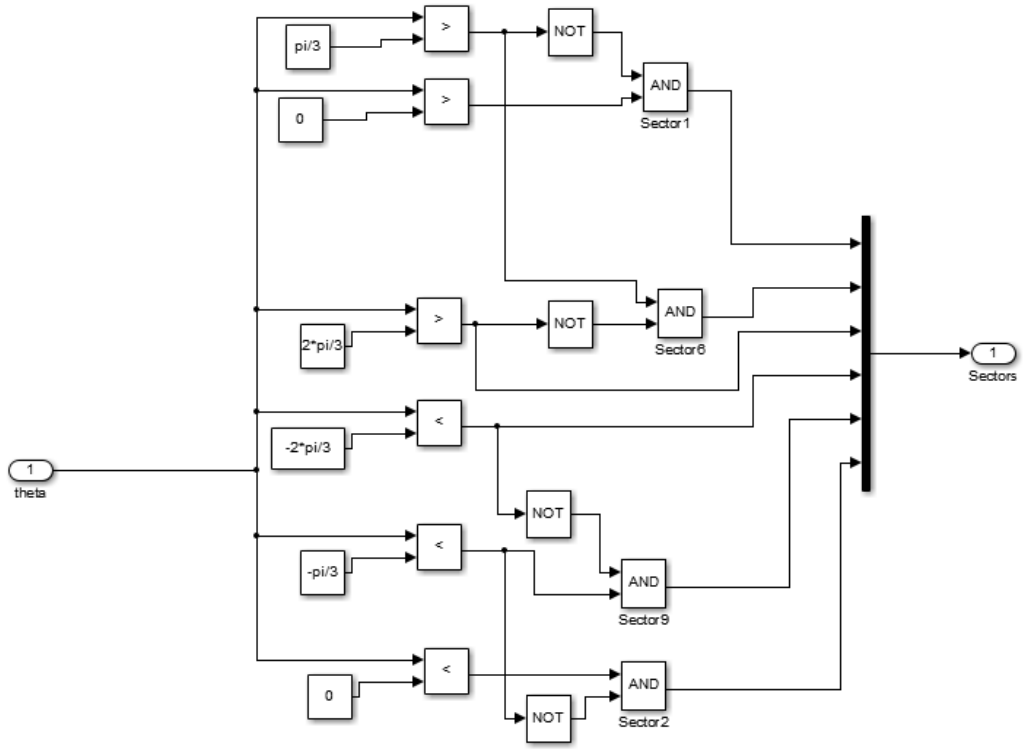

d. Subsystem

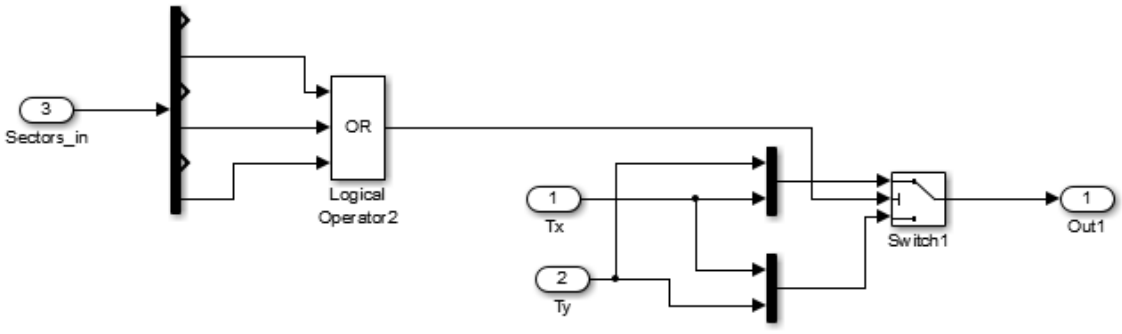

Switching pattern for sectors 2,4,6 are different

e. Subsystem 1

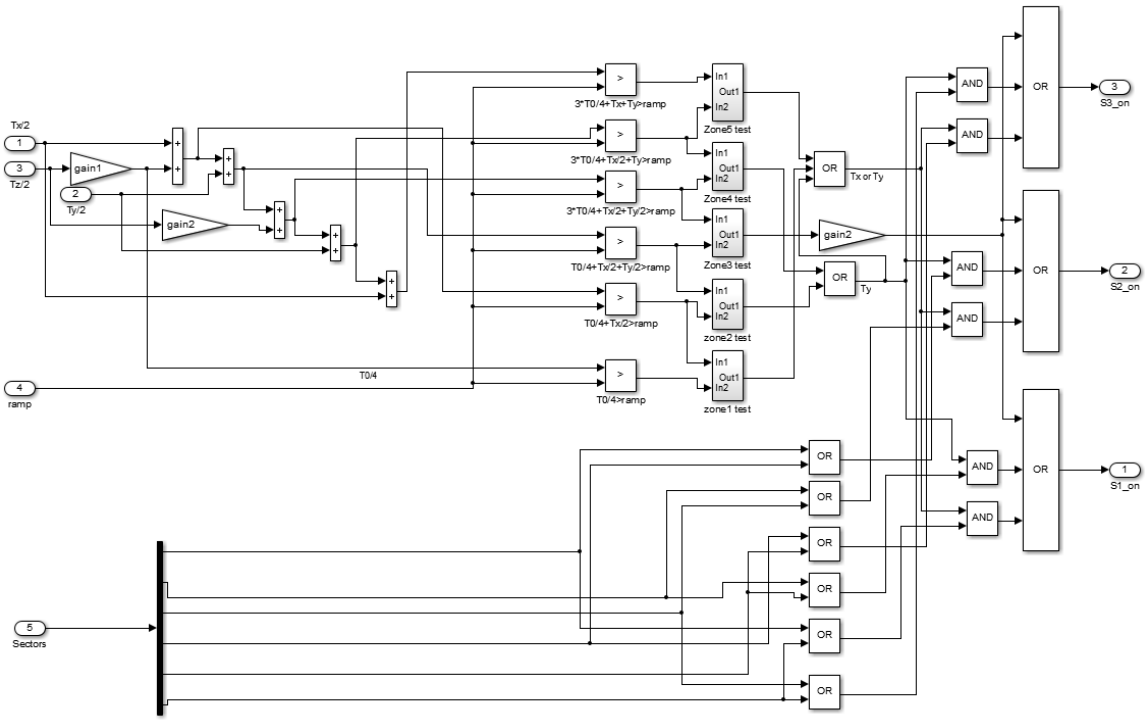

f. Zone 1-5 Test

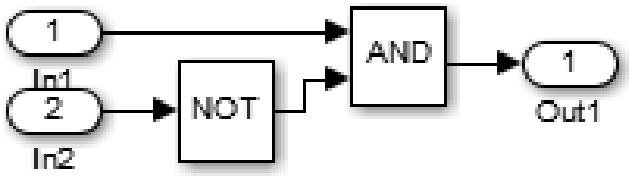

g. Subsystem 2

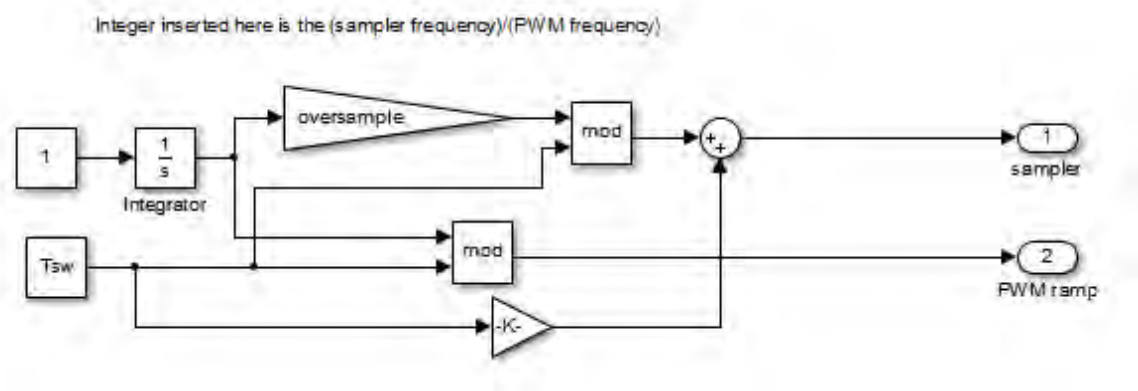

h. Triggered Subsystem

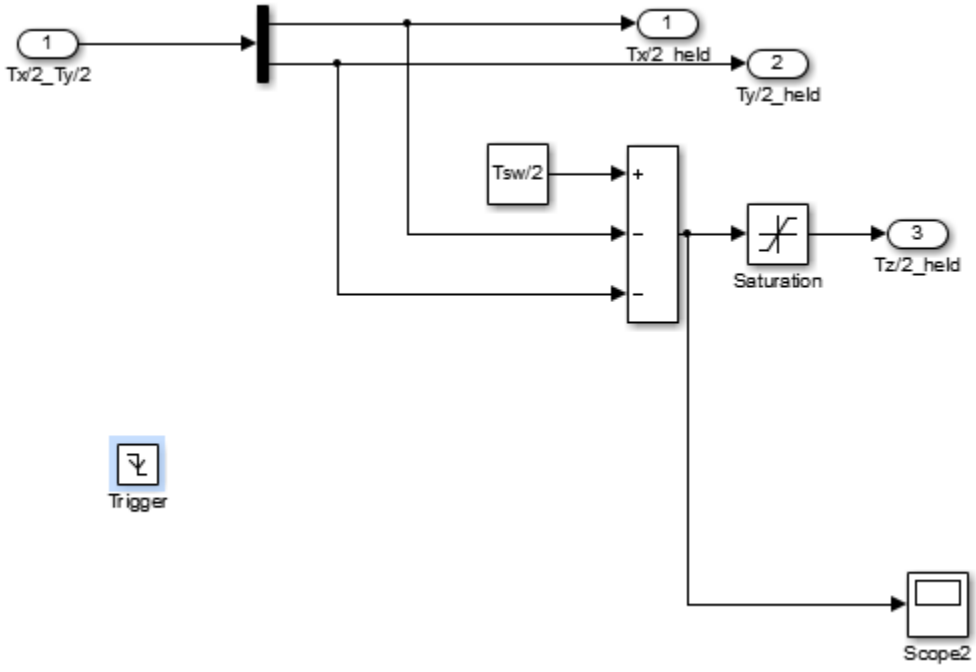

i. Voltage

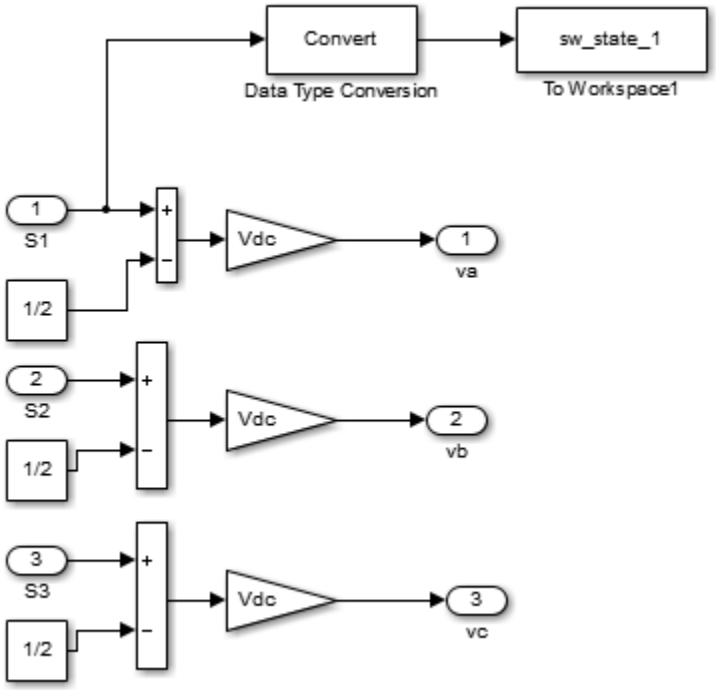

2. PI Controller

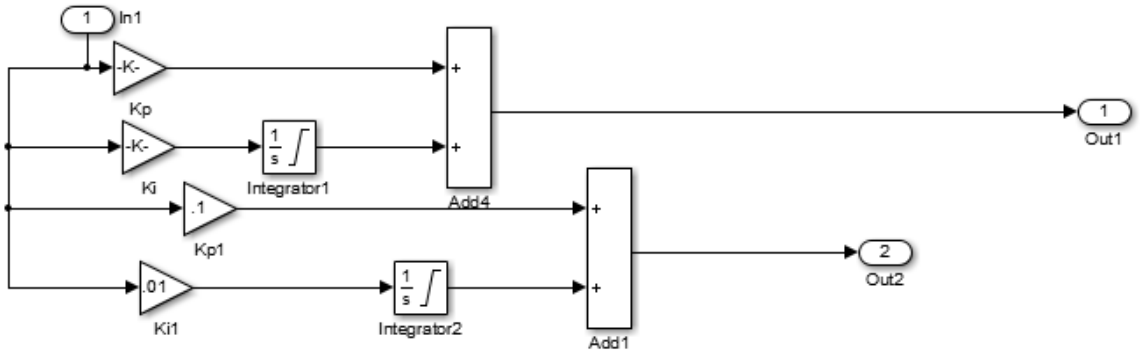

3. Inverse Transformation

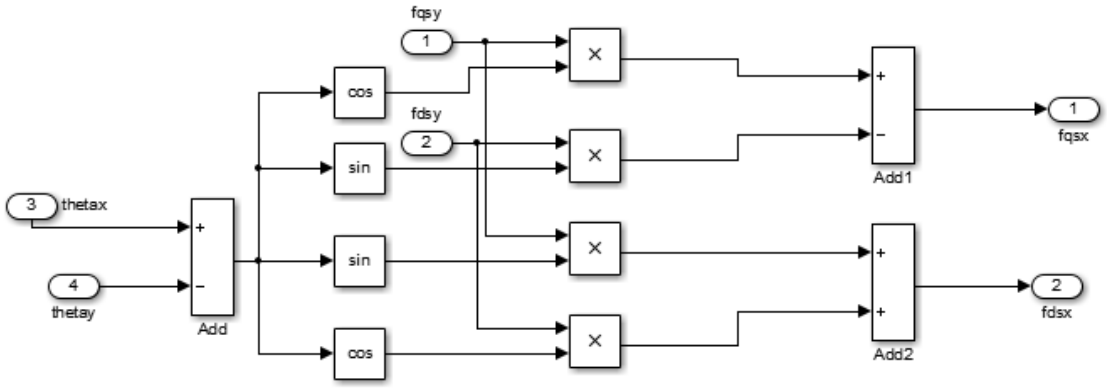

4. Inverse K_s Transformation

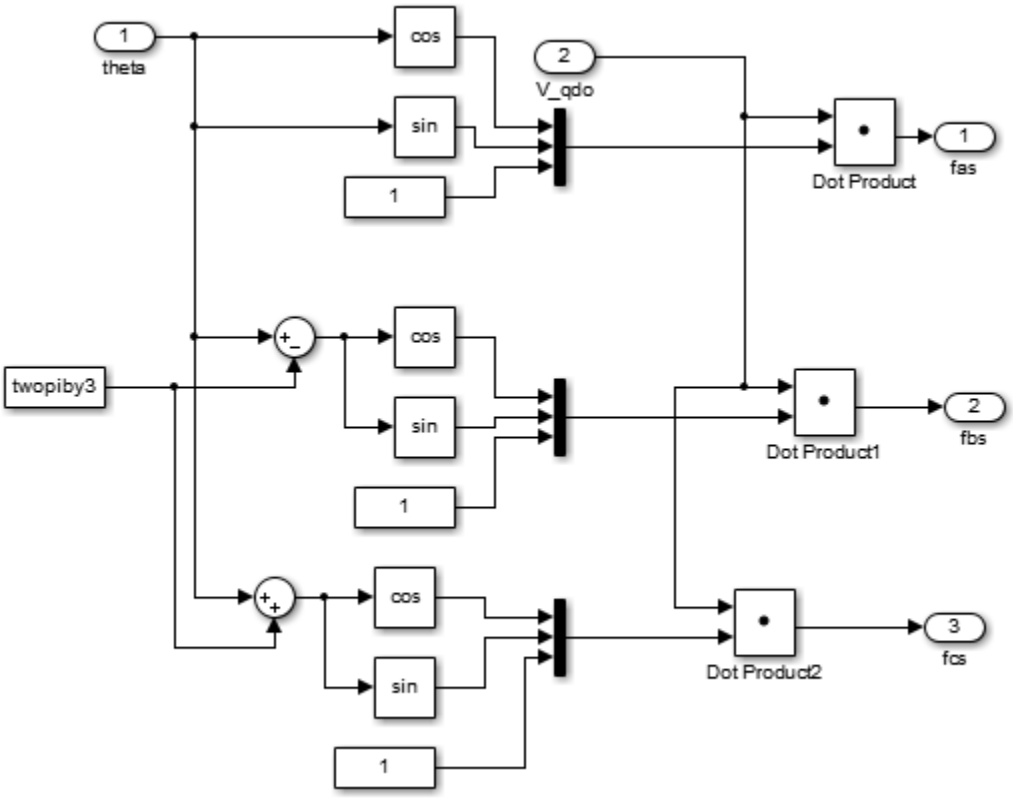

C. INDUCTION MACHINE

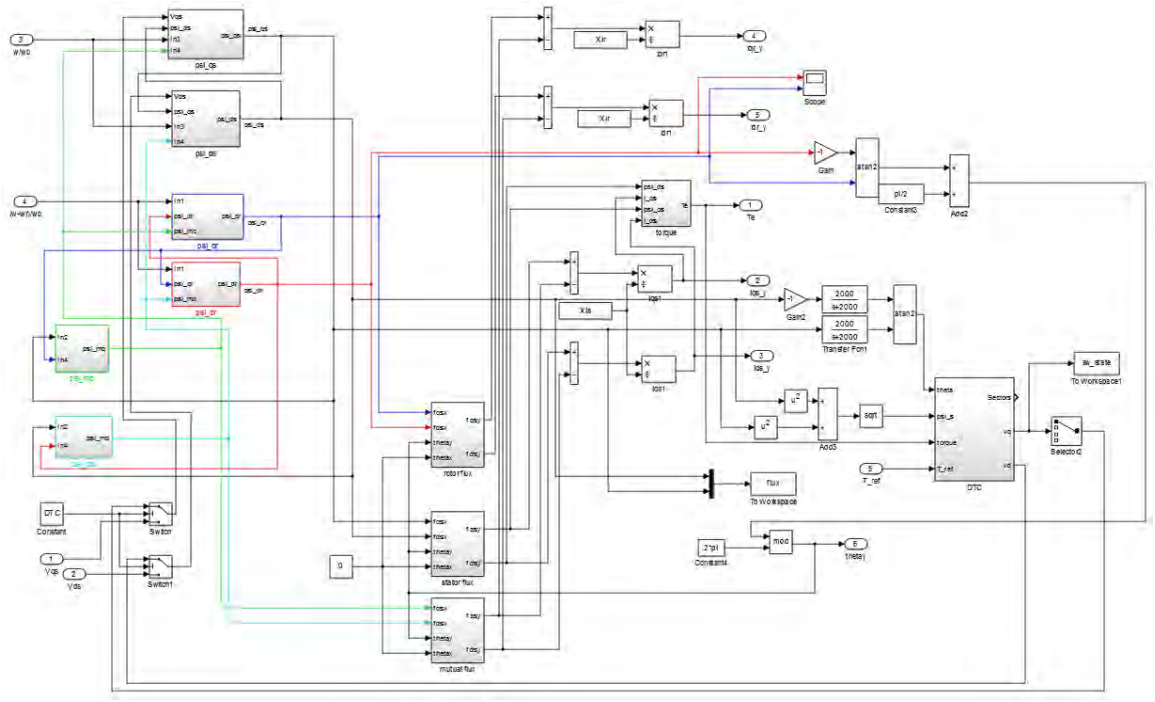

1. DTC

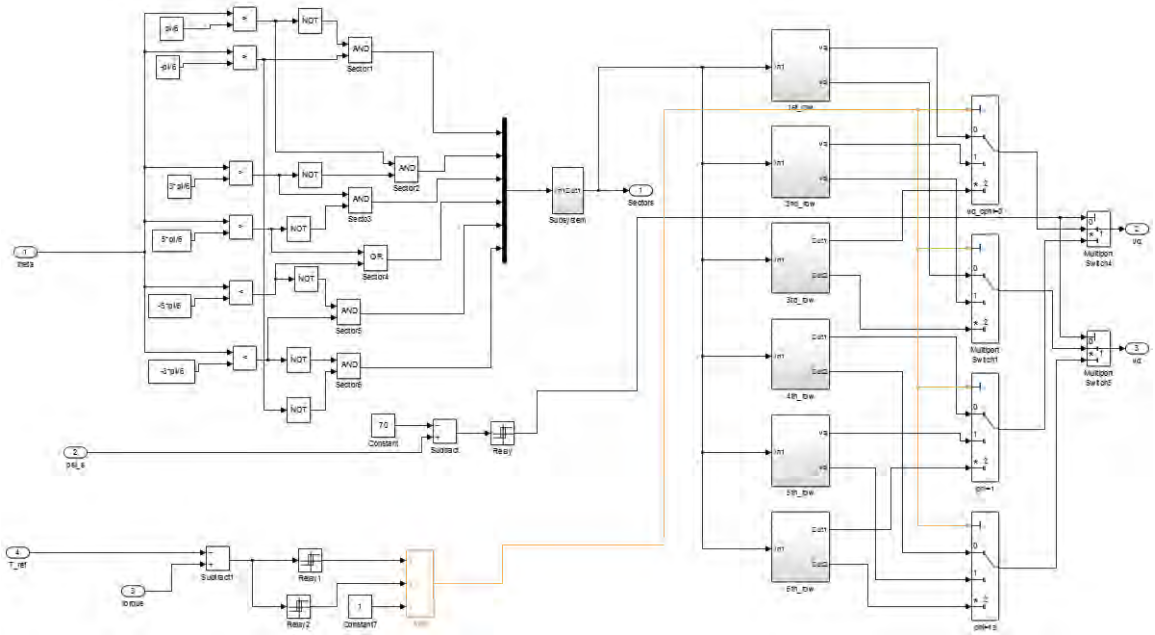

a. First Row

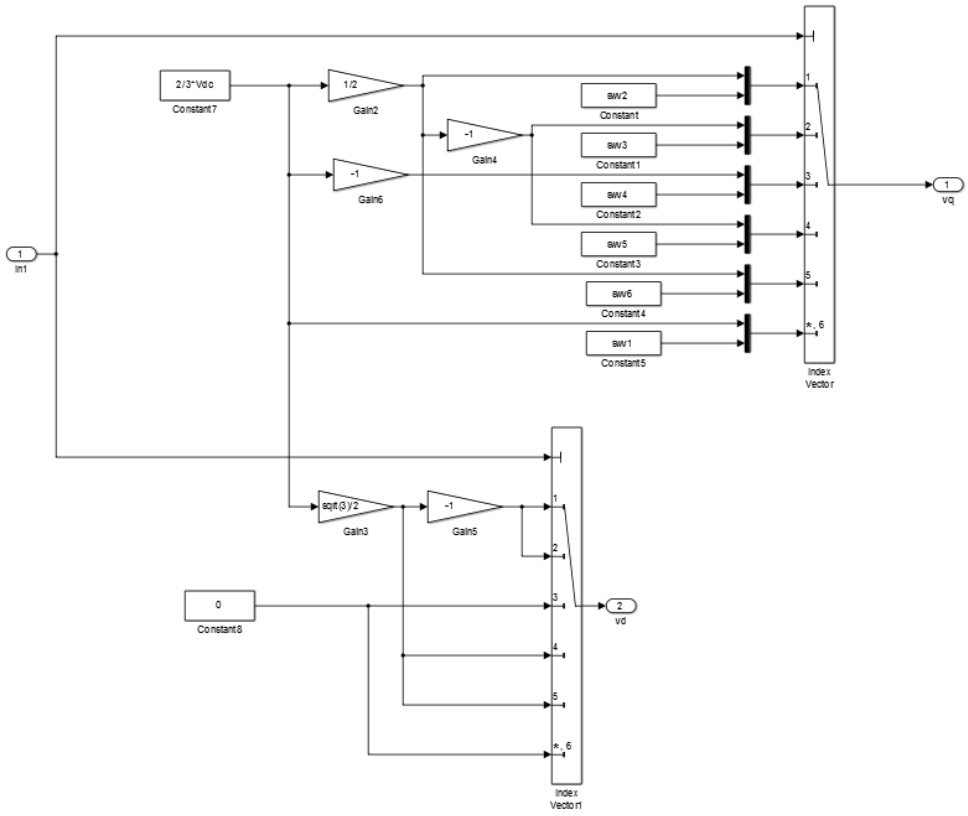
2/3*Vdc
Constant7
1/2
Gain2
-1
Gain4
-1
Gain6
sw2
Constant
sw3
Constant1
sw4
Constant2
sw5
Constant3
sw6
Constant4
sw1
Constant5
Index
Vector
1
vq
1
In1
sqrt(3)/2
Gain3
-1
Gain5
0
Constant8
2
vd
Index
Vector1

b. Second Row

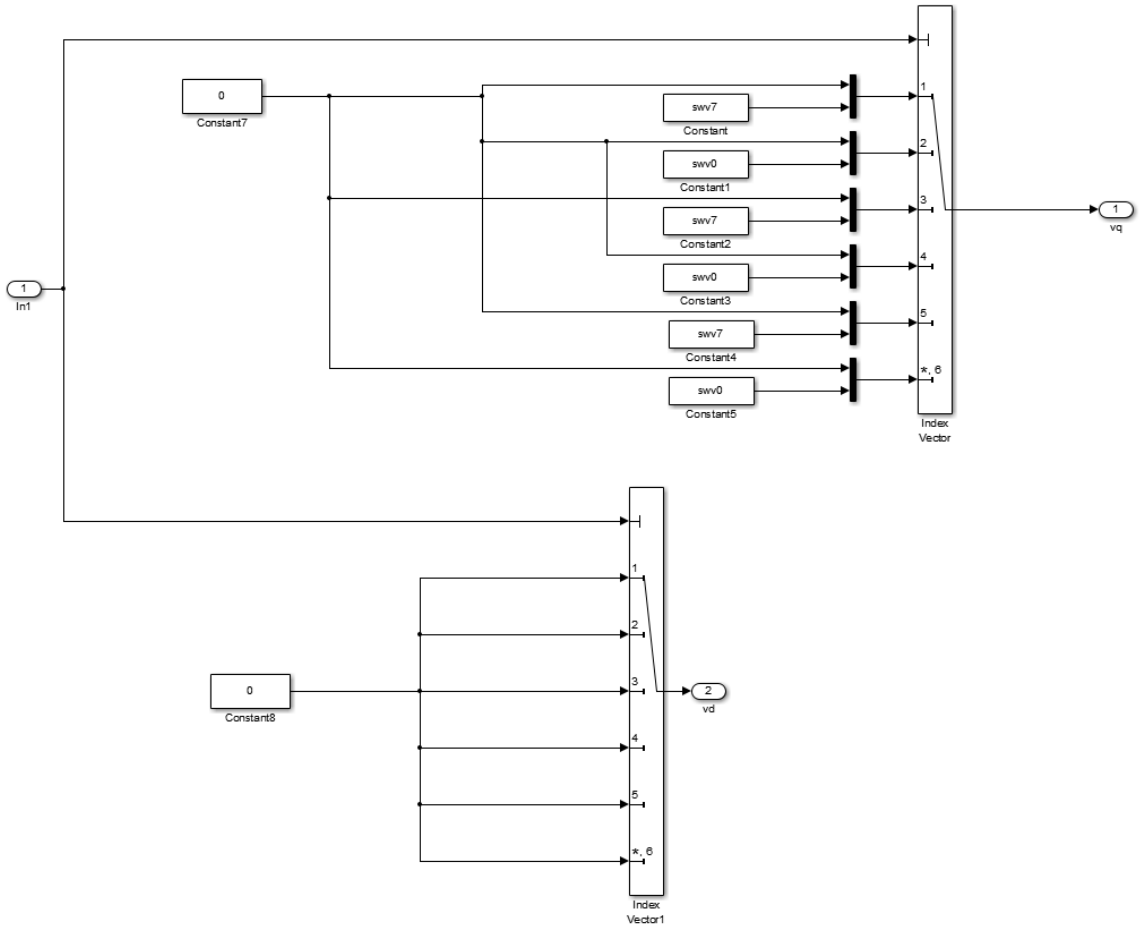
0
Constant7
swv7
Constant
swv0
Constant1
swv7
Constant2
swv0
Constant3
swv7
Constant4
swv0
Constant5
1
2
3
4
5
*, 6
Index
Vector
1
vq
1
In1
1
2
3
4
5
*, 6
Index
Vector1
0
Constant8
2
vd

c. Third Row

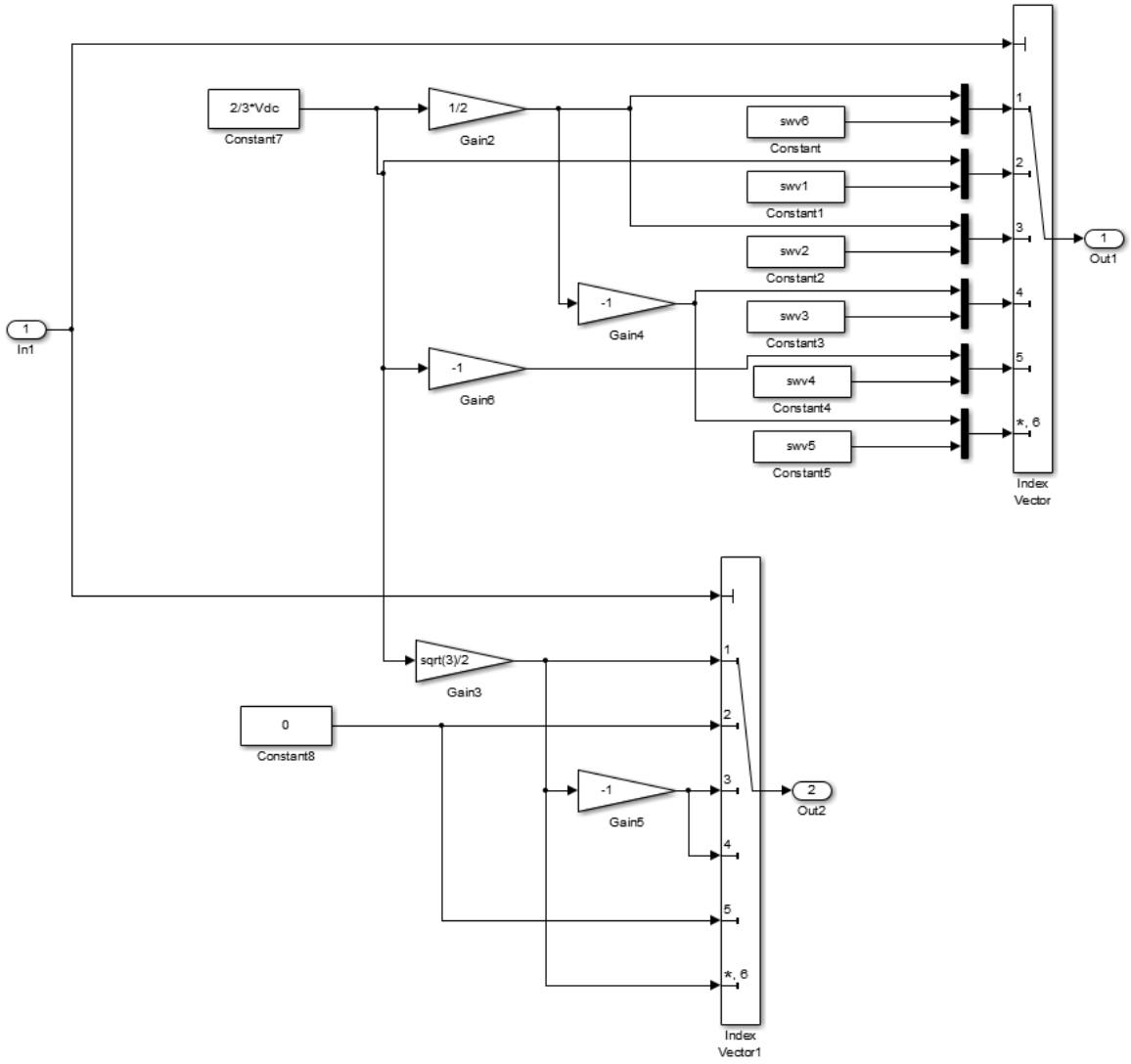
2/3*Vdc
Constant7
1/2
Gain2
swv6
Constant
swv1
Constant1
swv2
Constant2
-1
Gain4
swv3
Constant3
-1
Gain6
swv4
Constant4
swv5
Constant5
1
2
3
4
5
*, 6
Index
Vector
1
Out1
1
In1
sqrt(3)/2
Gain3
0
Constant8
-1
Gain5
1
2
3
4
5
*, 6
Index
Vector1
2
Out2

d. Fourth Row

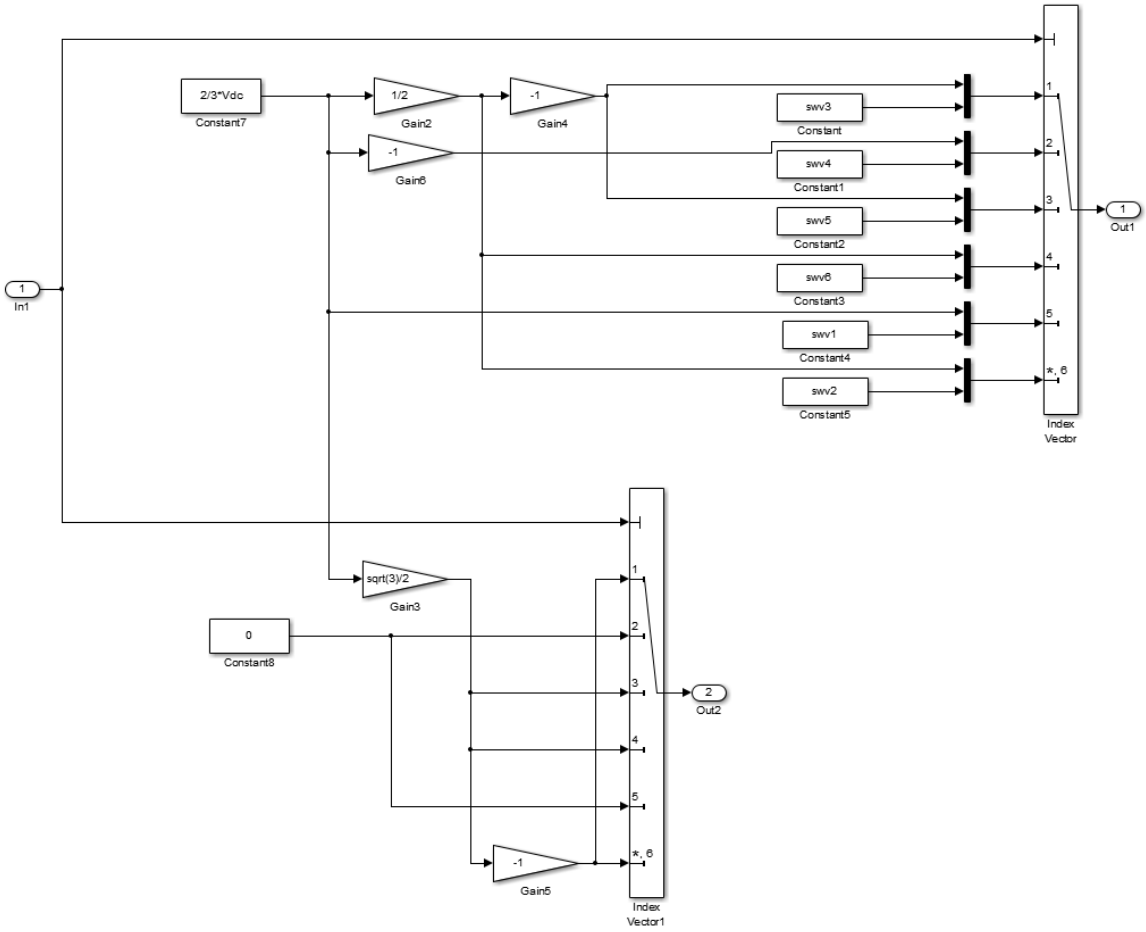
2/3*Vdc
Constant7
1/2
Gain2
-1
Gain4
-1
Gain6
swv3
Constant
swv4
Constant1
swv5
Constant2
swv6
Constant3
swv1
Constant4
swv2
Constant5
Index
Vector
Out1
In1
sqrt(3)/2
Gain3
0
Constant8
-1
Gain5
Index
Vector1
Out2

e. Fifth Row

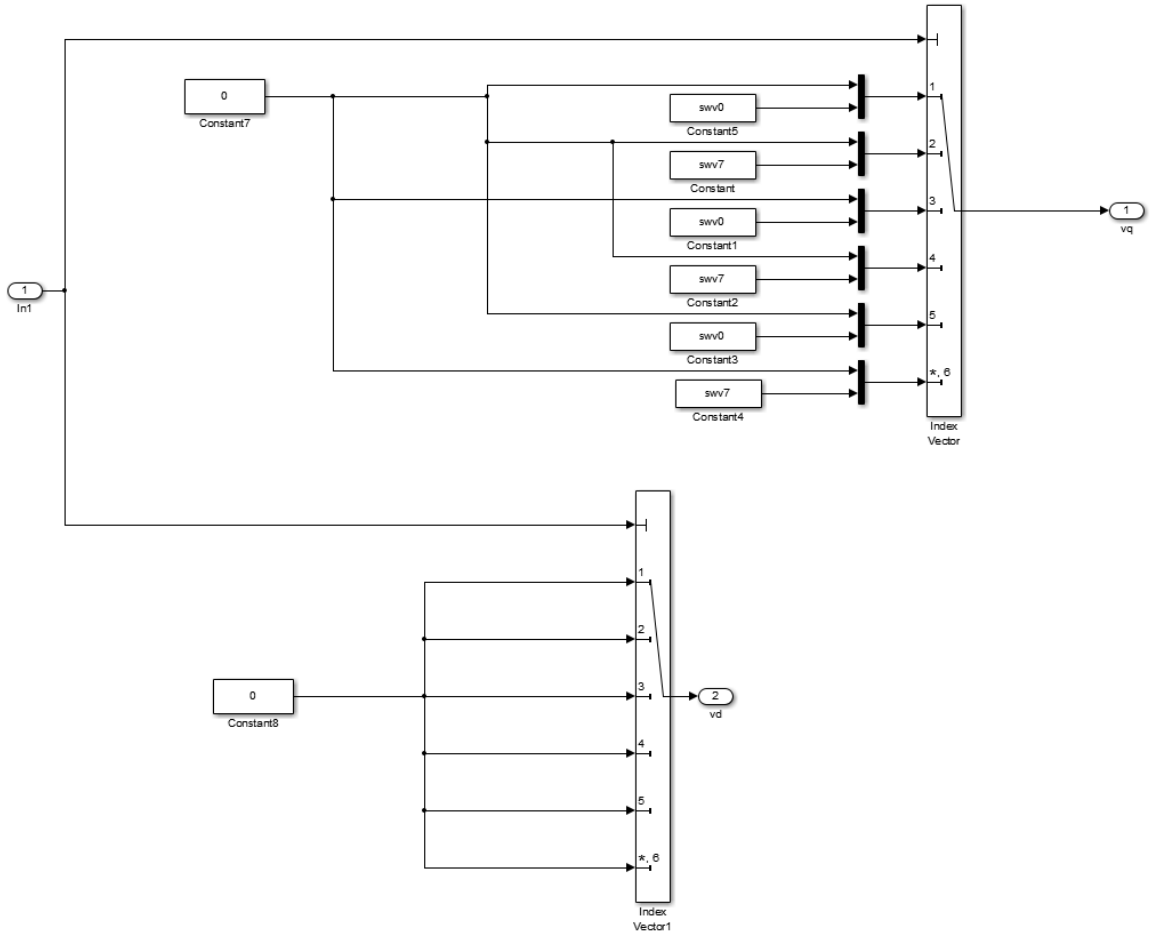
0
Constant7
swv0
Constant5
swv7
Constant
swv0
Constant1
swv7
Constant2
swv0
Constant3
swv7
Constant4
1
2
3
4
5
*, 6
Index
Vector
1
vq
1
In1
1
2
3
4
5
*, 6
Index
Vector1
0
Constant8
2
vd

f. Sixth Row

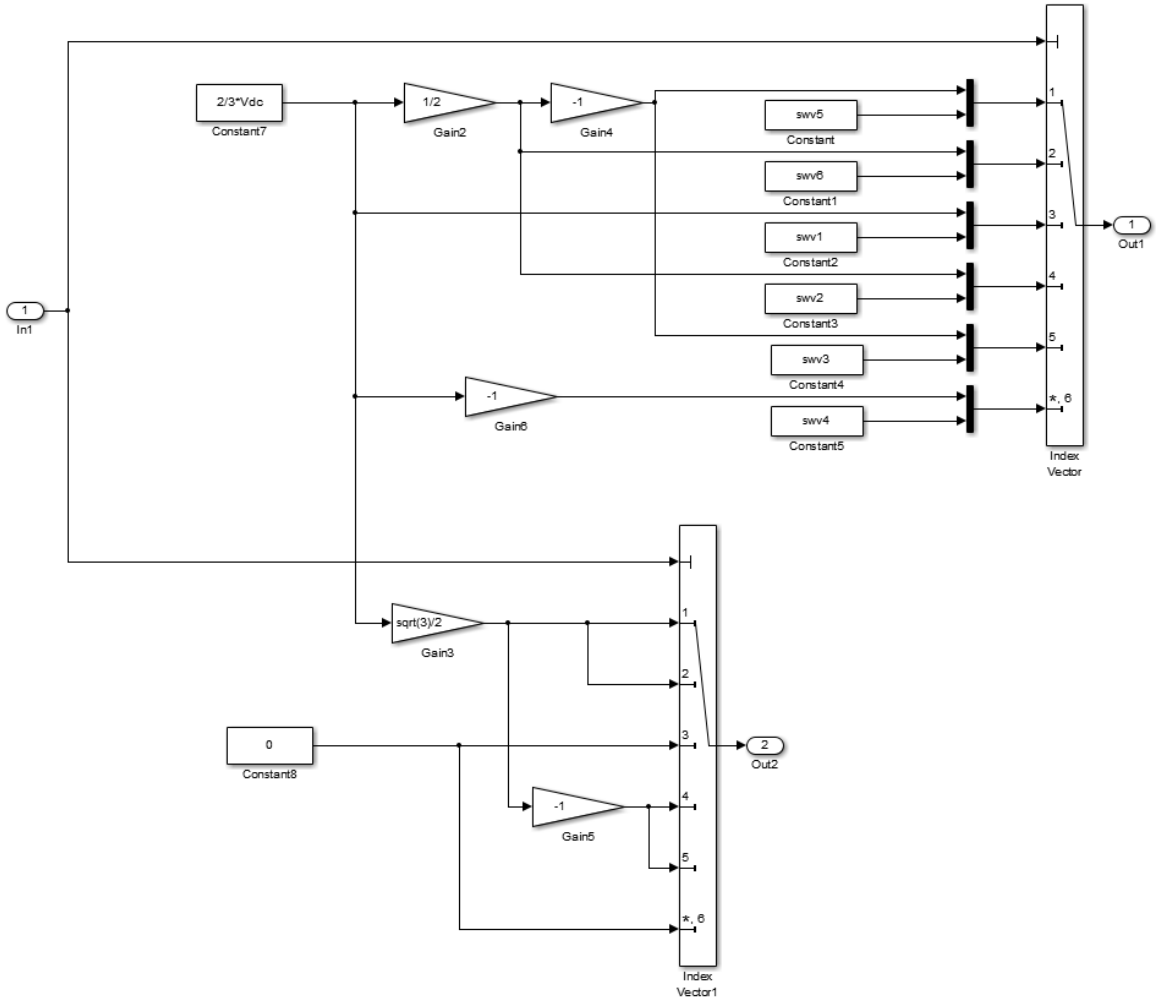
2/3*Vdc
Constant7
1/2
Gain2
-1
Gain4
swv5
Constant
swv6
Constant1
swv1
Constant2
swv2
Constant3
swv3
Constant4
swv4
Constant5
-1
Gain6
1
2
3
4
5
*, 6
Index
Vector
1
Out1
1
In1
sqrt(3)/2
Gain3
0
Constant8
-1
Gain5
1
2
3
4
5
*, 6
Index
Vector1
2
Out2

g. Subsystem

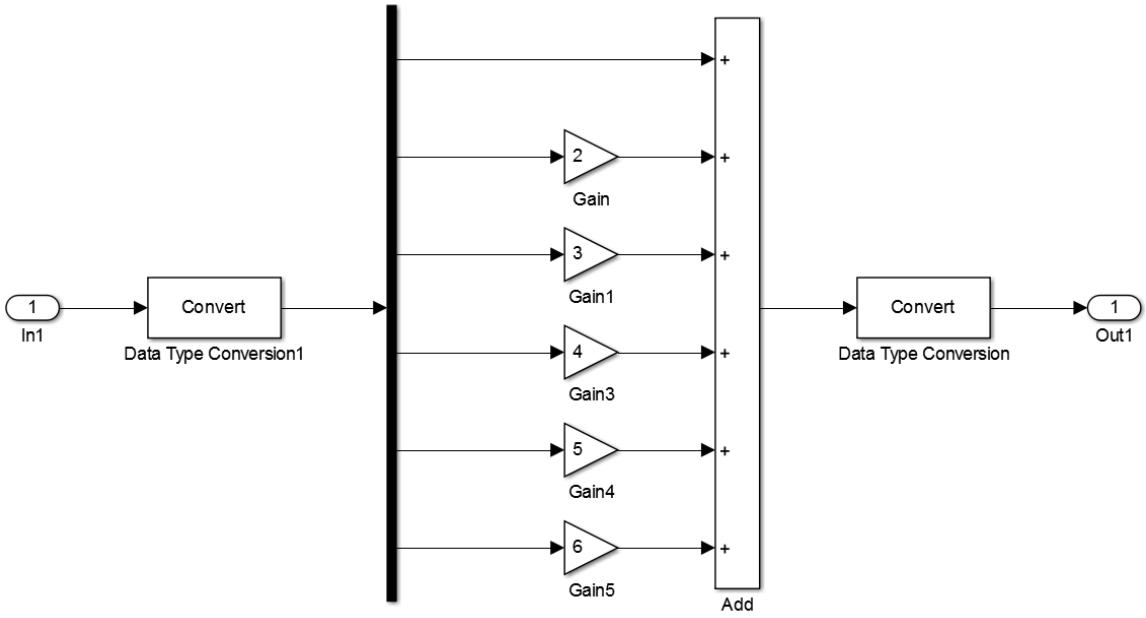

2. Mutual Flux

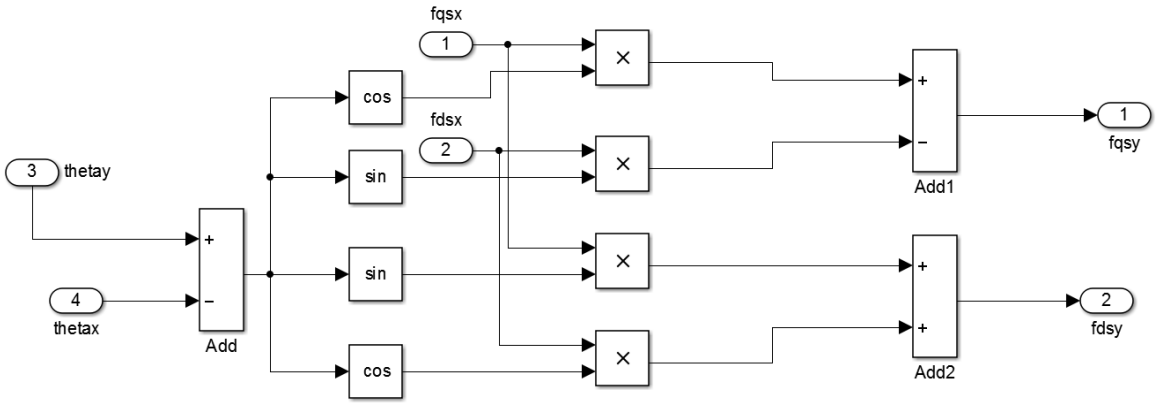

3. φ_{dr}

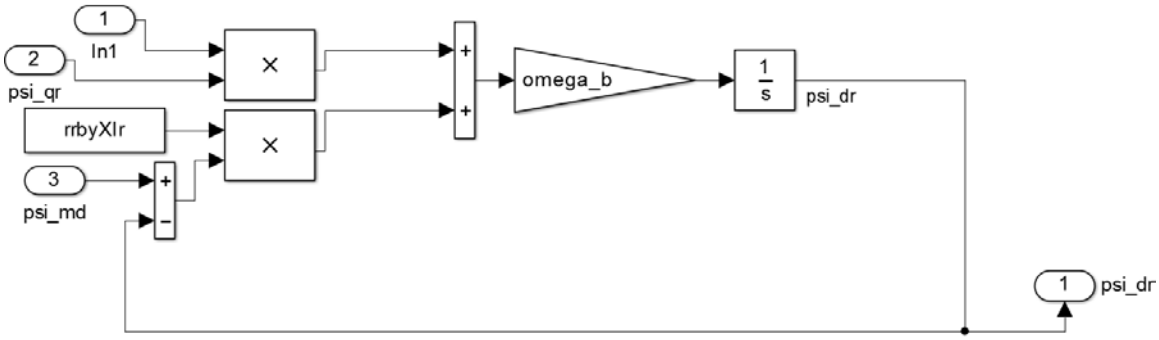

4. φ_{ds}

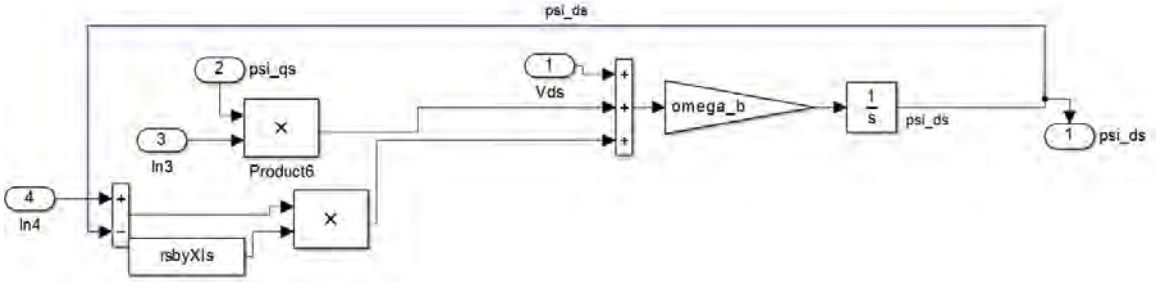

5. φ_{md}

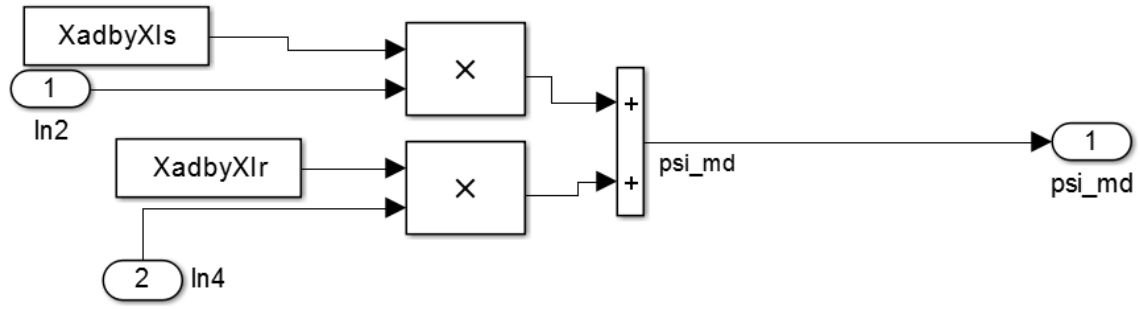

6. φ_{mq}

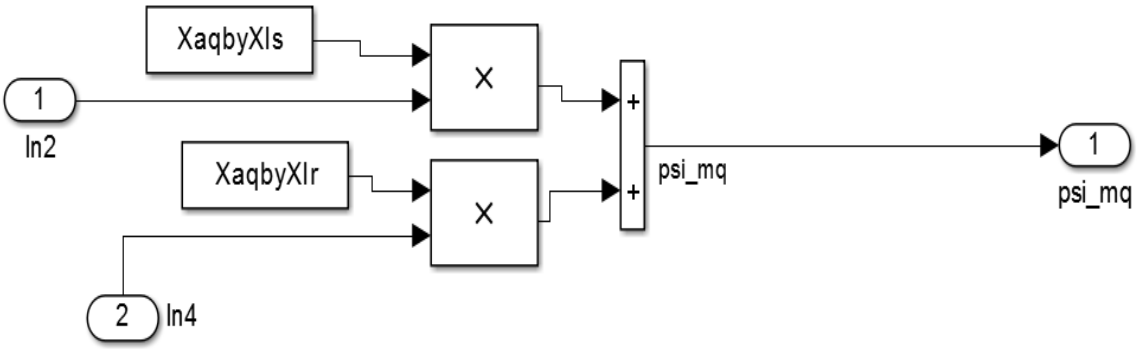

7. φ_{qr}

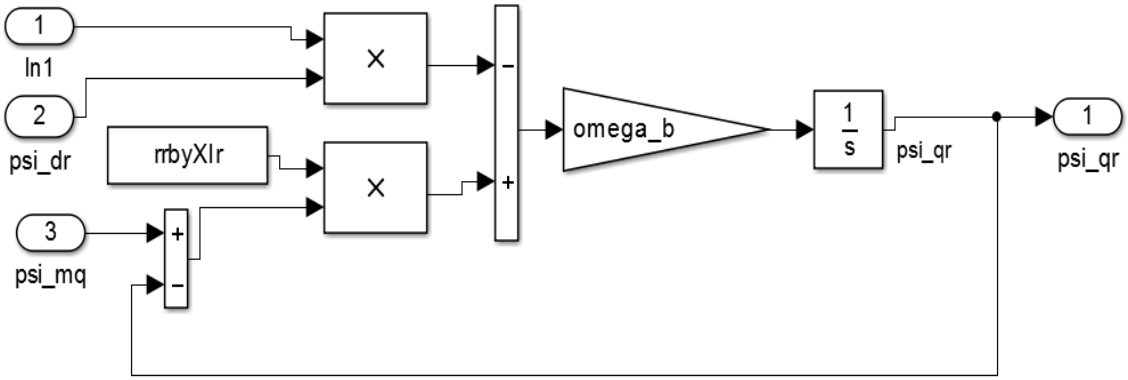

8. φ_{qs}

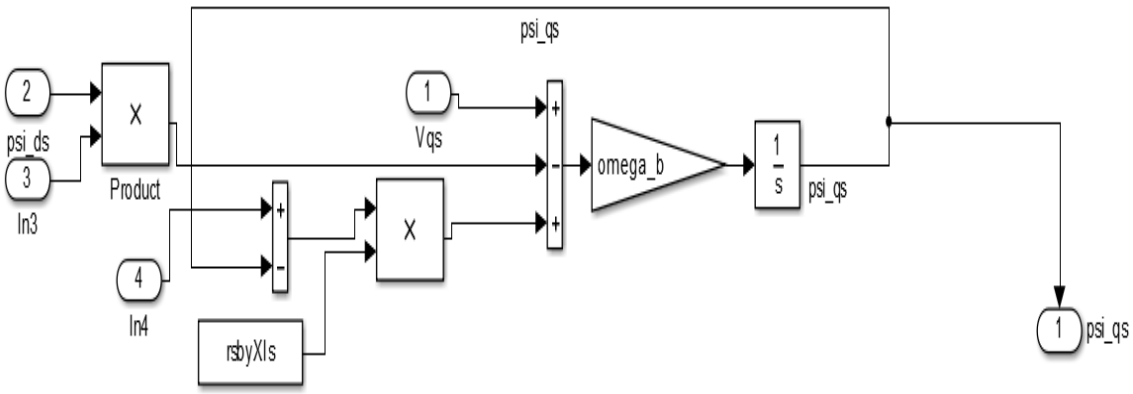

9. Rotor Flux

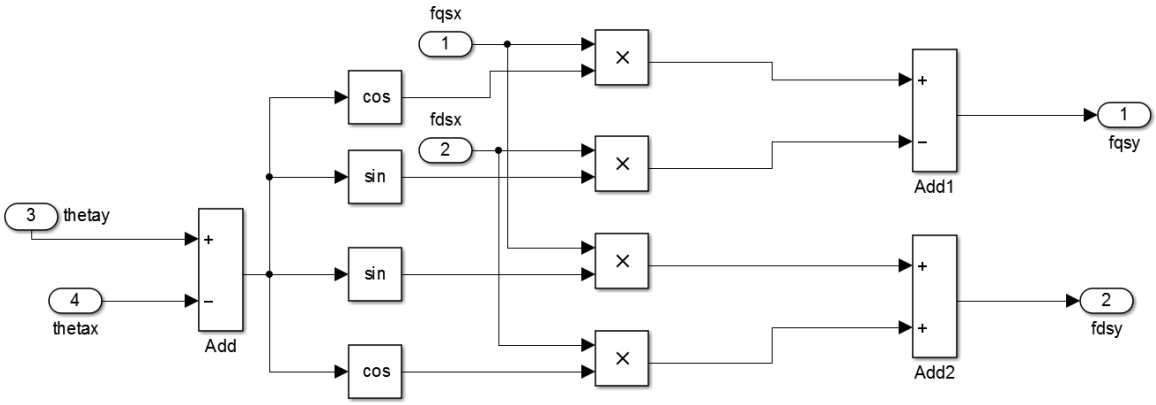

10. Stator Flux

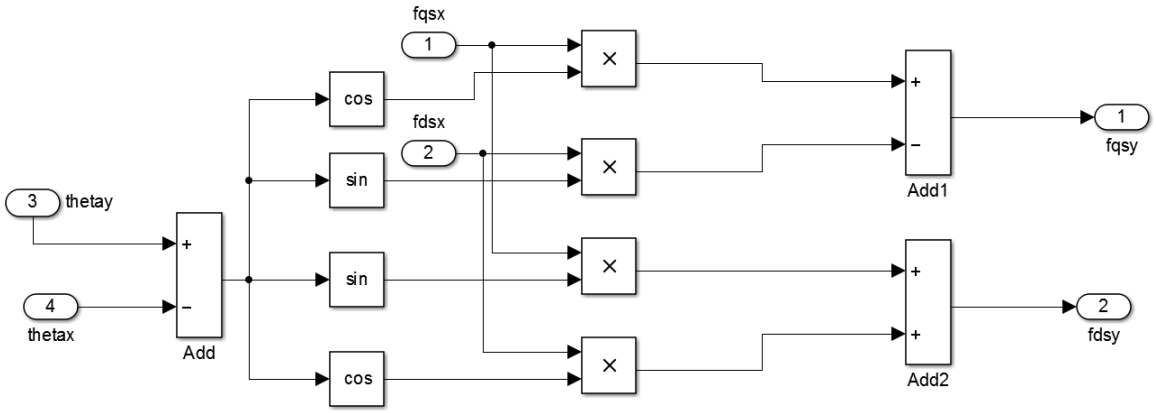

11. Torque

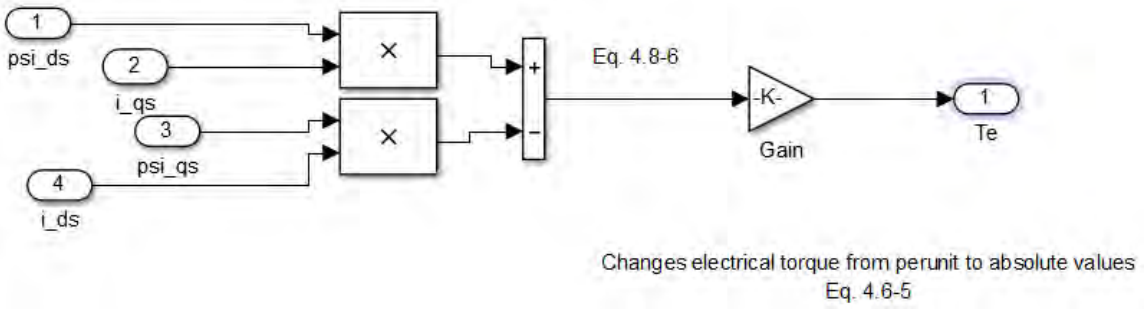

Changes electrical torque from perunit to absolute values
Eq. 4.6-5

D. SPEED

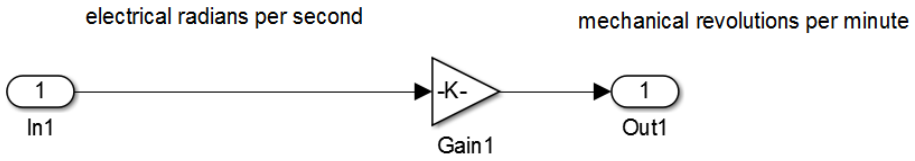

E. TORQUE EQUATION

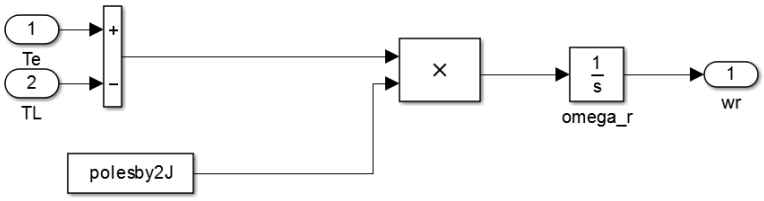

F. INVERSE K_s TRANSFORMATION

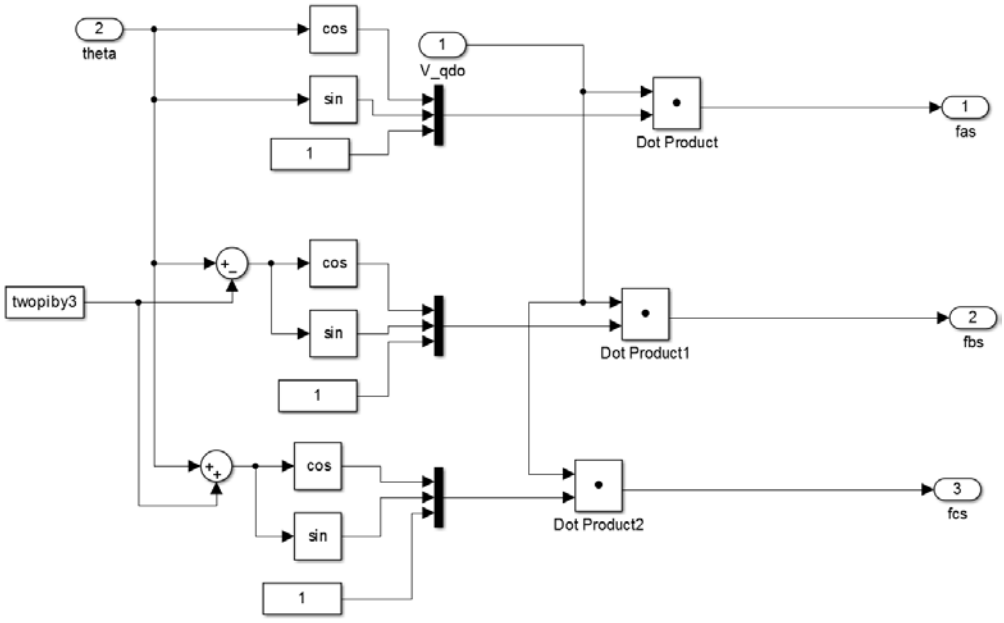

G. LOAD TORQUE

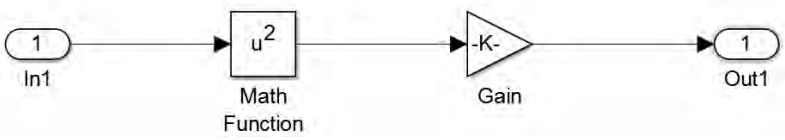

LIST OF REFERENCES

[1] J. N. Nash, "Direct torque control, induction motor vector control without an encoder," *IEEE Transactions on Industry Applications*, vol. 33, no. 2, March/April 1997.

[2] P. C. Krause, O. Wasynczuk, and S. D. Sudhoff, *Analysis of Electric Machinery and Drive Systems*. Piscataway, NJ: John Wiley & Sons, 2002.

[3] G. W. Edwards, "Wind turbine power generation emulation via doubly fed induction generator control," M.S., Naval Postgraduate School, 2009.

[4] V. Peter, *Sensorless Vector and Direct Torque Control.* Oxford, United Kingdom: Oxford University Press, 1998.

[5] S. Srilad, S. Tunyasrirut, and T. Suksri, "Implementation of a scalar controlled induction motor drive," in Bexco, Busan, Korea, pp. 3605–3610, 2006.

[6] A. Julian, "EC4130 laboratory experiment #3: three-phase induction machine," Naval Postgraduate School, Monterey, CA, December 2011.

[7] R. Brindha, "Implementation of V/f control of three-phase induction motor using microcontroller," S.R.M Engineering College, Tamil Nadu, India, June/July 2006.

[8] C. R. Nave, "Faraday's law," Georgia State University, Atlanta, GA, 2013.

[9] C. U. Ogbuka, M. Eng, and M. U. Agu, "A modified closed loop V/f controlled induction motor drive," *The Pacific Journal of Science and Technology*, vol. 10, no. 1, May 2009.

[10] D. Casadei, F. Profumo, G. Serra, and A. Tani, "FOC and DTC: Two viable schemes for induction motors torque control," *IEEE Transactions on Power Electronics*, vol. 17, no. 5, September 2002.

[11] Texas Instruments Europe, "Field orientated control of 3-phase AC-motors," Literature Number: BPRA073, February 1998.

THIS PAGE INTENTIONALLY LEFT BLANK

INITIAL DISTRIBUTION LIST

1. Defense Technical Information Center
   Ft. Belvoir, Virginia

2. Dudley Knox Library
   Naval Postgraduate School
   Monterey, California